GOLD AND BASE METAL MINERALIZATION OF THE DOLPHIN INTRUSION-RELATED GOLD DEPOSIT, FAIRBANKS MINING DISTRICT, ALASKA

By

Luke M. Raymond, B.S.

A Thesis Submitted in Partial Fulfilment of the Requirements

for the Degree of

Master of Science

In

Geology

University of Alaska Fairbanks

August 2018

APPROVED:

Dr Rainer Newberry, Committee Chair
Dr. Jessica Larsen, Committee Member
Dr. Mary Keskinen, Committee Member
Dr. Paul McCarthy, Chair,
Department of Geosciences
Dr. Anupma Prakash, Interim Dean,
College of Natural Science and Mathematics
Dr. Michael Castellini,
Dean of the Graduate School

Abstract

The Dolphin deposit is an intrusion-related gold deposit (IRGD) located approximately 30 km north of Fairbanks, Alaska. The deposit is in--and adjacent to--a composite mid-Cretaceous pluton intruding amphibolite facies metamorphic rocks. An NI43-101 compliant gold resource estimation for the deposit (utilizing a 0.3 g/t cut-off grade) is 61.5 Million tonnes (Mt) at 0.69 g/t indicated (1.36 million oz = Moz) and 71.5 Mt at 0.69 g/t inferred (1.58 Moz).

Due to extensive hydrothermal alteration of the intrusion, identifying rock types in hand sample and thin section, as well as by standard compositional techniques (e.g., SiO_2 vs. $Na_2O + K_2O$), has proven problematic. By plotting wt % TiO_2 vs. P_2O_5 obtained from XRF analyses and four-acid digest ICP-MS data, two distinct population clusters appear. By comparison with least-altered intrusive rock analyses from the Fairbanks district, the igneous units were originally granite and tonalite. Because there is no gradational transition through an intermediate granodiorite unit, they were most likely derived from two separate magmatic bodies rather than *in-situ* fractionation from a single parent. Tonalite is concentrated along the northern and eastern margins of the stock with granite composing the rest of the body. Tonalite xenoliths in granite and granite dikes intruding tonalite prove that tonalite is the older unit.

Investigations of hydrothermal alteration (based on chemical analyses, X-ray diffraction, and thin section examination) show albitic and advanced argillic (kaolinite-quartz) alteration are the dominant styles with sericite common throughout. Advanced argillic is a low temperature (<300°C) low pH alteration style that has not been previously identified in intrusion related gold deposits (IRGDs) in interior Alaska. Albitic alteration probably resulted from higher temperature, more neutral pH fluids.

Gold investigations show that gold occurs as coarse-grained Au°, aurostibite, and maldonite in quartz + sulfide veins; fine-grained Au° in the oxide zone; and in many forms in disseminated sulfide. These forms include Au° inclusions in pyrite and arsenopyrite; solid-solution Au within compositionally zoned arsenopyrite; and as Au° nanoparticles in pyrite and probably arsenopyrite. Using UAF's JEOL JXA-8530F microprobe, I found that solid-solution gold occurs only in arsenopyrite with strong compositional zoning. Such grains are always small (< 0.2 mm) and commonly have low As cores; gold-bearing mantles with moderate % As; and higher As rims. In contrast, compositionally homogenous arsenopyrite does not contain detectable solid-solution gold. Pyrite is commonly arsenian and carries dissolved gold (if any) near detection limits. Gold mineralization has not been tied to any one lithology or alteration style; however, gold does seem to correlate with abrupt changes in alteration, especially between sericite + albite and kaolinite + sericite alteration. Gold-bearing, zoned arsenopyrite is predominantly associated with advanced argillic alteration and apparently represents a rapid growth, disequilibrium phenomenon.

Table of Contents

List of Figures

List of Tables

List of Appendices

1 Chapter 1 Introduction

1.1 Introduction to Dolphin Deposit

The Dolphin deposit is an intrusion related gold deposit (IRGD) hosted by the Dolphin pluton and located in the southern part of the Livengood A-1 quadrangle in the Fairbanks Mining District. The pluton is located approximately 30 kilometers north of Fairbanks and 9 km northwest of Ft. Knox Gold Mine (Figure 1-2). Historic lode and placer mining has taken place in the immediate vicinity of the pluton and the pluton is crudely depicted on the geologic map of Hill (1933); however, significant mineralization in the pluton itself was not discovered until the mid-1990's. The Dolphin pluton is one of hundreds of mid-Cretaceous composite plutons that intrude metamorphic rocks of the Yukon Tanana Terrain (YTT), only some of which are gold-bearing.

Figure 1-1: Alaska image showing location of Dolophin area image, modified from Abrams et al.(2016).

Figure 1-2: Image showing location of Dolphin pluton and nearby features, modified from Google Earth.

There are similarities between Dolphin and other IRGDs of interior Alaska as well as poorly understood differences. Understanding of differences and similarities is limited due to limited knowledge of the Dolphin deposit as well as of the others. While Dolphin is only 9 km from the Fort Knox deposit in a pluton of the same age, it contains considerably more sulfide minerals (typically > 10% vs. < 1% for Fort Knox) and little obvious Bi or Mo minerals.

1.2 Introduction to Intrusion-Related Gold Deposits

Interior Alaska is home to a suite of mid-Cretaceous to early Tertiary IRGDs. These deposits are hosted primarily in intrusions or in the immediate wall rock and comprise a distinct class of magmatic-hydrothermal systems (Lang and Baker, 2001). McCoy et al. (1997) argue that there is a magmatic source for some or much of the fluids and metals in interior Alaska intrusion related gold deposits and that they

are associated with subduction related, I-type, ilmenite series plutons. Geochemically, they are enriched in Bi± Te ± As.

1.2.1 Mineralization

Two major styles of mineralization have been identified in IRG deposits: (1) a common style with high % sulfide (e.g., Livengood, Donlin Creek, Vinesale Mountain), and (2) a less common style with low % sulfide (e.g., Fort Knox, Shotgun). The former (high-sulfide type) contains pyrite and arsenopyrite with gold as microscopic to submicroscopic inclusions and as solid solution in sulfides. Gold occurs as fine-grained inclusions and solid solution in arsenopyrite at Livengood and as solid-solution in arsenopyrite and lesser pyrite (< 1 ppm) at Donlin (Goldfarb et al., 2004; Francis, 2008; Kunter et al., 2013). In contrast, gold in low-sulfide deposits is present as native gold and Bi-Au intergrowths; pyrite and arsenopyrite are both rare and rarely host gold, as at the Fort Knox deposit (Bakke, 1995). Pogo is broadly similar to Fort Knox; it contains more sulfide than does Fort Knox but much or most of the gold is in quartz outside of the sulfide minerals.

1.2.2 Alteration

Little has been published concerning alteration and its relation to gold in IRGDs. At Fort Knox, early veins containing K-feldspar and with K-feldspar rims are cut by veins and shear zones with muscovite-calcite-chlorite assemblages. At Donlin, alteration associated with Au mineralization is primarily argillic, composed of illite with minor dickite and smectite (Francis, 2008). Three principal stages of alteration are described at Livengood (Kunter, et al., 2013) as secondary biotite, albite and muscovite (sericite). Biotite is recognized as the oldest alteration style, followed by albite, then sericite. Carbonate (largely ankerite) was introduced with and subsequent to alteration. Dating of sericite alteration indicates mineralization and alteration were contemporaneous with dike emplacement (Kunter et al., 2013). Shotgun contains widespread and abundant albitic alteration with intense sericitic alteration overlapping the upper zones (Rombach and Newberry, 2001; Van Wyck and Armitage, 2013).

1.3 Geologic Setting

1.3.1 Regional Geology - Interior Alaska and the Yukon-Tanana Terrane

The Dolphin Pluton is located in the west-central part of the Yukon Tanana Terrane (YTT), an arcuate belt extending from the southeastern Yukon Territory into interior Alaska (Figure 1-3). The YTT is bounded by the Denali fault to the south and is partly bounded and partly offset by the Tintina fault in the north.

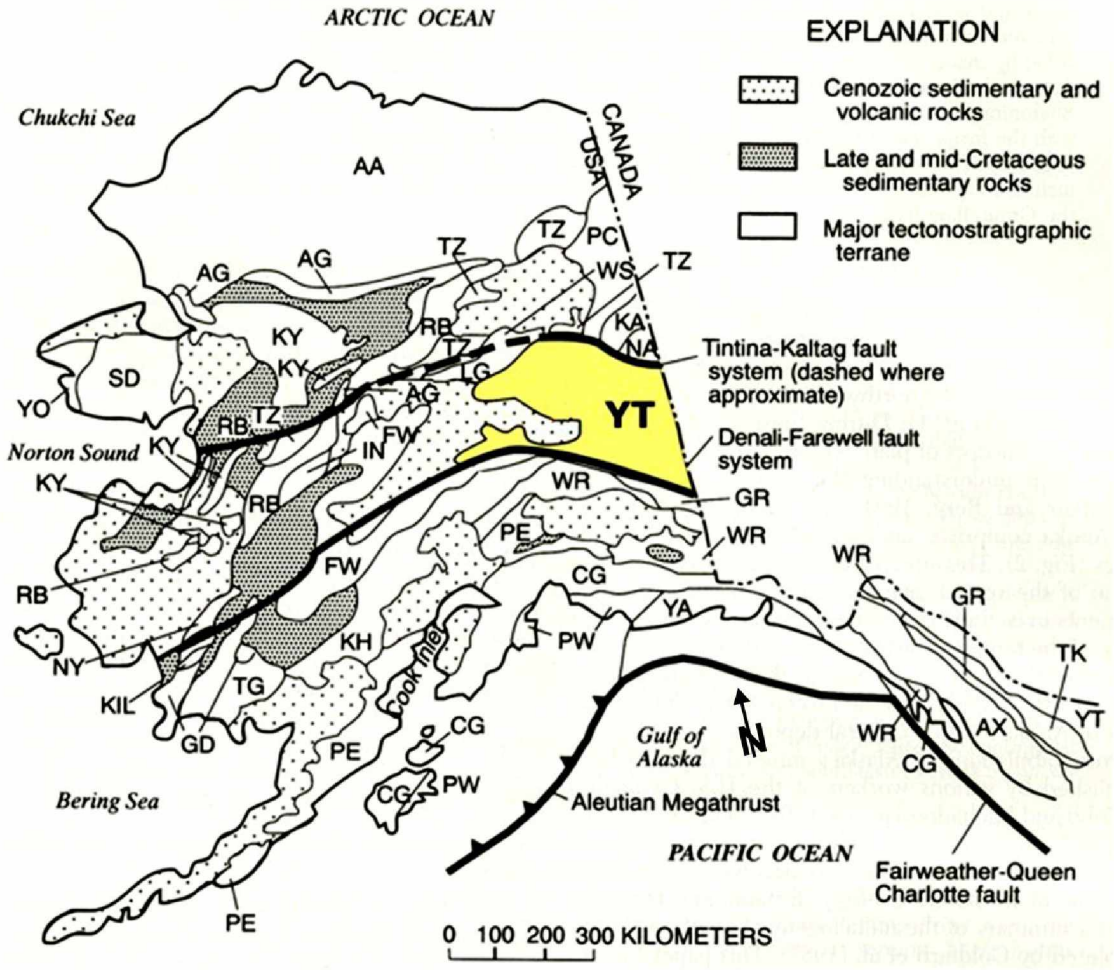

Figure 1-3: Map of Alaska showing the extent of the Yukon-Tanana Terrain (YT), modified from Goldfarb, 1997.

The YTT consists of metasedimentary, metavolcanic, and metaplutonic rocks of Proterozoic to Upper Paleozoic ages that have undergone several episodes of deformation and metamorphism. These regionally metamorphosed rocks have been subdivided into several sub-terranes based on ages of last metamorphism and metamorphic P-T paths (Dusel-Bacon et al., 2002). In the immediate Fairbanks area, the predominant unit is the Fairbanks Schist. Some workers break out the eclogite facies rocks just north of Dolphin (Figure 1-4) as a different terrane, while others lump it with YTT.

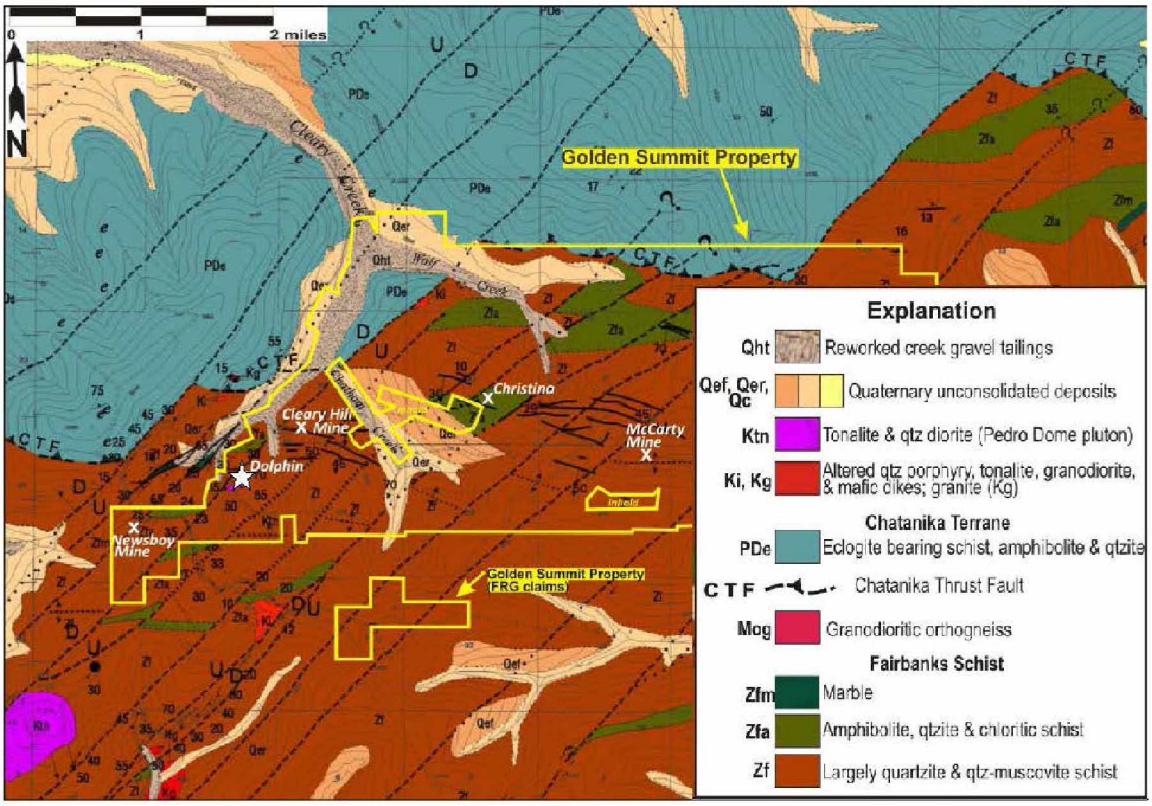

Figure 1-4: Local geology of the Golden Summit property. Geology from Newberry et al., 1996; modified from Adams and Giroux, 2011.

Three distinct clusters of igneous rock intrude the metamorphic rocks of the YTT (Abrams and Giroux, 2013): 215-188 Ma (Late Triassic – Early Jurassic), 110-85 Ma (Mid to Late Cretaceous), and 70-50 Ma (Late Cretaceous – Eocene). In the immediate Fairbanks area, the 110-85 Ma group is further divided into quartz-poor 110 Ma plutons and quartz-rich 88-94 Ma intrusions (Newberry, 1996); Dolphin belongs to the latter. Mortenson et al. (2000) identifies a 95-90 Ma suite of granite, granodiorite, quartz-monzonite and diorite plutons referred to as the "Tombstone" suite.

1.3.2 Project Geology

The Dolphin Pluton is located in the southern part of the Livengood A-1 quadrangle in the Fairbanks Mining District at latitude 65.061° N, longitude -147.117° W. The pluton is located on Freegold Ventures Ltd. Golden Summit property. Several historic gold mines are located on the property (Figure 1-4) and Kinross Gold's open pit Ft. Knox gold mine is located 9 km to the southeast (Figure 1-2). Three styles of gold occurrences have been identified on the property: 1) intrusive-hosted sulfide-quartz stockwork veins and veinlets (such as the Dolphin gold deposit), 2) auriferous sulfide-quartz veins (exploited by historic underground mines), and 3) low-sulfide gold-bearing veins and veinlets (Abrams and Giroux, 2013). The Dolphin gold deposit is hosted in the Dolphin stock, which is the only known

intrusive body on the Golden Summit property. The Dolphin stock is approximately the same age as the nearby Fort Knox pluton, which hosts the Fort Knox gold deposit (Abrams and Giroux, 2013).

Mapping of extensive trenches in the Cleary Hill mine area suggests that numerous low-angle structures are present in the Golden Summit project area, some of which are mineralized. The bulk of veins are WNW-striking, but NE-striking faults with left-lateral motion cut veins and are locally veins (Robinson et al., 1990). Post-mineral north-south faults with normal motion clearly cut veins (Hill, 1933). Airborne magnetic data in this part of the Fairbanks District indicate the presence of district scale northeast trending faults which appear to postdate N60-80E fold axes (DGGS, 1995). Gold mineralization in the general Dolphin area postdates regional and district scale folding and is contemporaneous with or slightly younger than district-scale northeast trending faults and mid-Cretaceous plutons (Abrams et al., 2016).

1.4 Previous work

1.4.1 Introduction

Since the turn of the twentieth century, placer and lode gold operations have extracted gold in the Golden Summit area. Of the 9.5+ million ounces (Moz) of placer gold mined in the Fairbanks Mining District, 6.75 Moz were recovered from streams that drain the Golden Summit area (Freeman, 1991). Prior to World War II, 537,021 ounces of lode gold were extracted from high grade quartz veins near the Dolphin deposit including the Cleary Hill Mine, the largest historic underground gold producer in the area (281,000 oz; Adams and Giroux, 2011).

Modern surface exploration on the property by a series of companies began in 1969, and major amounts of trenching and drilling have been completed on numerous targets. In 1991 Freegold Ventures Ltd. acquired the property and since then has conducted extensive geologic mapping, soil sampling, trenching, rock sampling, geophysical surveys and core, reverse circulation, and rotary air blast drilling on the project (Abrams and Giroux, 2013)

1.4.2 Dolphin Deposit

Gold mineralization was discovered in the Dolphin pluton in 1995 during reverse-circulation drilling which was being conducted to follow up on anomalous Au in soil samples. In 1998, a single diamond-core drill hole was drilled in the northern margin of the pluton followed by limited drilling in 2004, and more extensive drilling in 2011-2013. In total, 35 diamond core drill holes have been drilled into the pluton. Au 30g fire assay-AAS with 33 element four-acid digest ICP-AES geochemical assays were conducted on drill core which was sawed in half until the middle of drill hole GSDC1217, after

which the halved core was assayed for gold only. All core was logged, sawed, sampled, photographed and stored by Avalon Development Corporation at their warehouse in Fox, Alaska.

A 2016 Preliminary Economic Assessment (Abrams, et al., 2016) contains a resource estimate of the Dolphin deposit. A conceptual open pit model was created and only blocks which fall in the pit were included in the estimate (Table 1-1 and Table 1-2). While the conceptual pit was designed to exploit the intrusive rock of the pluton, it is not apparent if, or how much, adjacent metamorphic rock is included in the pit and resource estimate.

Table 1-1: Dolphin zone indicated resource within conceptual pit (Abrams et al., 2016)

Au Cut-off (g/t)	Tonnes> Cut-off (tonnes)	Grade > Cut-off		
		Au (g/t)	Contained	
			kg Au	ozs Au
0.20	82,650,000	0.58	47,610	1,531,000
0.25	71,140,000	0.63	45,030	1,448,000
0.30	**61,460,000**	**0.69**	**42,410**	**1,363,000**
0.35	53,460,000	0.74	39,770	1,279,000
0.40	46,690,000	0.80	37,260	1,198,000

Table 1-2: Dolphin zone inferred resource within conceptual pit (Abrams et al., 2016)

Au Cut-off (g/t)	Tonnes> Cut-off (tonnes)	Grade > Cut-off		
		Au (g/t)	Contained	
			kg Au	ozs Au
0.20	95,920,000	0.58	55,350	1,779,000
0.25	82,910,000	0.63	52,400	1,685,000
0.30	**71,500,000**	**0.69**	**49,260**	**1,584,000**
0.35	61,640,000	0.75	46,050	1,480,000
0.40	52,690,000	0.81	42,730	1,374,000

1.4.2.1 Gold Mineralogy and occurrences

Based on two samples, McCoy and Olson (1997) reported early, higher temperature arsenopyrite containing Au with Bi inclusions and lower temperature arsenopyrite associated with base metal sulfides and lacking significant Au grade. Microprobe analysis of the high gold sample revealed gold occurred as >5-micron inclusions with 1) wormy intergrowths of Bi and Au 2) a Bi-S mineral and 3) a Bi-Te-S

mineral. Abrams and Giroux (2013) indicate cyanide bottle roll gold recovery of 35-75% for unoxidized gold-bearing samples, which indicates that some of the gold is present in sulfide at too small grain size to be extracted by cyanide solution. Di Prisco (2013) analyzed 26 drill core samples collected from mineralized intervals from 9 drill holes at Dolphin to identify the nature and characteristics of gold-bearing minerals. He found gold grains in 16 of the 26 samples. Di Prisco (2013) noted that gold is predominantly associated with arsenopyrite (typically as inclusions) and most gold grains had diameters of <8 microns. Besides native gold, Di Prisco (2013) identified one grain of aurostibite ($AuSb_2$). Di Prisco (2013) did not report any Bi minerals and suggested that some gold must occur as nanoparticles or solid solution in sulfide.

1.4.2.2 Rock types and alteration

Abrams and Giroux (2013) identified five intrusive phases in the Dolphin pluton. These are 1) fine- to medium-grained, equigranular to weakly porphyritic biotite granodiorite, 2) fine- to medium grained, equigranular to weakly porphyritic hornblende-biotite tonalite, 3) fine-grained biotite granite porphyry, 4) fine-grained biotite rhyolite to rhyodacite porphyry, and 5) fine-grained, chlorite-altered mafic dikes. Granodiorite and tonalite make up the majority of the pluton with granite, rhyolite-rhyodacite and mafic phases occurring largely as dikes. Dikes of granodiorite cutting tonalite have been observed in core, and altered granitic dikes cut both. My experience logging core was that rock type distinctions were frequently problematic. Intrusive rocks have undergone extensive hydrothermal alteration which makes identification in hand sample difficult, and the intermittent drilling of the pluton over the years has resulted in frequent changes in core logging geologists who did not always log intrusive rocks consistently.

That Abrams and Giroux (2013) use the terms "altered" and "unaltered" granodiorite and tonalite, suggest multiple phases of intrusion and hydrothermal alteration. No basis, however, is given for the various rock types identified. Previous reports (Abrams and Giroux, 2013; Adams and Giroux, 2011) suggest several types of alteration overprint the Dolphin intrusive rocks. The most common alteration types identified are silicification, sericitization and albitization with carbonate alteration (calcite or less commonly dolomite or iron carbonate) found locally. Alteration can range from weak to intense and Abrams and Giroux (2013) consider alteration generally indicative of higher gold values; particularly when strong silicification and sericitization are present. Strong sericite alteration is characteristic of shear zones, but weak to moderate sericite alteration is ubiquitous throughout the deposit. Albitic alteration occurs as patchy alteration of groundmass plagioclase, and as megascopic envelopes adjacent to early stage quartz veins which has been interpreted to be evidence of an earlier higher temperature event compared to sericite shear zone alteration events. Detailed core logging (as reported in Abrams and

Giroux, 2013) suggests a paragenetic sequence of alteration and mineralization events at the Dolphin deposit starting with early sericite alteration and disseminated arsenopyrite ± pyrite through sheeted auriferous quartz-sulfide veining to coarse grained pyrite dominated ± base metal sulfide veining (no quartz associated).

1.5 Objectives

The objectives of this research project were to increase understanding of the lithology, alteration and mineralizing history of the Dolphin intrusion-related gold deposit and to attempt to relate gold grade to any aspect of the deposit. Based on my preliminary observations, igneous units and distribution of the pluton, alteration styles and distribution, association of intrusive units and alteration to gold mineralization (if any), and style of gold mineralization have not been sufficiently described. In conducting my research, I have identified two intrusive units that make up the pluton, identified dominant alteration styles and created 3D models of petrology and dominant alteration, and identified styles of gold mineralization.

2 Lithology and Alteration

2.1 Introduction

The lithology and alteration history of the Dolphin pluton and associations with gold mineralization are poorly understood. Previously, as many as five different intrusive units have been identified at Dolphin and extensive hydrothermal alteration has made identification in hand sample difficult if not impossible in many instances. Numerous core logging geologists and core logging procedures have been used throughout the core drilling process which, despite best efforts, has resulted in inconsistent lithology and alteration assignments, complicating the pluton and obscuring any associations of rock units or alteration with gold grade. Through geochemical analysis and transmitted light microscopy I have identified two intrusive units at Dolphin: granite and tonalite. I also identified albitic, sericitic, advanced argillic, and calcite alteration in intrusive rock. With this data I was able to create three-dimensional models and cross-sections of the pluton.

2.2 Sample creation and methods

Physical samples for this study were collected from diamond core drill samples (see section 1.4.2) of intrusive rocks of the Dolphin pluton. Sample intervals were selected based on gold grade, logged lithology, alteration, and sulfide content. Samples were cut into slabs approximately one centimeter thick parallel with the previous cut surface. I created 195 polished pucks for XRF analysis following the routine outlined in Deal (2012) from these samples. 50 pressed powder pellets were created following procedures in Deal (2012) from drill core assay pulps. 51 polished thin sections were analyzed by reflected and transmitted light petrography and electron probe microanalysis (EPMA). All EPMA analyses were completed with a JEOL JXA-8530F electron microprobe located in the Advanced Instrument Laboratory at the University of Alaska Fairbanks. Four-acid digest ICP-MS geochemical assays were used to determine lithology and alteration of intrusive rock at Dolphin. Assay procedures and quality control measures are outlined in Abrams et al. (2016).

2.3 Rock types

2.3.1 Introduction

Prior to this study, as many as 6 different intrusive rock units had been reported to make up the Dolphin pluton. All intrusive rocks have undergone some extent of hydrothermal alteration, in many areas pervasively so. Due to this alteration, it has proven difficult to identify intrusive rocks in hand sample or thin section. Because all of the plutonic rocks (even those logged as ‘unaltered’) contain visible calcite and (or) muscovite (and hence, are really altered), it was necessary both to find some way to identify the original rock types and to assess chemical alteration.

2.3.2 Methods and Results

Blum (1983) gives extensive chemical analyses for unaltered mid-Cretaceous plutonic rocks from throughout the Fairbanks district and his compilation is the primary basis for comparison to Dolphin. Additional analyses are given in Burns et al. (1991) and Newberry (1996). Elements that are resistant to changes during chemical alteration show systematic variation with igneous rock type. These elements are part of the four-acid digest package employed on a dozen Dolphin drill holes and are critical for sorting out rock types. The two that best fit these criteria are Ti and P, usually expressed in chemical analyses as wt % TiO_2 and % P_2O_5. A plot of these two elements for rocks identified by mineral staining and point counting (Figure 2-1, left) shows a systematic increase in both the most felsic (granite) to the least felsic (tonalite).

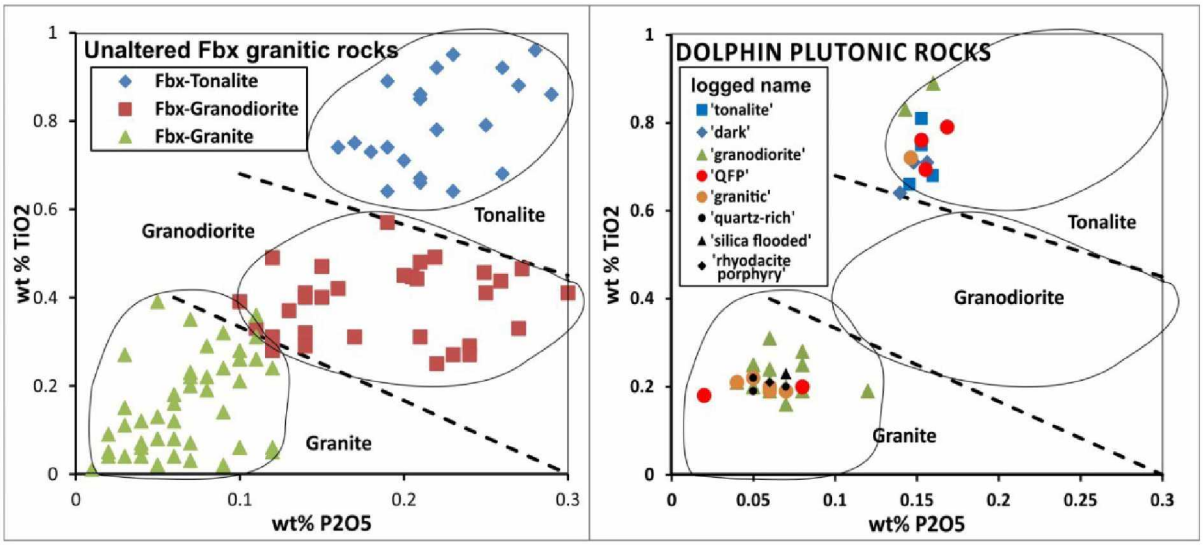

Figure 2-1: P_2O_5 vs. TiO_2 for unaltered plutonic rocks of the Fairbanks district (left, data from Blum, 1983; Burns et al., 1991; and Newberry, 1996) and for 45 Dolphin slabs (right, analyzed by XRF). Dolphin rocks appear to have original compositions of either tonalite or of granite, with nothing in-between the two.

Employing the boundaries between granite, granodiorite, and tonalite defined using data from Blum (1983), Burns et al. (1991), and Newberry (1996), initial lithology investigations began with XRF analyses of 45 polished puck slabs, the results of which suggest that the bulk of the plutonic rocks at Dolphin, regardless of how originally logged, are either granite or tonalite (Figure 2-1, right). Importantly, there is a significant compositional gap between the two major intrusion types, which makes the two difficult to directly relate to each other. Further, rocks identified as 'quartz feldspar porphyry' have compositions of both granite and tonalite, apparently indicating two different types of porphyry (dikes?) present.

I identified approximately 3,000 four-acid digest ICP-MS analyses in 20 Dolphin drill holes as likely from plutonic rock from core logs. For these analyses I converted the concentrations of elements into oxides (e.g., ppm Ti to wt% TiO_2) and then plotted P_2O_5 vs. TiO_2 by logged rock type (Figure 2-2).

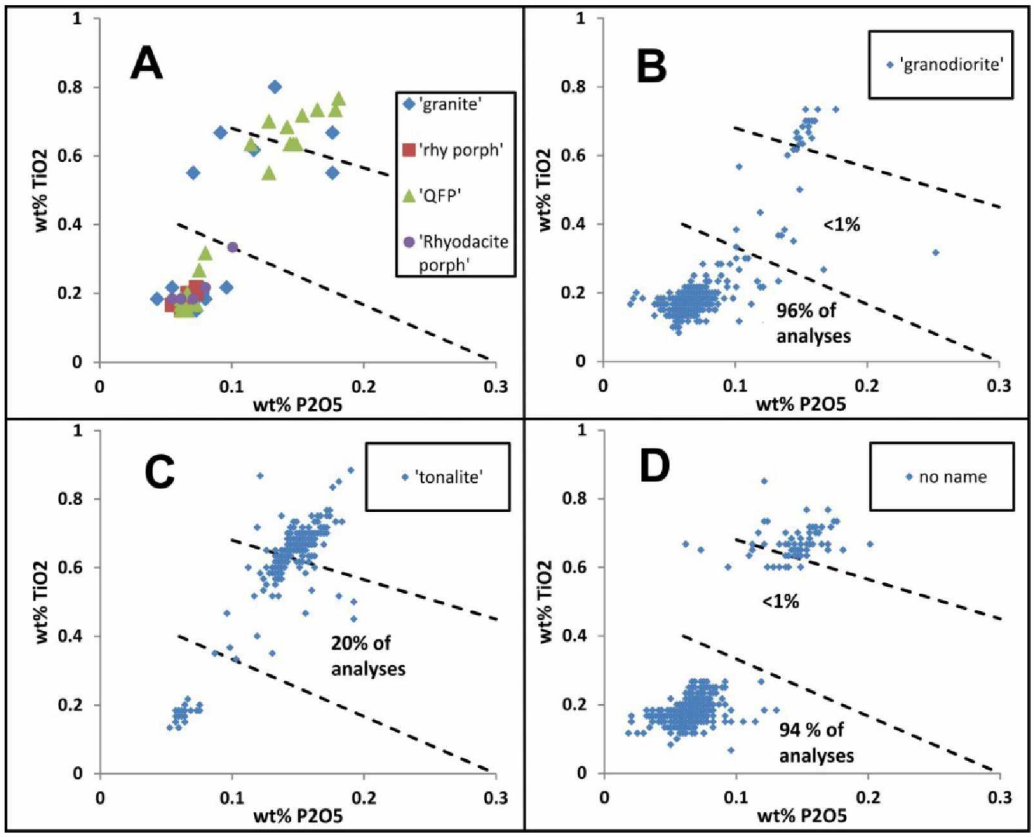

Figure 2-2: P_2O_5 vs. TiO_2 for Dolphin four-acid digest analyses of likely plutonic rocks. A = data for rocks logged as granite, rhyolite porphyry, QFP (quartz-feldspar porphyry), or rhyodacite porphyry. B = data for rocks logged as granodiorite. C = data for rocks logged as tonalite, D = no log, rocks are probably plutonic. Rock type fields (black dashed) from Figure 2-1.

As with the slab XRF analyses, the vast bulk of the four-acid digest concentrations fall into the 'granite' or 'tonalite' fields as defined by the Blum (1983), Burns et al. (1991), and Newberry (1996) data. Rocks identified as 'rhyolite porphyry' and 'rhyodacite porphyry' are not readily distinguished; all their compositions fall into the granite field (Figure 2-2A). Rocks logged as 'quartz feldspar porphyry' mostly fall into either the granite or granodiorite fields. Of the rocks logged as granodiorite (Figure 2-2B) 96% of the analyses fall in a small cluster centered on 0.07% P_2O_5 and 0.18% TiO_2 (i.e., 'granite') < 1% of the analyses fall into the 'granodiorite' field and 3% plot as tonalite. Of the rocks logged as tonalite (Figure 2-2C), approximately 20% fall in the 'granodiorite' field, but the vast bulk plot in a low-TiO_2 or a high-TiO_2 cluster. I checked core photographs or inspected drill core to establish that most of the rocks with 'granodiorite' Ti-P concentrations represent mixed intervals of tonalite and granite that were lumped

together in a single 5-foot assay interval. This occurred due to sampling over lithology contacts or in samples of granite that contain tonalite xenoliths.

Based on this use of the four-acid digest compositional data, the relative abundance of tonalite in each drill hole with compositional data can be calculated. Tonalite identification based on logging is more tenuous, given that the logged name frequently doesn't match the composition (Figure 2-2C), but the bulk of rocks with analyses that were logged as tonalite do have tonalitic (or mixed) composition.

A plan map showing relative abundance of tonalite in each of 25 drill holes (Figure 2-3) shows that the central part of the pluton is completely devoid of tonalite and that tonalite is most abundant in the northeastern margin of the body (also see section 2.5).

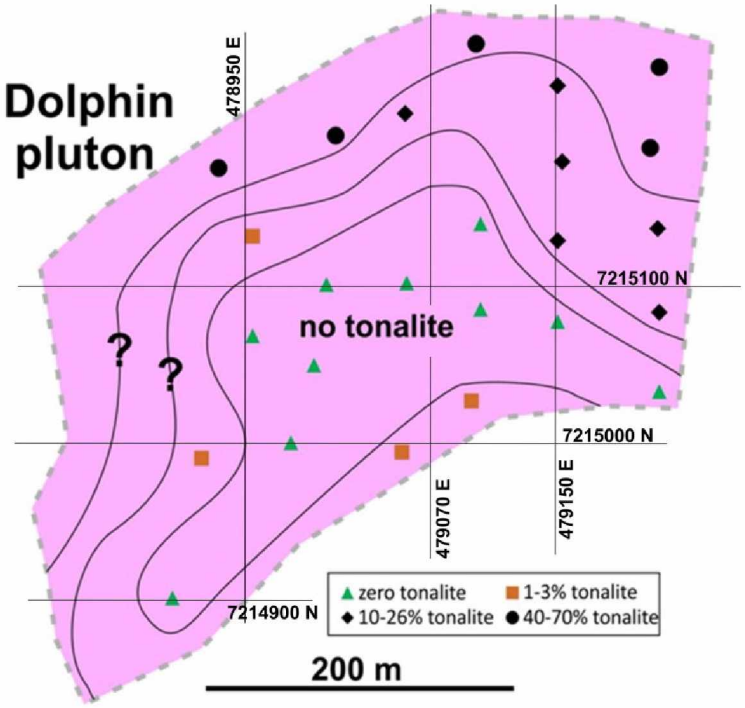

Figure 2-3: Map showing relative abundance of tonalite in the Dolphin pluton based on Ti-P assignments (most holes) or on drill logs (5 holes on the far eastern edge of the pluton). The central part of the pluton is entirely granite. UTM lines shown for reference; the three N-S lines correspond to leapfrog cross-section lines (see ahead).

The higher abundance of tonalite towards the margins, and especially the northern and northeastern margin of the Dolphin pluton (Figure 2-3), might suggest that the tonalite is an early chilled mafic margin on the pluton. Evidence that this is false is supported by the lack of compositional gradation between tonalite (high-TiO_2) and granite (low-TiO_2); plutonic rocks with intermediate TiO_2 contents are essentially missing. Further, granite-tonalite contact patterns are extremely complex. Drill hole 1132 for example (Figure 2-4), shows lithology switches back-and-forth between granite and tonalite after the first

580 feet, with a drill thickness of each from 1 foot to 180 feet. However, tonalite xenoliths are found in granite and granite dikes that intrude tonalite, which shows that tonalite is older than granite. How much older is not known.

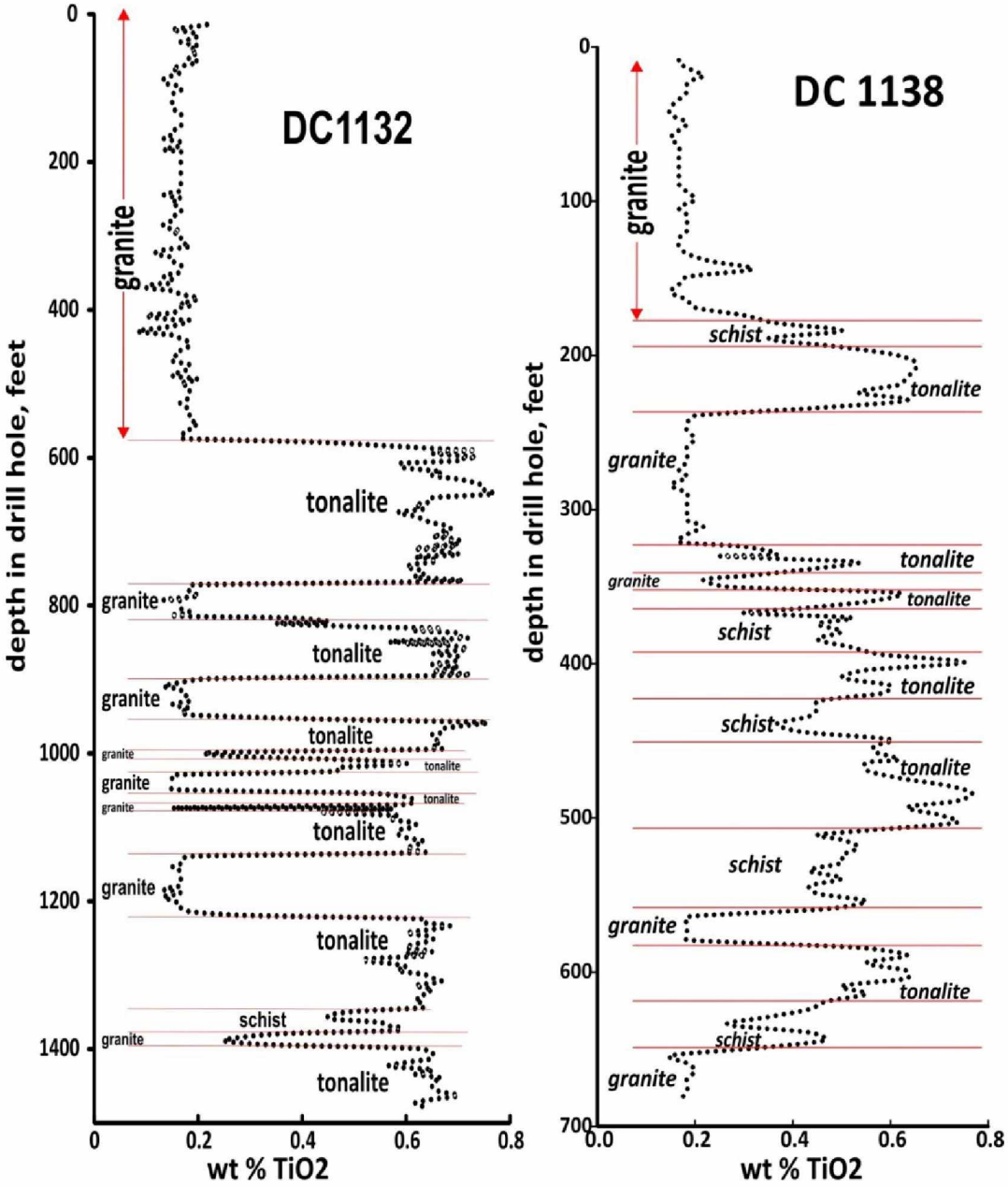

Figure 2-4: Weight % TiO_2 (dotted black) versus depth for drill hole 1132 (left) and 1138 (right). The rapid changes in TiO_2 with depth indicate sharp contacts between granite (low-Ti), tonalite (high-Ti), and schist (medium-Ti).

Unfortunately, chemical analyses alone are not sufficient to distinguish plutonic from metamorphic rock at Dolphin, which makes assigning rock types to those holes problematic. However, for approximately 10,000 four-acid digest analyses of likely metamorphic rocks (drill holes well outside of the Dolphin pluton), only about 300 (3%) fall into the fields defined by the bulk of the granite and tonalite

analyses (Figure 2-5). Because both plutonic and metamorphic rocks are variably altered, it is likely that all of the other elements available vary so much (e.g., Na_2O from ~0 to ~8% in Dolphin granite) as to not be useful for discrimination between plutonic and metamorphic rock. Especially where core photographs suggest non-igneous rocks, intermediate TiO_2 and P_2O_5 contents indicate metamorphic rocks are likely. That is, metamorphic rocks cannot be definitively identified by their compositions, but commonly can be identified.

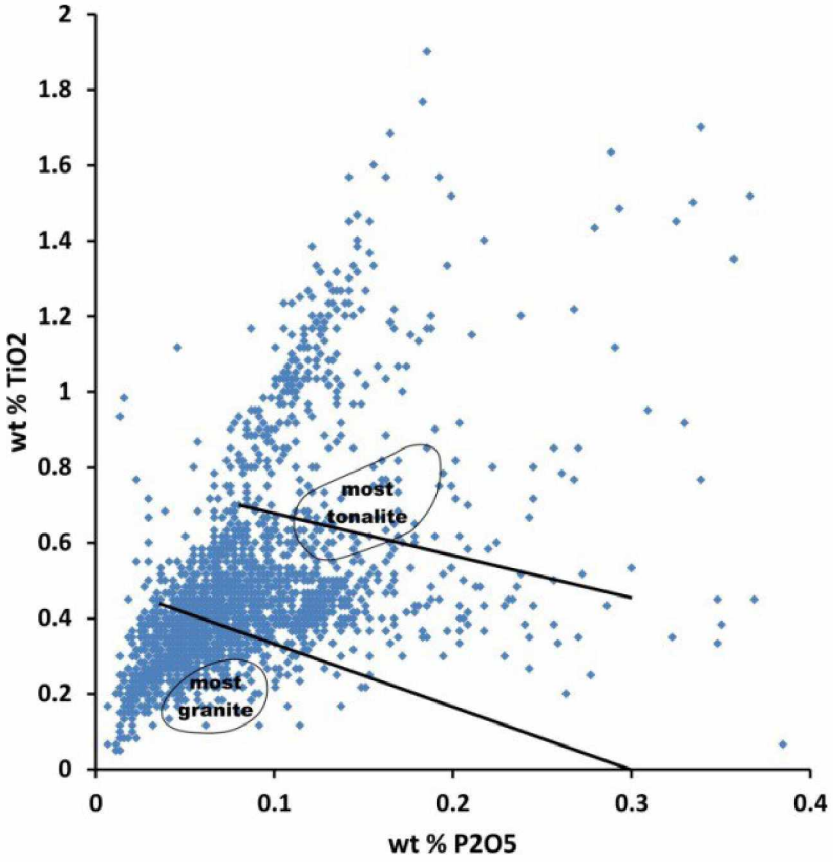

Figure 2-5: Weight % P_2O_5 vs. TiO_2 for ~ 12,000 four-acid digest drill core intercepts from likely metamorphic rocks in the general vicinity of the Dolphin pluton. The fields circled outline the compositional fields for the bulk of the Dolphin granite and tonalite.

I needed to clearly distinguish between the two phases (tonalite and granite) to create an accurate three-dimensional model of the pluton (section 2.5). As indicated, the drill logs were not always reliable, especially in areas of intense alteration and (or) shearing. To attack this problem, I first identified Dolphin drill core intervals of entirely granitic rock by examining core logs and core photos for each drill hole in the pluton. In many instances, sample intervals crossed contacts between intrusive and metamorphic rocks, which commonly occurred at or beyond the margin of the pluton (e.g., dikes in the country rock).

For these samples I was not able to use geochemistry to identify the intrusive units as the contained metamorphic rocks skewed the data.

Once sample intervals containing only intrusive units were identified, the P_2O_5 vs TiO_2 values were plotted for each drill hole that contained four-acid ICP-MS assay data. Based on the discrimination shown on Figure 2-1, I assigned points that plotted above $wt\%\ TiO_2 = -0.7667 * wt\%\ P_2O_5 + 0.63$ as tonalite and points below $wt\%\ TiO_2 = -0.8333 * wt\%\ P_2O_5 + 0.4$ as granite (Figure 2-6). In instances where the point fell between these lines, core logs and photos were investigated to determine the cause. The most common reason is the sample interval contained both tonalite and granite. This happens where the sample interval crossed a lithologic contact, but also where granite contains tonalite xenoliths. The other common causes are schist clasts mixed with intrusive rocks, fault zones, and highly altered zones (as Ti and P are not perfectly immobile). In only four cases ('+' symbol, Figure 2-6), I could not determine why the point plotted outside of the tonalite or granite fields.

I used 3,424 four-acid digest assays derived largely from intrusive units. Based on the approach described in this section, 3,023 assays are from granite, 330 are from tonalite, and 71 are mixed rock types or otherwise unassignable (Figure 2-6). Of the 71 unassigned, 3 are from gouge in fault zones, 3 are from an area of intense alteration, 15 are granite-schist mixtures, 33 are granite-tonalite mixtures, 6 are a mixture of granite-tonalite-schist in a fault zone, and 7 are tonalite-schist mixtures. I also analyzed 50 pressed pellets created from drill core pulps from holes GSDC1301, GSDC1302, GSDC1304, and GSDC1305, as none of these drill holes have assay data outside of gold grade. In all cases, these analyses plotted in the fields of granite or tonalite (Figure 2-6).

For drill holes that do not have compositional data, I assigned lithology to intervals based on core logs, comparison to lithology of surrounding holes that do have assay data, and core photos. A lithology was then assigned to each interval based on my best determination of which intrusive unit it belonged to. This lithologic assignment was then used to create a 3D model of the pluton (see ahead).

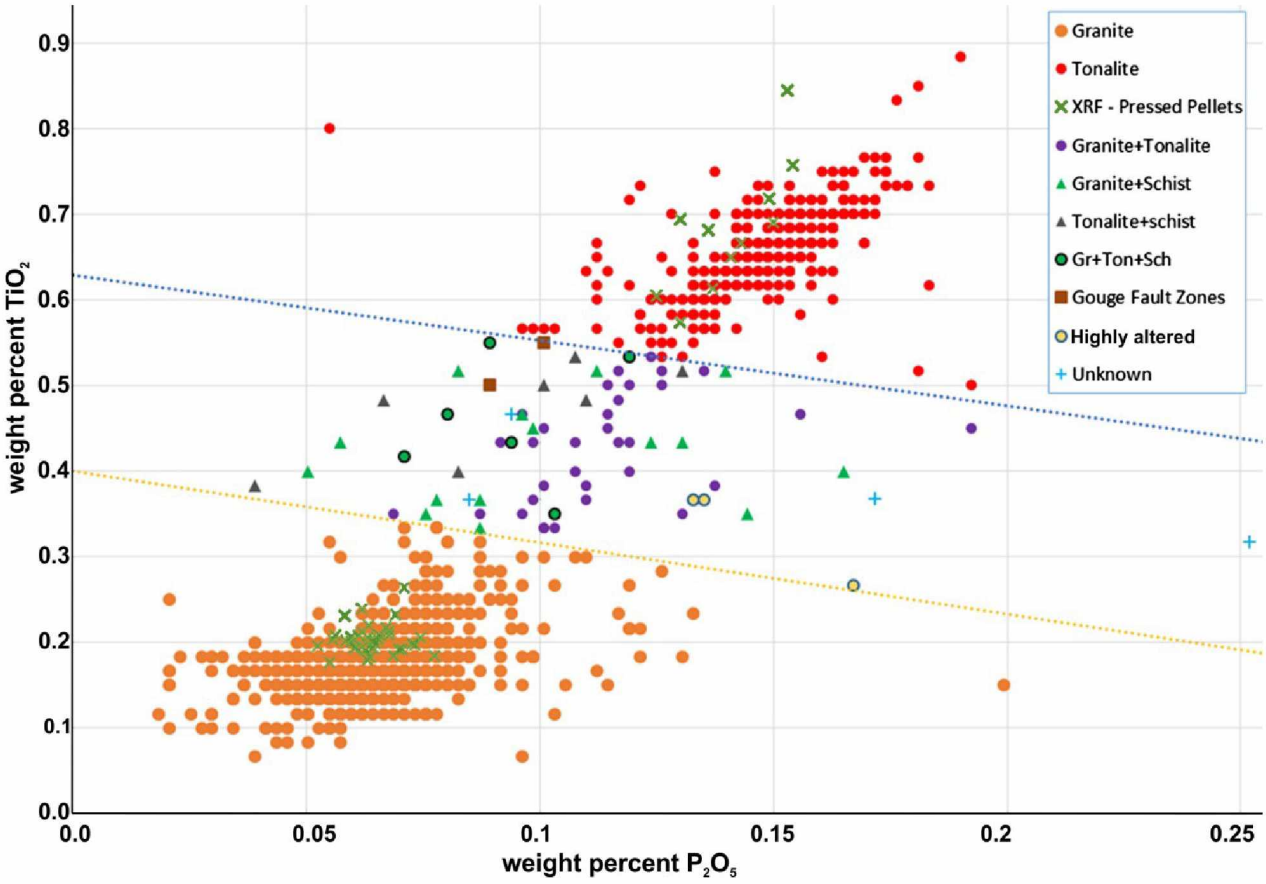

Figure 2-6 - Plot showing TiO_2 vs P_2O_5 values for 3,425 4-acid digest ICP-MS assay samples and 50 XRF pressed powder pellets from (mostly) Dolphin intrusive rocks. Abbreviations: Gr = granite, Ton = tonalite, Sch = schist.

2.4 Intrusive Units

2.4.1 Granite

Granite makes up the majority of the Dolphin stock. It is the younger of the two intrusive units as is evident by tonalite xenoliths in granite. Least-altered granite is equigranular to weakly porphyritic, and fine to medium grained (Figure 2-7). Typical granite contains approximately 10% biotite, which is partly altered to muscovite + chlorite + rutile in even the least altered samples. The feldspar always displays some alteration to sericite and plagioclase is commonly mantled by a thick to thin zone of albite. Alkali feldspar is typically intergrown with albite. Granite with porphyry textures (feldspar + quartz phenocrysts 1-3 mm in diameter in a very fine-grained invariably altered matrix) is common in granite dikes, which cut all units, including equigranular granite.

Figure 2-7: Typical least-altered granite from Dolphin drill core, showing sub-equigranular texture.

2.4.2 Tonalite

Tonalite is the older intrusive unit and makes up a small part of the Dolphin stock. It is primarily located in the northeast portion of the pluton and rarely on the western and southern margins (Figure 2-3). Tonalite is biotite rich, equigranular to weakly porphyritic, and fine to medium grained (Figure 2-8A). Least-altered tonalite contains 5% 1-2 mm hornblende phenocrysts (completely surrounded by biotite, hence, invisible in hand specimen), 50-60% 1-3 mm strongly zoned plagioclase crystals (Figure 2-8B), 10-15% 0.2-0.5 mm subhedral biotite grains, and 20-30% 0.5 mm, interstitial quartz. Even the least-altered samples contain some alteration of plagioclase and especially of hornblende.

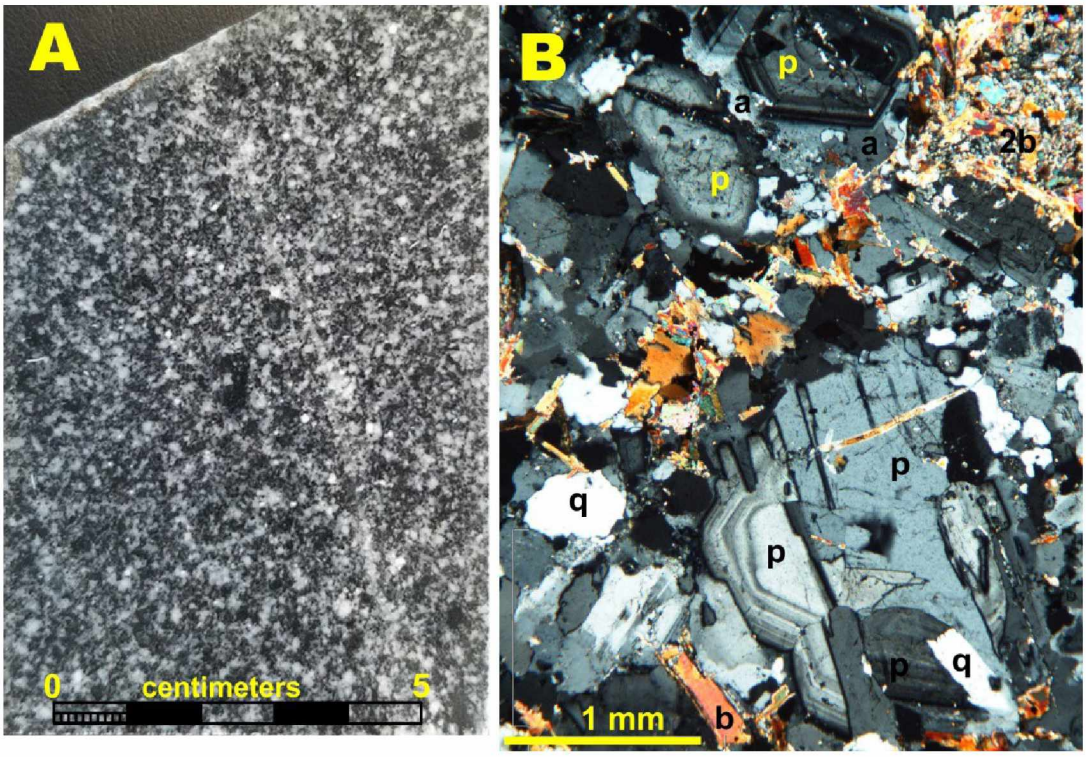

Figure 2-8: Typical least-altered tonalite (A) in hand specimen, from Dolphin drill core, showing sub-equigranular texture and thin albite veinlet and (B) in thin section (plane polarized light) showing 2-3 mm plagioclase grains with extensive oscillatory zoning (p) and commonly a mantle of albite (a) with 0.2-0.5 mm grains of biotite and quartz and a clot of secondary biotite (2b) probably as a replacement of hornblende.

2.4.3 Porphyry

Intrusive rocks that have been logged as "porphyry" at Dolphin have been shown through Ti-P analysis (e.g., Figure 2-2A) to have either granite or tonalite composition. There is nothing geochemically different from these "porphyries" and other intrusive rocks of the pluton. I have identified two different types of rock logged as having porphyry texture. The first is "quartz porphyry", which is extremely altered rock in which all minerals except quartz were converted to sericite and (or) kaolinite (e.g., Figure 2-9). This leaves quartz "phenocrysts" floating in a fine-grained sericite and (or) kaolinite matrix. It is not a true porphyry (phenocrysts in an aphanitic matrix) as it was originally a sub-equigranular rock but alteration has destroyed the original texture. This type is usually altered granite, as quartz is usually too fine-grained in the tonalite to easily identify, even where all other minerals are destroyed.

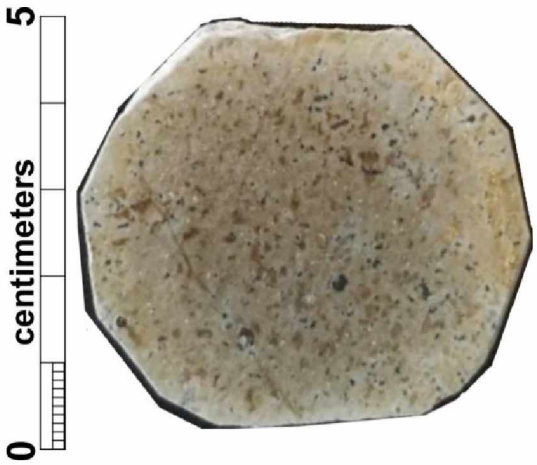

Figure 2-9: Photo of "porphyritic" texture caused by intense alteration; grey 1-2 mm spots are quartz grains in an entirely sericite ± kaolinite (altered) matrix.

The other style of porphyry texture is sub-millimeter, euhedral feldspar ± quartz phenocrysts in a dark, aphanatic matrix, referred to as 'quartz-feldspar porphyry', even where quartz is not obvious. This porphyry texture is present along the margins of thin granite dikes and margins of tonalite intrusions. I interpret it to be the result of rapid cooling along a chilled margin. Feldspar crystallizes first in both intermediate (tonalite) and felsic (granite) magma allowing euhedral box-shaped feldspars (± rare quartz) to form. Thermal quenching causes the remaining melt to quickly solidify, creating a dark, very fine-grained matrix. In my experience, these rocks rarely contain significant obvious quartz. The granite versions (e.g., Figure 2-10A) have a slightly paler-colored matrix and usually fewer feldspar phenocrysts. The tonalite versions (e.g., Figure 2-10B,C) possess darker matrix and higher abundance of (commonly) smaller feldspar grains. Typical granite porphyry dikes are 5-10 feet wide and intrude tonalite, schist, and equigranular granite (Figure 2-11).

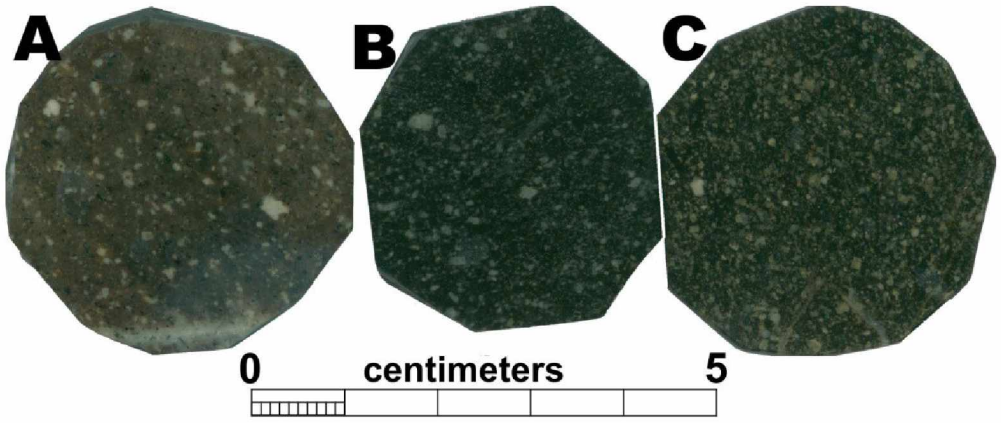

Figure 2-10 – Samples of core logged as 'QFP'. A is from a 3ft wide granite dike in granite; B and C are from tonalite near schist contacts. White spots are feldspar phenocrysts.

Figure 2-11: Dark granite porphyry dike intruding equigranular granite in drill hole GSDC1137

2.5 3D model and cross-section

Leapfrog Geo is 3D implicit modelling software which allows the user to import drill hole data and create 3D models and cross-sections based on that data. As with any software, the results and quality of the product exported is a product of the truthfulness and quality of the data that is imported. Leapfrog provided me with an academic research license which I used to create models and cross-sections of the pluton for both lithology and alteration.

Drilling near the margins of the pluton has encountered dikes and (or) sills(?) in schist, but their orientations are unknown. The Leapfrog model has extended the intrusive units to the edge of the model

area, which results in the straight edges of the pluton. This is an artificial contact. It actually fingers out in a complex manner.

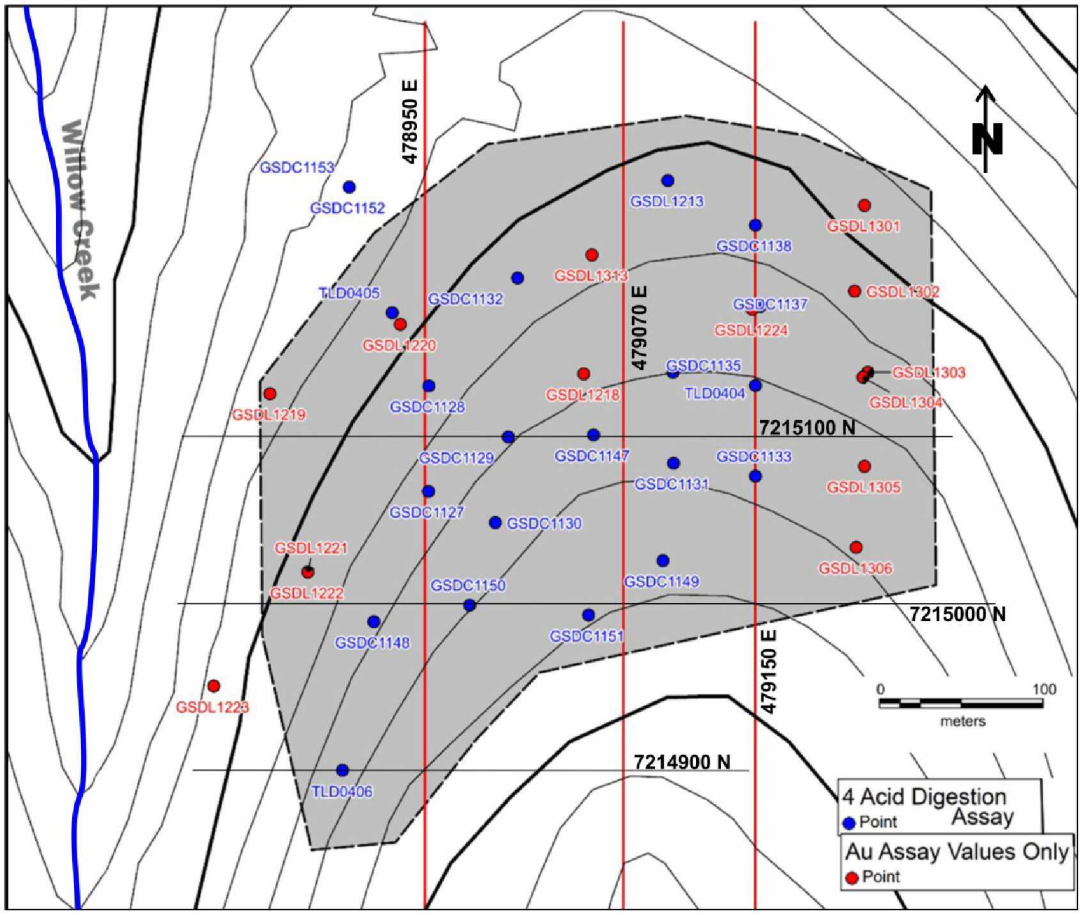

Figure 2-12: Map showing approximate outline of Dolphin pluton (gray) with drill hole collar locations and cross-section lines (red) with additional UTM lines (black).

I created cross-sections of the pluton at UTM 479150, 479070, and 478950E (Figure 2-12). Due to the fact that four-acid ICP-MS data are not available for all drill holes in the pluton, these 3 lines were selected to include the maximum number of holes for which four-acid ICP-MS data are available while providing good distribution through the pluton.

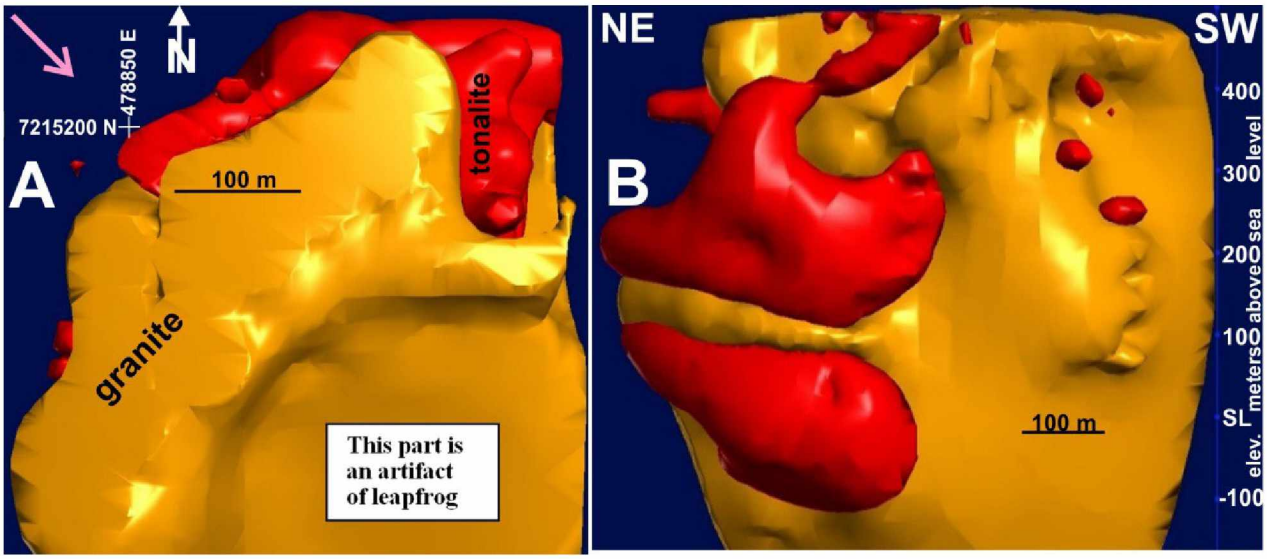

Figure 2-13: Plan view(A) and isometric view looking SE (B) of the Dolphin pluton, showing tonalite (red) is mostly restricted to the northeastern margin of the granite (orange) body. The igneous units intrude schist (dark blue) which entirely surrounds the pluton. Pink arrow on A indicates the direction of the view for B. As seen in B, a granite dike cuts the tonalite body approximately in half. Images made using the Leapfrog(c) software.

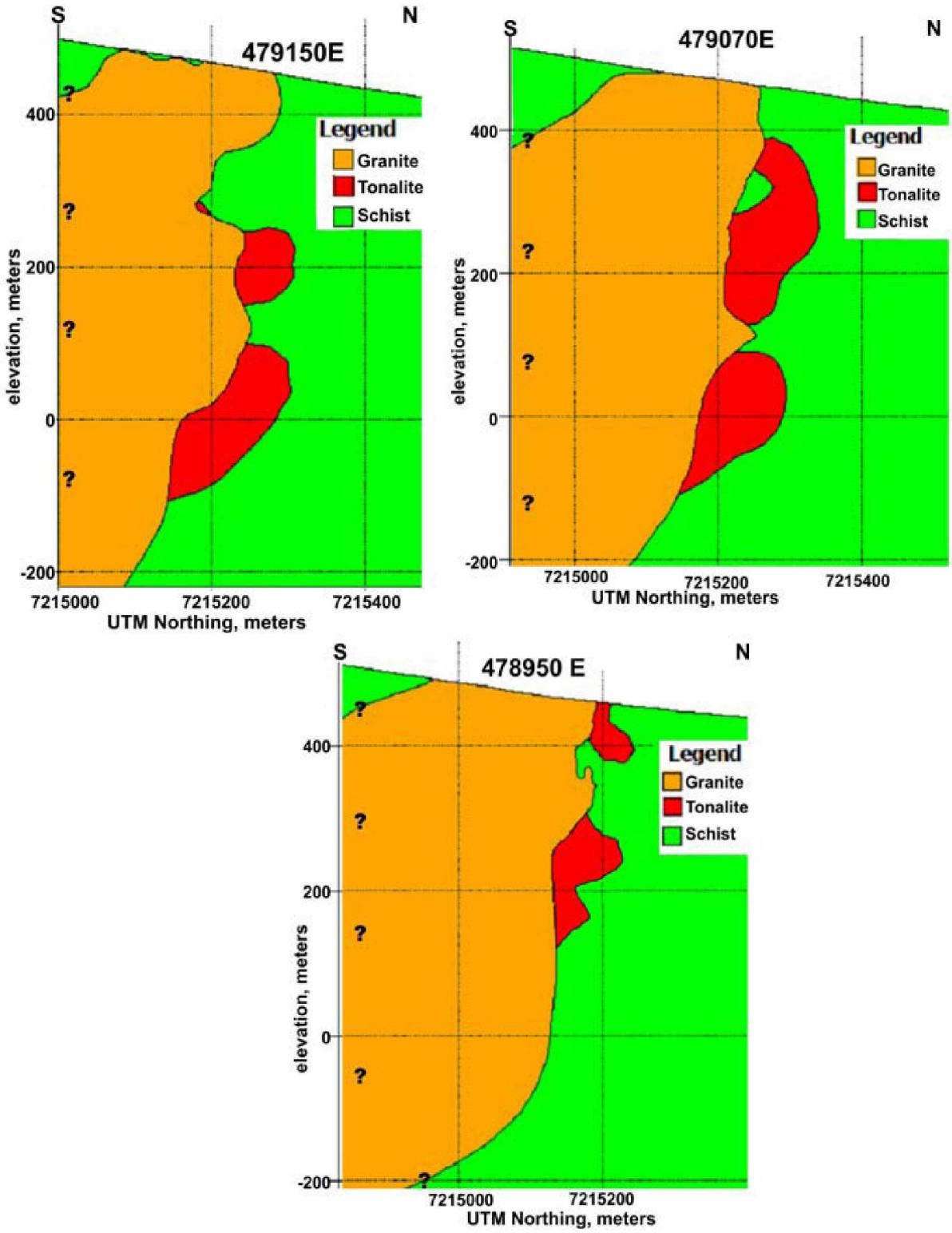

Figure 2-14: N-S geologic cross-sections (looking W) through the Dolphin pluton, with 200 m grid. Upper left = Western-most section, along UTM 479150 east. Upper right = central cross-section along UTM 479070 east. Lower central = Eastern-most section, along UTM 478950 E. Cross-section lines are shown on Figure 2-12.

Unfortunately, I could not show the detailed inter-tonguing between granite, tonalite, and schist which are seen in individual drill holes (e.g., Figure 2-4). Drill hole 1138, for example, is at the north end of the easternmost cross-section, and the depiction of the northern contact area (Figure 2-14) is much less complex than seen in the drill hole (Figure 2-4, right). With that proviso in mind, three cross-sections (Figure 2-14) show a more-or-less continuous body of tonalite north of the main granite body. The tonalite plunges to the east, such that the tonalite is at the surface in the westernmost cross-section but is 200 m below the surface in the section 200 m to the east. It is clear in the sections that the tonalite is not a marginal phase to the granite, but rather is an earlier, somewhat dike-shaped body that is cut by the granite, especially seen in the central cross-section (Figure 2-14).

2.5 Discussion—Igneous Units

Identification of igneous units during core logging has been a difficult task due to the overwhelming extent of hydrothermal alteration present. During the 15-year interval over which Dolphin core has been logged, at least 6 different intrusive units were logged. Compositional data (Figure 2-1) indicate that the logged name commonly bears only a modest relationship to the composition-based name. My analysis of the four-acid digest compositional data, however, shows two distinct intrusive units. By comparing the TiO_2 and P_2O_5 concentrations in Dolphin intrusive rocks with unaltered granitic samples collected by Blum (1983), Burns et al. (1991), and Newberry (1996), two units can be identified: low Ti (granite) and high Ti (tonalite). Because there is no gradational transition through an intermediate granodiorite unit between these two, these units cannot reflect simple fractional crystallization. Two obvious possibilities are: (a) the two rock types were derived from a deeper body that underwent fractionation but failed to inject granodiorite and (b) the two rock types are derived from completely separate magmas. Tonalite is the older unit as evidenced through tonalite xenoliths in the granite unit and granite dikes intruding tonalite.

Au grade is found in both igneous units. If both the granite and tonalite were separately mineralized, one would expect higher grades in the tonalite (mineralized twice). If the tonalite was exclusively responsible for Au mineralization, granite should be barren. If the granite was exclusively responsible, both could be mineralized, but one might expect lower values in the tonalite. These models will be pursued in the mineralization chapter.

Many large hydrothermal-plutonic Cu-Mo-Au deposits are associated with stocks which possess porphyry textures ('porphyry Cu-Mo-Au deposits'). In those cases, the porphyry texture is thought to arise from rapid loss of magmatic water, which raises the solidification temperature without appreciably

changing the temperature. In the case of Dolphin, rocks identified as 'quartz porphyry' are simply highly altered granite. True porphyry-textured rocks are present, but they are very local in extent and most likely caused by local thermal quenching. At Dolphin, tonalite porphyry is easily confused with granite porphyry based on hand specimen appearance, but compositionally they are quite distinct. A larger proportion of the Dolphin tonalite has porphyry texture than does the granite. This is likely due to smaller tonalite intrusions that occurred early while the wallrocks were still relatively cool.

2.6 Hydrothermal Alteration

2.6.1 Introduction

The Dolphin pluton has undergone multiple overprinting hydrothermal alteration events. In order to better understand the conditions under which gold mineralization occurred, I used geochemical analysis and transmitted light petrographic microscope analysis to identify albitic, sericitic, advanced argillic, and calcite alteration in intrusive rock. I then attempted to model the spatial distribution of alteration styles based on Na_2O concentrations that are associated with gold mineralization. Abrams and Giroux (2013) identified common alteration styles at Dolphin as silicification, and sericitic, argillic, and albitic alteration with local carbonate alteration as calcite (rare dolomite or ankerite). They also claimed that sericitic alteration was earliest. Since their identifications were based exclusively on hand-lens descriptions, the potential for misidentification is high. My objectives were to better describe the types and spatial patterns of hydrothermal alteration and try to correlate alteration style with gold grade.

2.6.2 Methods

I conducted petrographic studies in transmitted light in order to discern alteration minerals. Quantitative energy-dispersive spectrometry (EDS) electron probe micro-analyses (EPMA) of these thin sections was conducted in some instances to identify minerals and quantify elemental concentrations. In addition, I employed limited X-Ray diffraction (XRD) analyses to confirm the presence of kaolinite. Geochemistry from the 3,425 samples identified as from plutonic rocks and 50 powder pressed pellets analyzed by XRF were used to determine and assign styles of alteration based on Na_2O, K_2O and CaO concentrations. Based on the style of alteration assigned to each sample, I created 3D models and cross-sections of zones of alteration within the pluton using Leapfrog Geo 3D modelling software.

2.6.3 Petrographic Analysis

Fifty-one polished thin sections were made and analyzed for alteration assemblages. Through transmitted light petrography I have seen evidence of widespread hydrothermal alteration with several different alteration types present. I also employed qualitative microprobe analysis on very fine-grained mineral clumps and employed X-ray diffraction on most of the polished thin sections. Using these

methods, I identified alteration minerals including calcite, sericite, kaolinite, chlorite, and (or) secondary biotite in every sample.

One of the complications to the alteration is that except for quartz, granitic minerals are unstable under lower greenschist facies conditions (T~ 300° C) and extensive fluid passing through granitic rocks would tend to convert rock minerals stable at these conditions. In particular, hornblende and biotite are unstable relative to chlorite, plagioclase is unstable relative to albite + a calcium mineral, and alkali feldspar (Na-K solid solution) is unstable relative to albite + muscovite. At Dolphin the usual secondary calcium-rich mineral is calcite. Consequently, even where there has been no change at all in the rock chemical composition (aside from addition of CO_2 and H_2O), the minerals that experienced this low-temperature fluid are 'altered', i.e., not magmatic and contain the assemblage quartz + albite + muscovite + chlorite $\pm$ residual alkali feldspar. Such rocks could be considered to have experienced 'propylitic' alteration, but that term carries some baggage, and is usually not employed for rocks with significant calcite and fine-grained muscovite (sericite). I will use the term 'weakly altered' instead and note that all of the Dolphin igneous rocks I examined contain at least some calcite and sericite and should be considered at least weakly altered.

2.6.4 Systematic Description of Alteration

Replacement of primary hornblende in tonalite by secondary biotite (a type of potassic alteration) is the earliest alteration type (Figure 2-15). All hornblende I saw in thin section is at least partly rimmed by aggregates of very fine-grained pale biotite 'shreds', giving an overall scaly appearance (e.g., Figure 2-15A). With increasing degree of potassic alteration (increase in rock potassium by virtue of low-K hornblende replaced by high-K biotite), small islands of hornblende are left in a sea of biotite (Figure 2-15B). In many cases, I see only clumps of shreddy biotite with disseminated, fine-grained pyrrhotite that have overall hornblende shapes but no residual hornblende (Figure 2-15C). Because biotite at Dolphin is so commonly replaced by sericite and (or) chlorite, however, it is difficult to gauge how common this was at Dolphin. I saw no evidence for secondary K-feldspar, but if it was white it would be impossible to distinguish from secondary albite. Certainly, the only K-rich rocks (> 4% K_2O) are those with abundant (>50%) muscovite, so there is no compositional evidence for secondary potassium feldspar. Consequently, although there was probably some early potassic alteration, there is now little evidence for it.

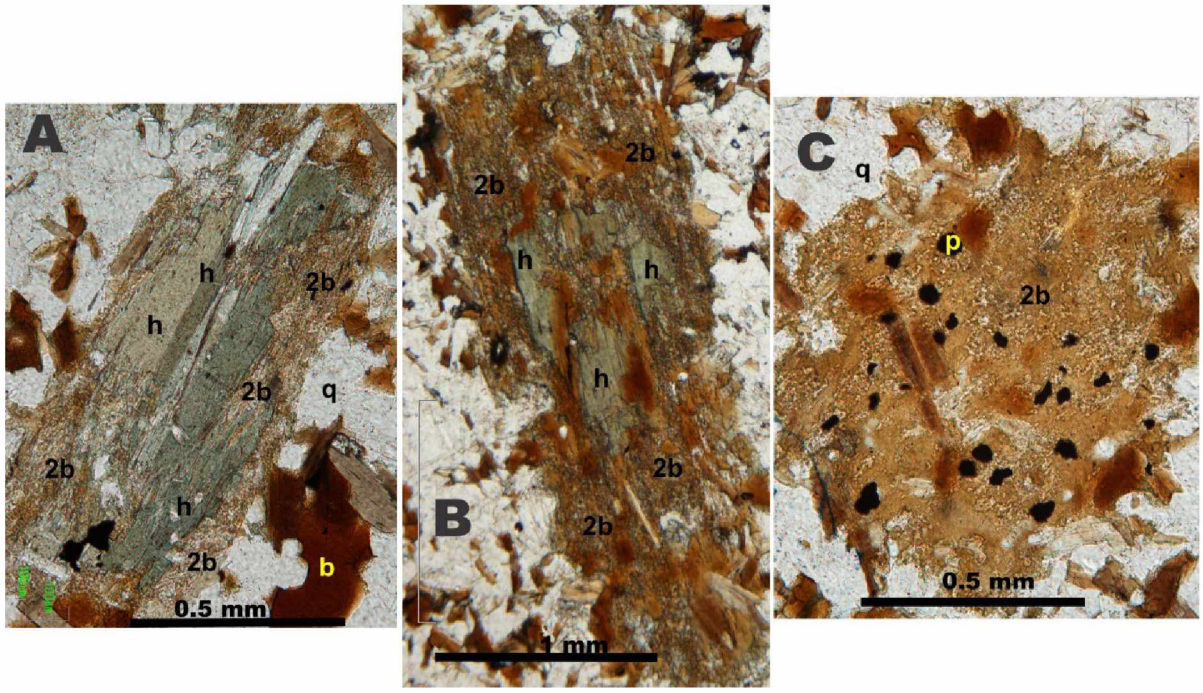

Figure 2-15: Photomicrographs (plane polarized light) showing progressive increase in degree of replacement of primary hornblende (h) by secondary biotite (2b) + pyrrhotite (p) from A (least replaced) to C (completely replaced). Secondary biotite (2b) is distinguished from magmatic biotite (b) as the former is pale brown, .01-.02 mm 'scaly' intergrowths.

Albitic alteration (rock with abnormally abundant albite) is most common in the core of the granite pluton and is rare on the northeastern and eastern margins. That said, the highest Na_2O concentrations measured at Dolphin are in the upper 50 feet of drill hole 1132 (average 7% Na_2O), near the north-central contact (Figure 2-12) of the Dolphin pluton. However, because albite results from the low-temperature decomposition of plagioclase, the mere presence of albite doesn't make a rock possess albitic alteration. It is most definitively recognized by an increase in the Na_2O concentration in rocks but lacking chemical analyses such a definition is problematic.

Weak albitic alteration is difficult to recognize (Figure 2-16A), especially because the associated calcite and muscovite are much easier to identify in core. Such rocks were typically logged as sericite or calcite-altered. On a smooth, wet surface, however (Figure 2-17) such alteration is seen as tiny white albite inclusions in grey translucent quartz. As the strength of albitic alteration increases, quartz abundance drops (Figure 2-16C) and eventually quartz disappears (Figure 2-16D). Albitically altered rocks typically contain about 20-25% muscovite + calcite (Figure 2-16) but the proportions of the two vary. Intense albitic alteration results in a creamy-white, hard rock with a vague 'pseudo-magmatic'

texture caused by the intergrown calcite, muscovite, and sulfides (e.g., Figure 2-16D). I have found up to 9.8 wt% Na_2O in Dolphin rocks, equivalent to 83 wt% albite.

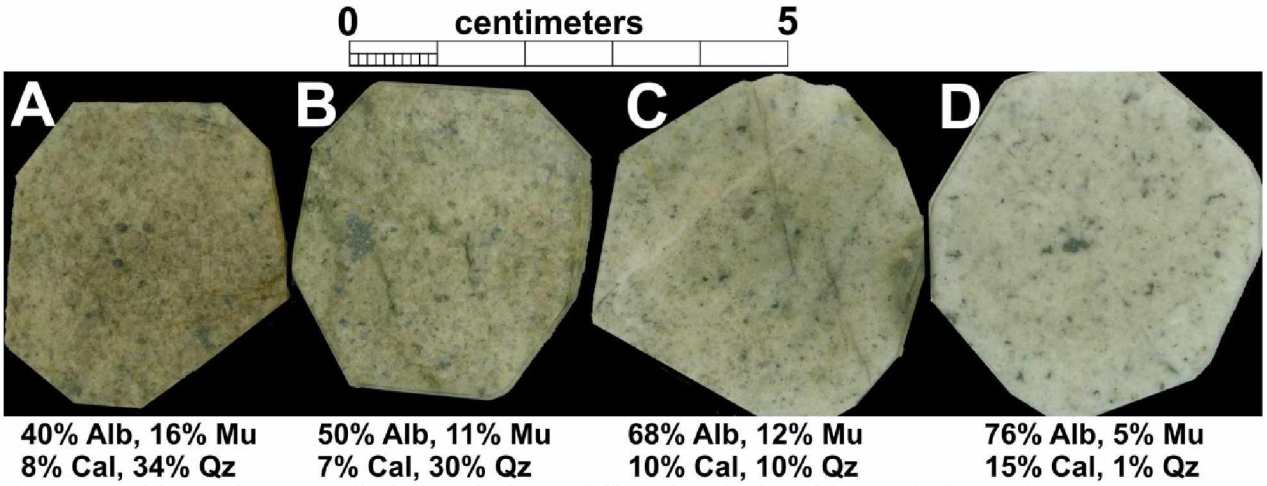

Figure 2-16: Slabs showing progressive increase in degree of albitic alteration in Dolphin granite from A (least) to D (most). Mineral abundances are calculated from XRF major element analyses.

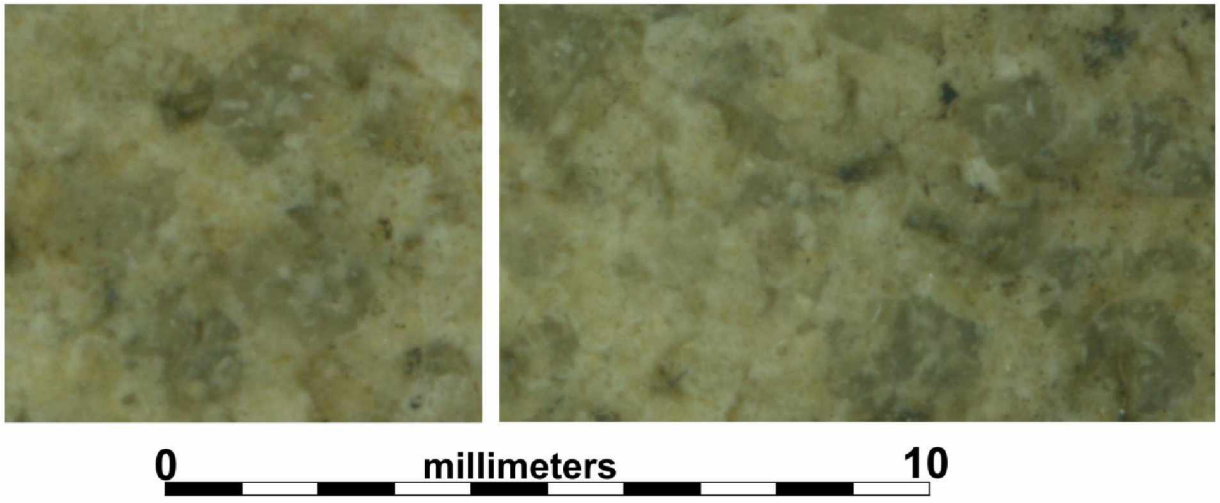

Figure 2-17: Close-ups of slab A, Figure 2-16 showing characteristic texture of weak albitic alteration, namely, tiny white albite inclusions in quartz. With progressive albitization, quartz is completely replaced. Magnification ca. 10x.

Because hydrothermal albite rarely displays polysynthetic twinning, it is difficult to recognize in thin section (it is easily confused with both quartz and alkali feldspar). Microprobe analyses of selected slides from rocks with high Na_2O concentrations, however, indicate that albite is the only mineral in appreciable abundance with significant Na. Consequently, calculated % albite is simply proportional to

rock wt% Na_2O. Comparison of Na_2O calculated from four acid-digest ICP-MS data to logged 'albitic alteration' suggests it was correctly recognized perhaps 10-20 % of the time.

Figure 2-18: Drill core from hole 1127, 750 (upper left)-757 (lower right) feet, showing intense albitic alteration zone 1 m wide (white) and thin (1-2 mm wide) albite alteration zones. The white band in the upper left is a 1 cm wide calcite vein that cuts across a 5 cm wide pale grey intense albite zone. None of the albite zones are cored by quartz veins.

Areas of intense albitic alteration occur as white zones 1 mm to 1 m wide (e.g., Figure 2-18). They are not albite veins, i.e. a crack filled with secondary albite, but rather are zones in which all the primary minerals have been replaced by 70-80% albite, with accessory calcite, muscovite, pyrite-arsenopyrite, and locally chlorite. The 1 m wide albite zone in hole 1127 was logged as 'leucogranite' and I suspect other zones were logged similarly. In this case the grey rock above and below the intense albite contains enough albite (35-40%) to be considered weak albitic alteration.

Feldspars are very commonly replaced by sericite and (or) kaolinite, but I have never seen evidence for replacement of phyllosilicate by feldspar (including albite) at Dolphin. Consequently, I think albitic is the earliest major alteration type at Dolphin. Schistose rocks surrounding the Dolphin pluton commonly contain 4-5.5 wt% Na_2O, i.e., about 30-45% albite. It seems likely that at least some of this albite is also secondary. Drill hole intercepts with high Na_2O concentrations occasionally host high (>1 ppm) Au concentrations, but lower values are more characteristic. The average Au concentration in drill core with > 4% Na_2O is 0.3 ppm.

Sericite is the most recognized secondary mineral at Dolphin, visible as soft white 0.2-0.5 mm flakes, and sericitic alteration has historically been the most logged alteration type. That is, most Dolphin

rocks, regardless of alteration type, contain at least modest amounts (>5%) of fine-grained white mica. I identified sericite in every thin section I examined and in many instances feldspar and biotite have been largely replaced by sericite (e.g., Figure 2-19). However, 'classic' sericitic alteration, that is rock consisting primarily of sericite + quartz + sulfide, is actually quite rare at Dolphin. A rock with 30% sericite (muscovite) must contain at least 4 wt% K_2O; out of nearly 3000 four-acid digest analyses of Dolphin granite, only 10 (0.3%) have that much K. The problem is, how much sericite is enough to be called 'sericitic' alteration? Without chemical analyses, this is a serious problem.

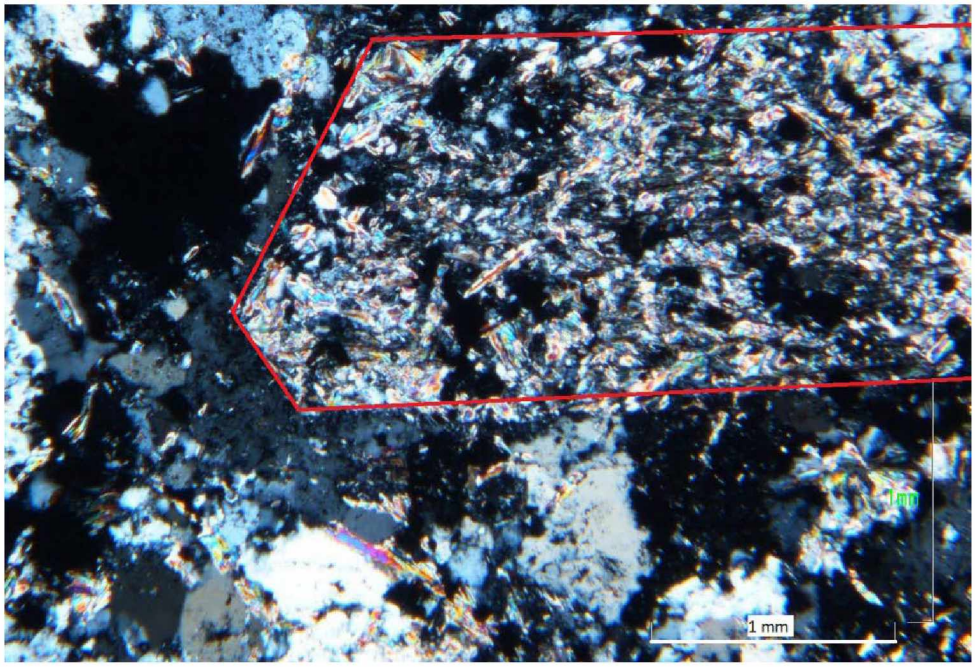

Figure 2-19: Photomicrograph in crossed polarized light showing complete replacement of feldspar (outlined in red) by sericite (fine-grained white mica) + quartz. White scale bar at bottom is 1 mm.

'Argillic' alteration has been noted in drill core logs. Technically, 'argillic' refers to smectite-group clays and is not readily (or easily) distinguished from simple weathering. In contrast, the presence of kaolinite indicates 'advanced argillic' alteration. Kaolinite had not been noted at Dolphin prior to this investigation, yet it is surprisingly common. Kaolinite is much finer-grained than sericite; a soft white rock that lacks visible mica flakes invariably contains significant kaolinite (e.g., Figure 2-20). However, this mineral is only reliably distinguished from sericite through X-ray diffraction or with the electron microprobe. In thin section kaolinite is so fine-grained and has such low birefringence that it is easily confused with epoxy-filled holes. In contrast, I verified the presence of kaolinite through petrographic examination, by X-ray diffraction, and by the electron microprobe (it has a distinctive composition).

Conversely, I found no evidence for pyrophyllite (an Al-silicate sometimes present with kaolinite) using both techniques.

Sericite is always present with kaolinite in the thin sections I examined and based on rock chemical analyses, the two are commonly together. Rocks containing significant kaolinite rarely show evidence for significant feldspar (i.e., hard, white, opaque minerals). Rocks with substantial kaolinite generally contain some, but not much, calcite.

Kaolinite is most frequently noted in logs as 'argillic' alteration where the kaolinite abundance (from chemical analyses) is greater than 25%. Rocks with less kaolinite have invariably been logged as sericitic alteration. In some cases, kaolinite-rich rocks were logged as 'leucogranite.' As with sericitic alteration, the problem is one of where to draw the line between 'advanced argillic' and sericitic alteration, especially in the absence of compositional data.

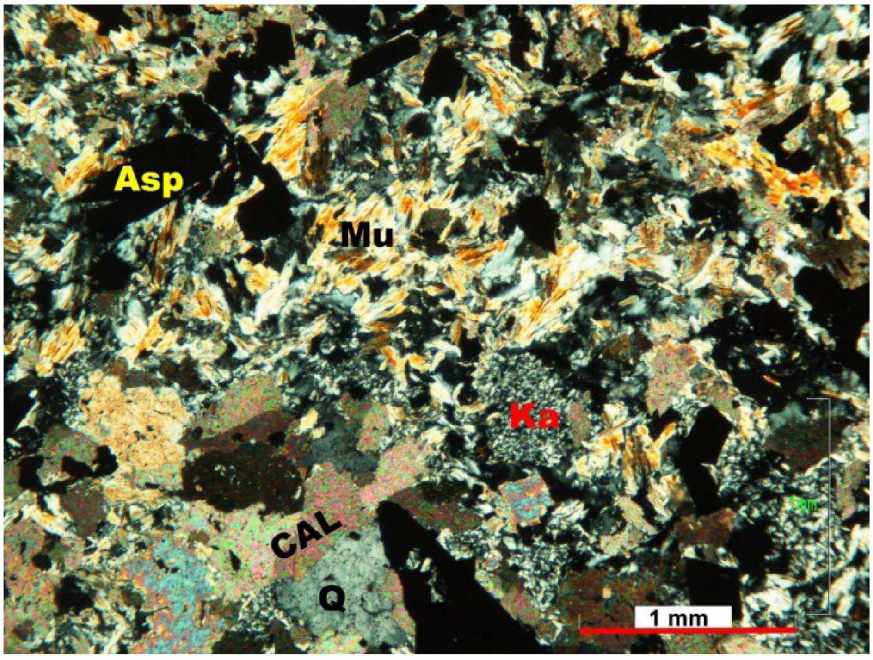

Figure 2-20: Photomicrograph (cross polars) of a sample displaying advanced argillic alteration: relatively coarse muscovite (Mu) with coarse quartz (a) and calcite (CAL) and extremely fine-grained kaolinite (Ka) intergrown with arsenopyrite(Asp).

2.6.5 Alteration recognized through rock compositions

I focused on alteration in the Dolphin granite because most of the analyses are from granite. Using the set of 2,800 four-acid digest analyses for rocks that were likely granite (section 2.3.2) allows some clarification of the alteration types and their complications. Relative to typical unaltered Fairbanks district

granite, Dolphin granite is depleted in K (Figure 2-21, left) and enriched in Ca (Figure 2-21, right). This is consistent with a background of pervasive K-feldspar replacement by sericite (essentially muscovite) + calcite, seen in even the least altered rocks. Albitic alteration results in Na enrichment, but the presence of substantial K and Ca confirms petrographic observations that the alteration assemblage is usually albite + muscovite + calcite rather than simply replacement of feldspars by albite. Conversely, loss of Na indicates plagioclase destruction, but decrease in K in such rocks indicates that plagioclase is replaced by sericite + calcite, not by K-feldspar. (Muscovite contains less K than does K-feldspar.) Rocks with essentially zero Na_2O are common; these invariably contain much more Al than K, so must contain significant kaolinite ($Al_2Si_2O_5(OH)_4$) $\pm$ muscovite. Many of these still contain substantial Ca (Figure 2-21, right), so the actual assemblage is kaolinite + muscovite $\pm$ calcite.

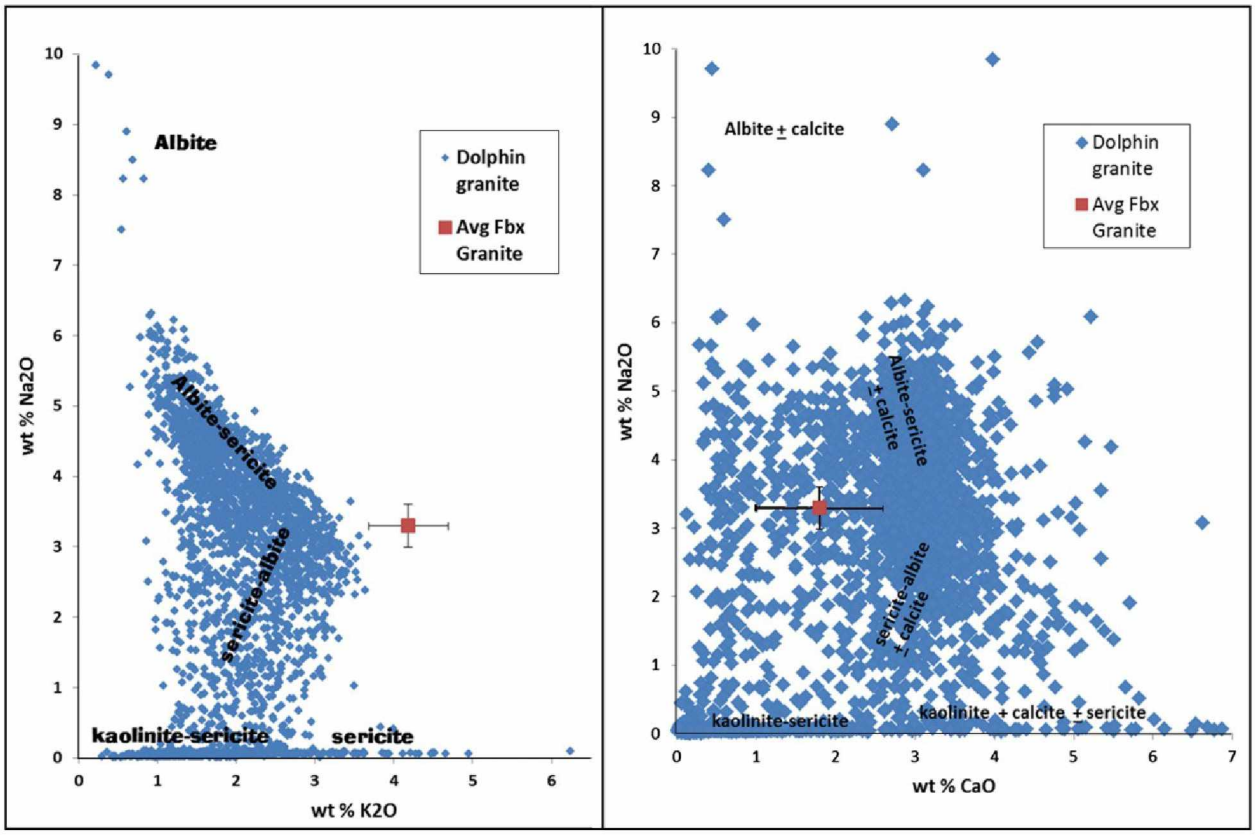

Figure 2-21: Na_2O vs. K_2O (left) and Na_2O vs. CaO (right) for 2800 analyses of altered Dolphin granite, based on four-Acid digest ICP-MS. Average Fairbanks granite from data in Blum (1983) and Newberry (1996).

The compositional data allow for extraction of two major alteration types: albite $\pm$ sericite (Na-addition) and sericite-kaolinite (complete Na loss). The former applies to granite (low-TiO_2 igneous rock) with > 3.7 wt% NaO_2; the latter to granite or tonalite with < 0.1 wt% NaO_2. For the Dolphin drill holes that have four-acid digest compositional data, I determined the % of the granite in each drill hole which

exhibits (a) significant Na addition and (b) total Na loss. Interestingly, for all but one drill hole, each hole either has more than 30% of the granite enriched in Na (albitic alteration) or more than 30% completely leached of Na (sericite-kaolinite alteration), but not both.

A map with locations of drill holes possessing significant amounts of the alteration types (Figure 2-22) shows that a zone with significant albitic alteration is confined to the middle-southern part of the pluton; in contrast, strong Na leaching is restricted to the northeast and eastern margins. In a general way, the region of strong albitic alteration (Figure 2-22) corresponds to the region of only granite in the central part of the pluton (Figure 2-3), and the area where tonalite is present (Figure 2-3) also contains extensive kaolinite-sericite alteration (Figure 2-22). However, the situation is more complicated than that because holes in the south-central part of the pluton (479050 E – 479150E, 7215200 N – 7215020 N) only intersected granite, but display extensive Na-leaching (Figure 2-22).

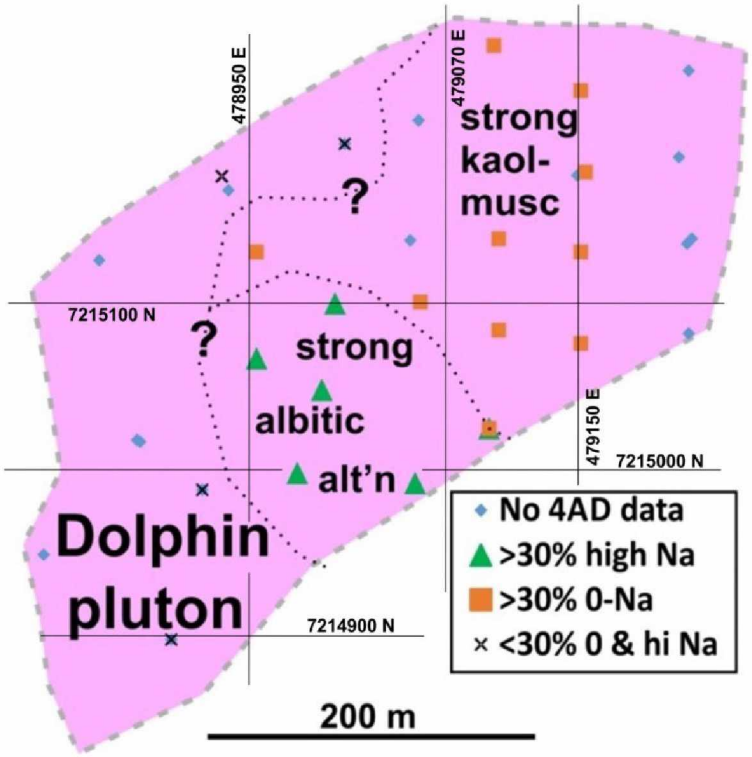

Figure 2-22: Map of the Dolphin pluton showing locations of drill holes with significant amounts of excess Na (albitic alteration) and complete leaching of Na (sericite-kaolinite alteration), based on 4-Acid digest compositional data for 5 foot core intervals of granite. UTM lines in black; the three N-S lines correspond to the leapfrog cross-sections.

A tie between tonalite and kaolinite-sericite alteration is suggested by the patterns seen in drill holes GSDC1132 and 1138 (Figure 2-23). As noted previously, variations in TiO_2 concentrations mostly track intervals of granite (low Ti) vs. tonalite (high Ti) with some schist (intermediate Ti) intercepts. Most

likely they represent a single original body of tonalite that was intruded by at least six granite dikes. Notably, low Na concentrations (kaolinite-sericite alteration) are commonly present in these drill holes at and near intrusive contacts. However, low-Na zones are also present in massive granite in the upper 200-500 feet of both drill holes (Figure 2-23). Thus, granite dike contacts could have served as conduits for the lower pH fluids responsible for kaolinite-sericite alteration. That such zones are also seen in massive granite indicates that additional conduits (faults?) were utilized.

Drill hole GSDC1149 was the only drill hole that contained more than 30% granite intercepts with both Na-enriched and highly Na-depleted intervals (Figure 2-24). This seemed worth further investigation. Because the entire hole was in granite, I could make some simple calculations regarding mineral abundances. I assumed that all Na was in albite, all K in muscovite, and that the remaining Al not used by albite + muscovite was present as kaolinite. Figure 2-24 shows the calculated downhole mineralogy for that drill hole can be neatly divided into 'albitic' (> 30% and usually ~40% albite), 'Advanced argillic' (AA, >20% kaolinite and > 40% kaolinite + muscovite, usually with < 2% albite), and 'sericitic' (10-20% muscovite, < 5% kaolinite, < 30% albite) alteration assemblages.

Based on these definitions, 39% of drill hole 1149 experienced albitic alteration, 36% experienced advanced argillic alteration, and 26% experienced sericitic alteration. About half of the AA intercepts are separated from albitic alteration by a strip of sericitic alteration and half of them have AA directly adjacent to albitic. In part this is a function of the sampling, usually taken at five-foot intervals, and consequent mixing of alteration types in a single drill core sample.

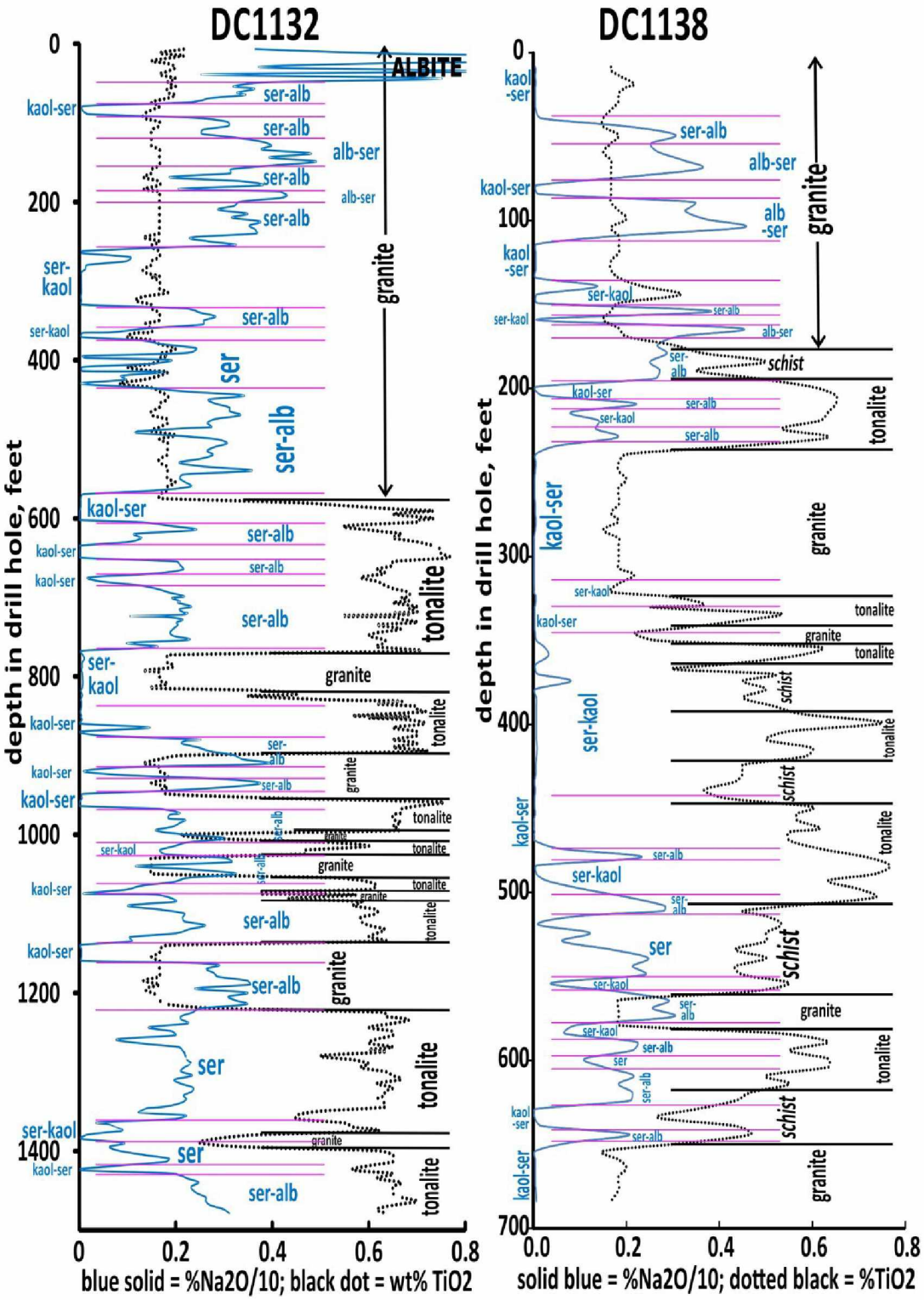

Figure 2-23: Wt% $Na_2O/10$ (solid blue line) and wt% TiO_2 (dotted black) versus depth for drill holes 1132 (left) and 1138 (right). Blue letters indicate the predominant alteration minerals given by the rock analyses. Ser = sericite, kaol = kaolinite, alb = albite. The rapid changes in TiO_2 with depth indicate sharp contacts between granite (low-Ti) and tonalite (high-Ti). Zones of extremely low Na_2O (effectively zero) are zones of kaolinite-sericite alteration. Major low-Na_2O zones are commonly at granite contacts, suggesting that the contacts acted as conduits for acidic fluid migration.

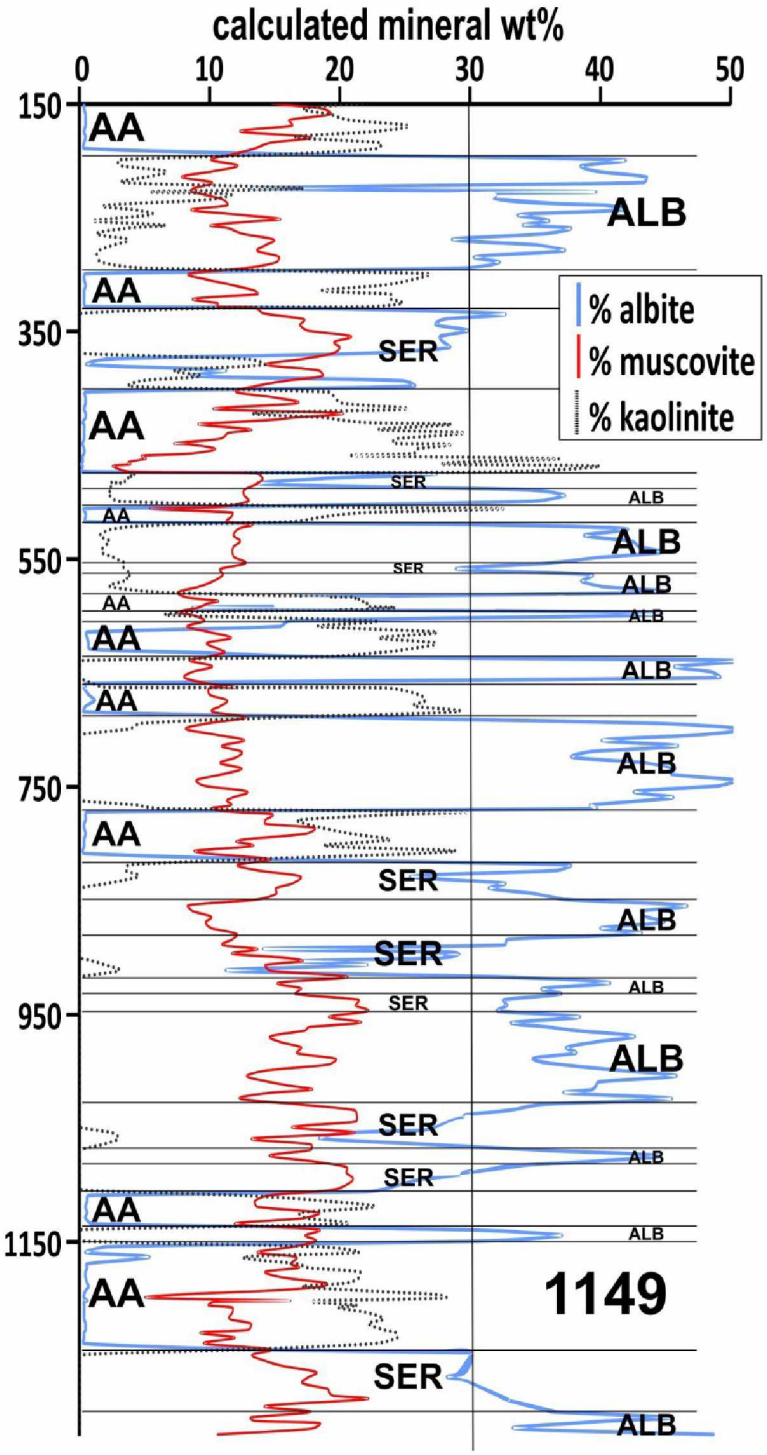

Figure 2-24: Calculated mineralogy (wt %) versus depth in drill hole for hole 1149. Minerals were calculated from the ICP-MS analyses for each assay interval as described in the text. Alteration assemblages assigned as AA (advanced argillic), ser (sericitic), and alb (albitic) based on calculated mineral abundances

While this compositional approach seemed promising, the calculated mineralogy is highly dependent both on the mineralogical model and on the assumption that the ICP-MS analyses have essentially no error. Not entirely valid mineral assumptions include the assumption that the only Al-bearing minerals in the core were albite, muscovite, and kaolinite (i.e., ignore chlorite and alkali feldspar), and the assumption that all minerals are chemically pure. Muscovite, in particular experiences significant phengite solid solution at moderate temperatures and really is not a pure phase. Trying to take all these other factors into consideration proved more complicated than I felt worthwhile and I continued analysis of the alteration by using simpler compositional variables.

Using the 3,425 sample assays from intrusive rock (see section 2.3), I assigned alteration to the 3,021 granite samples. Far fewer four-acid digest ICP-MS assays are available for the tonalite unit and the alteration is less well understood, therefore I restricted the analysis and modeling of alteration to granite only. I assigned alteration styles to each sample based on chemical composition when compared to average Fairbanks granite. Granite samples with >3.5 weight % Na_2O (equivalent to > 30 wt % albite) were labeled "albitic". Samples with < 3 weight % Na_2O but >0.25 weight percent Na_20 were labeled "sericitic". Samples with <0.25 weight percent Na_2O were labeled "advanced argillic" (Figure 2-25). Samples containing CaO >3.5 weight % were labeled calcite alteration. Samples that contain more than one style of alteration are common and terms such as albite-calcite alteration are applied. Of these 3,022 analyses, 290 are labeled "weakly altered", 183 are advanced argillic, 781 are advanced argillic + sericitic, 562 are sericitic, 863 are albitic, 51 are calcite, 85 are albite-calcite, 5 are advanced argillic - calcite, 37 are advanced argillic-sericite-calcite, and 164 calcite-sericite.

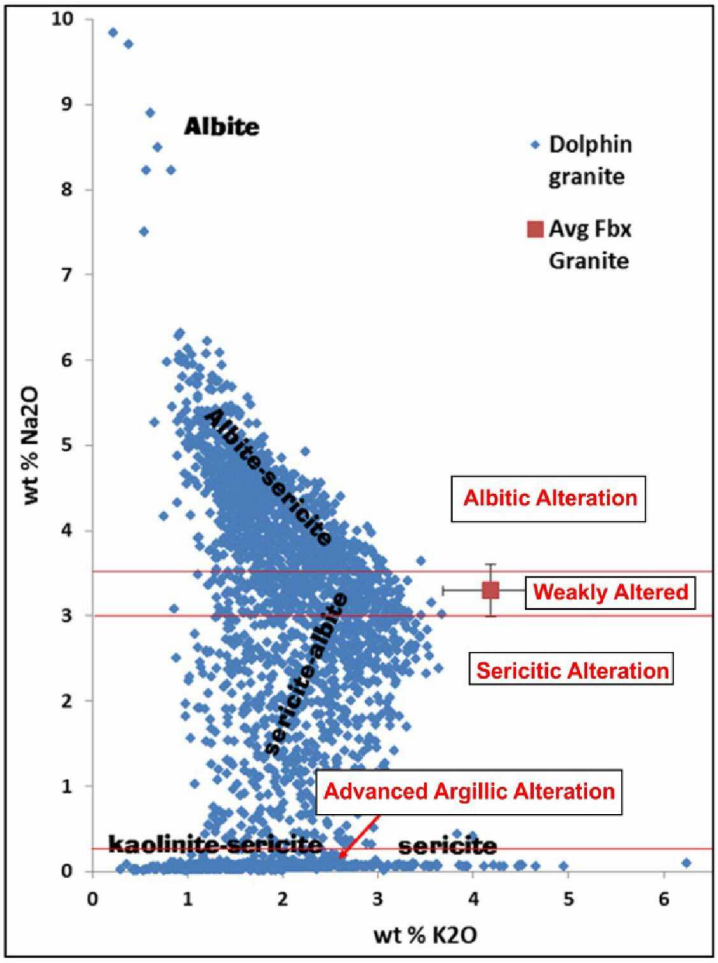

Figure 2-25: Assignment of alteration types in Dolphin granite based on Na_2O concentrations

2.6.6 3D modelling

Once an alteration type was assigned to each sample, I created a 3D model in Leapfrog Geo and created cross-sections of the pluton (see section 2.5) along UTM 479150, 479070, 478950 eastings (Figure 2-26). For Leapfrog 3D models, I grouped alteration into 4 types: 'albitic', 'advanced argillic', 'sericitic', and 'weakly altered'.

Compared to the complex interdigitating alteration types seen in individual drill holes (Figure 2-23; Figure 2-24), the Leapfrog models mostly show relatively large areas of consistent alteration. I am not sure how much confidence to put in them, but they seem to confirm my suspicions that advanced argillic and albitic are the two major alteration types at Dolphin, i.e., that 'sericitic' alteration per se is relatively scarce. All three cross-sections show advanced argillic alteration more abundant to the north, with a large zone of albitic in the center (Figure 2-26).

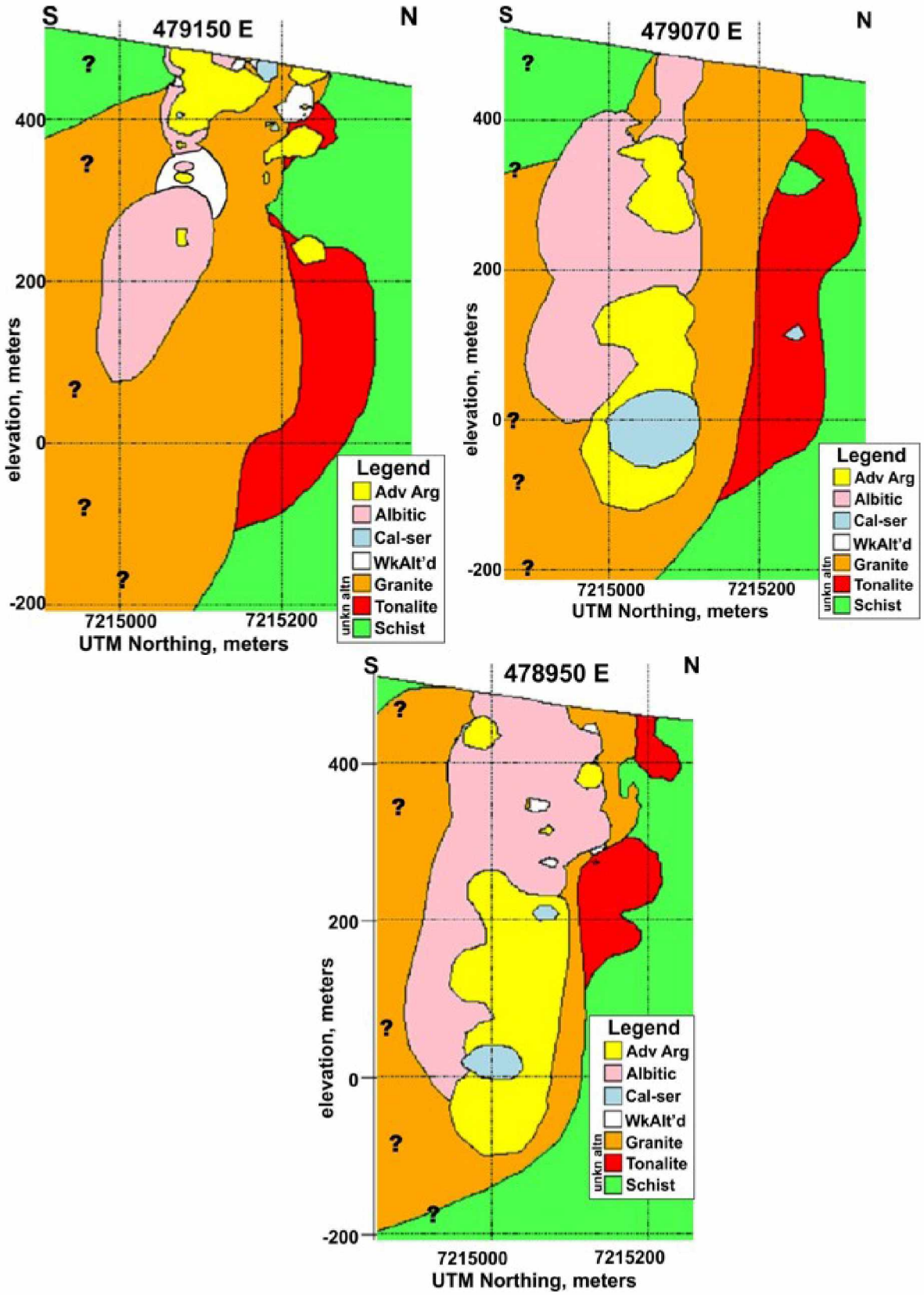

Figure 2-26: Alteration cross-sections through the Dolphin deposit, along the same lines as shown in Figure 2-14. Alteration type was not assigned where there was insufficient drill hole information.

2.6.7 Discussion—Hydrothermal Alteration

Abrams and Giroux (2013) suggests a paragenetic sequence of alteration and mineralization events at the Dolphin deposit starting with early sericitic alteration and disseminated arsenopyrite ± pyrite through sheeted auriferous quartz-sulfide veining to coarse grained pyrite dominated ± base metal sulfide veining (no quartz associated). My study, in contrast, shows that the hydrothermal alteration at Dolphin is dominated by albitic and advanced argillic alteration. Gagnon et al. (2004), based on LA-ICP-MS studies of fluid inclusions, showed that fluids responsible for albitic alteration have molar Na/K ratios of approximately 30:10 to 100:1. Similarly, Brathwaite et al. (2001) report lower Na/K ratios of 10:1-30:1 and more acidic pH associated with advanced argillic alteration. The upper thermal stability of kaolinite is approximately 300° C (Thompson, 1970), and is basically independent of pressure.

I modeled fluids responsible for albitic and advanced argillic alteration at Dolphin based on a fluid activity diagram at 300°C, calculated using the geochemists workbench software (Figure 2-27). Fluids with high Na/K (1, Figure 2-27) react with K-feldspar–bearing rocks by converting K-feldspar to albite. In doing so, the fluid loses Na^+ and gains K^+ until it reaches the stability of muscovite (2, Figure 2-27), at which point it converts K-feldspar bearing rock to muscovite + albite. Because the replacement of K-feldspar by muscovite is a $K^+ \leftrightarrow H^+$ exchange reaction, the fluid H^+ abundance drops and K^+ rises. Although Na^+ abundance in fluid also drops, the ratio of Na^+/H^+ rises, and the fluid path is from 2 to 3 (Figure 2-27). The fluid reaches equilibrium with the granite when its composition reaches 3. Note that the fluid that caused albitic alteration could have possessed a temperature higher than 300° but does not need to.

In contrast, a fluid with lower Na/K, but significantly more acid, would have lower (Na^+/H^+) and (K^+/H^+) ratios, making it stable with kaolinite (4, Figure 2-27). Such a fluid would react with practically all Na-K-Al silicates to form kaolinite. Doing so would cause the relative Na and K abundances to rise, until the fluid reaches equilibrium with muscovite (5, Figure 2-27). Further reaction would cause the fluid to replace feldspars by kaolinite + muscovite until equilibrium with albite + muscovite is reached. In other words, muscovite is the logical accompanying mineral for both low-pH (advanced argillic) and high Na (albitic) alteration.

"Classic" porphyry Cu-Mo-Au deposits are described as having a core zone with potassic alteration and with sericitic alteration variably superimposed. The Dolphin deposit might resemble that configuration, but with albitic instead of potassic and advanced argillic instead of sericitic alteration. Unfortunately, given the difficulties in identifying the major alteration types, the existing core logs are mostly useless for working out alteration patterns. Pursuing this topic further would simply require much additional compositional data.

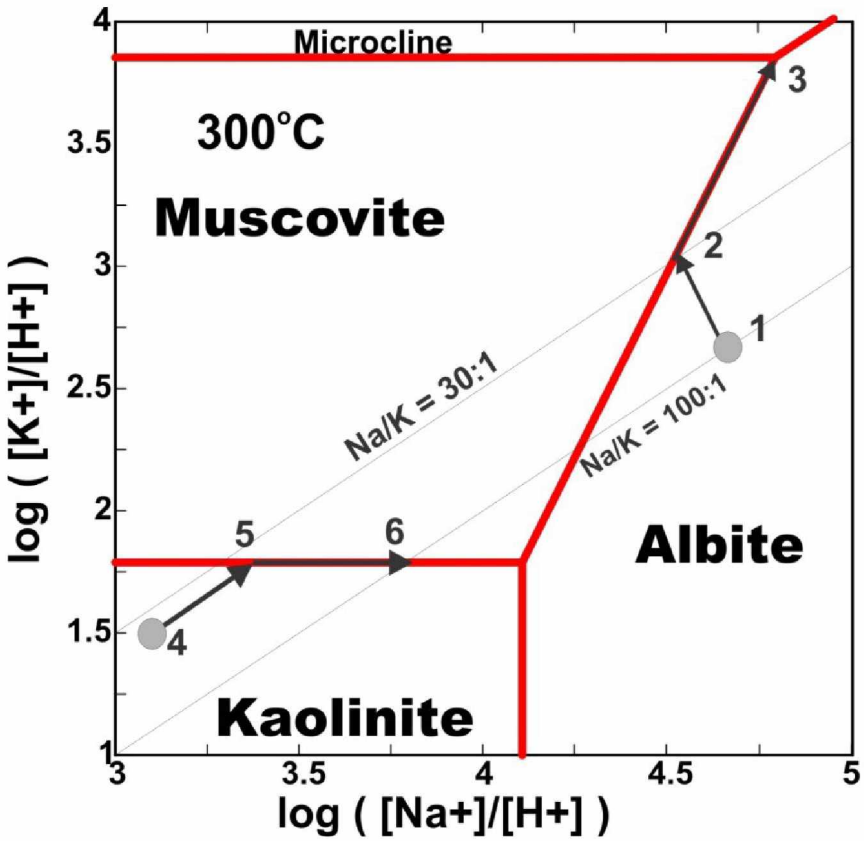

Figure 2-27: Activity diagram showing stability fields for major Na-K-Al minerals as functions of fluid composition at 300°C, calculated using the 'geochemists workbench' software. Fluid paths 1-2-3 and 4-5-6 represent hypothetical fluids causing albitic and advanced argillic alteration, respectively.

3 Mineralization

3.1 Introduction

Gold is the only known economic mineral at Dolphin. Gold is said to be associated with early high temperature auriferous quartz stockworks, later lower temperature auriferous sericitic shear zones, high grade gold-bearing quartz veins with low sulfide content, disseminated sulfides, and sulfide-quartz veins (McCoy and Olson 1997; Adams and Giroux, 2011; Abrams and Giroux, 2013). According to these workers, gold occurs as rare fine- to coarse-grained (0.1 – 2 mm) blebs in quartz veins, and more commonly intergrown with sulfides in sulfide veins, as fine-grained inclusions in pyrite and arsenopyrite, (least common) as Au + Bi from exsolution of maldonite (McCoy and Olson, 1997).

Dolphin has high sulfide content in comparison to other mid-Cretaceous intrusion-related gold deposits in Alaska (Raymond, 2017). Sulfides occur as disseminations in intrusive rock, as minor inclusions in quartz veins, and massive millimeter to >30cm thick sulfide veins. The principal sulfides are pyrite and arsenopyrite. Other common sulfides previously noted include jamesonite, stibnite, galena, and sphalerite. Also noted have been aurostibite (Di Prisco, 2013); bismuthenite and Bi-Te-S minerals (McCoy and Olson, 1997); and chalcopyrite, tetrahedrite, and pyrrhotite (Abrams and Giroux, 2013). Trace minerals are usually present as <10-20-micron inclusions in pyrite and arsenopyrite. The non-sulfide mineral scheelite ($CaWO_4$) occurs sporadically (Abrams and Giroux, 2013). Some of these mineral identifications (e.g., jamesonite) are based on hand specimen identification.

The purpose of this chapter is to better describe the various ore minerals present and their textures and intergrowths. I hope to use the minerals present to better understand the conditions of ore deposition. Table 3-1 is a summary of my observations concerning sulfide and associated minerals.

3.2 Sulfides

Pyrite and Pyrrhotite

Pyrite occurs as coarse euhedral grains or as "ragged" pyrite. Microprobe EDS and WDS analysis shows the pyrite is commonly arsenian (up to 7 weight percent As substituting for S), and commonly displays zoning with As-enriched rims. "Ragged" pyrite is composed of multiple grains of smaller pyrite crystals that appear to have annealed into a single larger mass. These smaller pyrite grains display irregular and complex As zoning. As-zoned pyrite commonly contains inclusions of arsenopyrite, boulangerite, chalcostibite, chalcopyrite, pyrrhotite, sulfosalts, and (or) rare gold in zones of low As (Figure 3-1), surrounded by As-rich, inclusion-free pyrite. Approximately 2/3 of the pyrite grains I analyzed by EPMA contain detectable (> 0.2%) As.

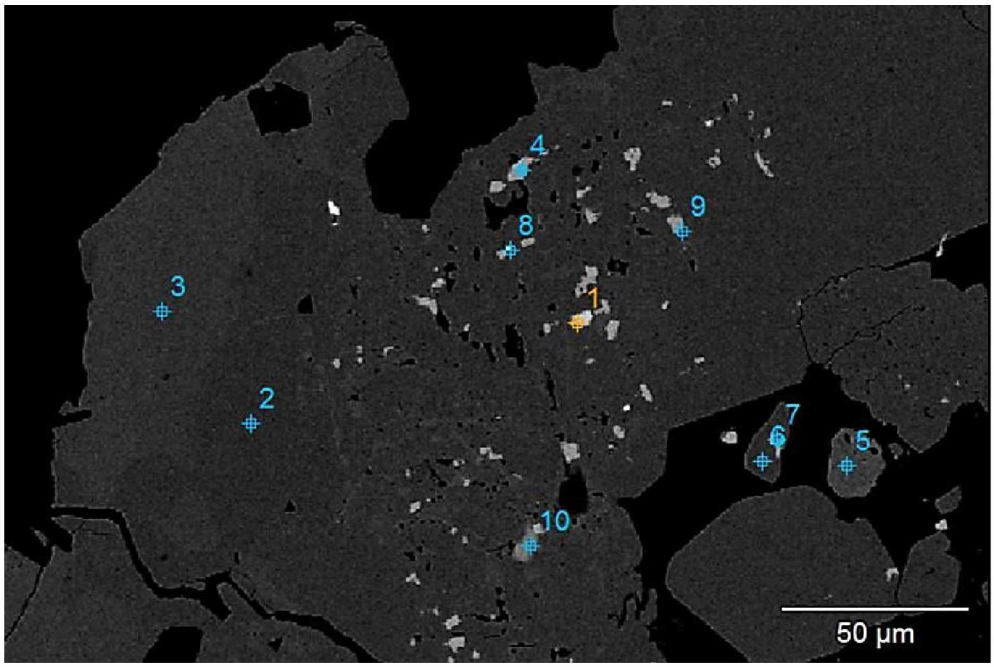

Figure 3-1: Backscatter electron (BSE) image of zoned arsenian pyrite with gold and sulfide inclusions 1) Chalcostibite 2) Pyrite 3) Arsenian Pyrite 4) Arsenopyrite 5) Zircon 6) Pyrite 7) Arsenopyrite 8) Gold 9) Arsenopyrite 10) Sphalerite. The brighter shaded rim of the pyrite grain contains 3.7 wt% As while the darker core contains <0.01% As.

Pyrrhotite is considerably less common than pyrite and is typically present as inclusions in arsenopyrite. It is present in significant abundance in several slides that contain secondary biotite with little additional alteration overprint, however.

Arsenopyrite

Arsenopyrite ($FeAs_{1-x}S_{1+x}$) is euhedral, fine- to coarse-grained, and occurs as isolated grains, intergrowths with pyrite, and microscopic inclusions in pyrite. I identified two types of arsenopyrite at Dolphin (Chapter 4). One type contains extensive compositional zoning with variations of up to 11 atomic % As in a single grain. This type of arsenopyrite carries Au in solid solution (chapter 4). The other type of arsenopyrite displays limited compositional zoning (usual range of 0.5-1 atomic % As) and does not contain appreciable Au. Arsenopyrite contains a variety of inclusions, but most notably pyrrhotite.

Stibnite- Bismuthinite

Stibnite (Sb_2S_3) is common in drill core from plutonic rock at Dolphin. It occurs as elongate needles microns to millimeters long, and as disseminated grains to massive accumulations. EDS analysis of stibnite shows variable Bi values, i.e., solid solution between stibnite and bismuthinite (Bi_2S_3; Figure 3-2). Lueth et al. (1990) showed that in a zoned vein system the bismuth-rich mineral precipitated early, near the fluid source, and the Sb-rich mineral precipitated later, and more distally. However, I found both $(Sb,Bi)_2S_3$ and Bi_2S_3 in the same sample in several cases (Table 3-1).

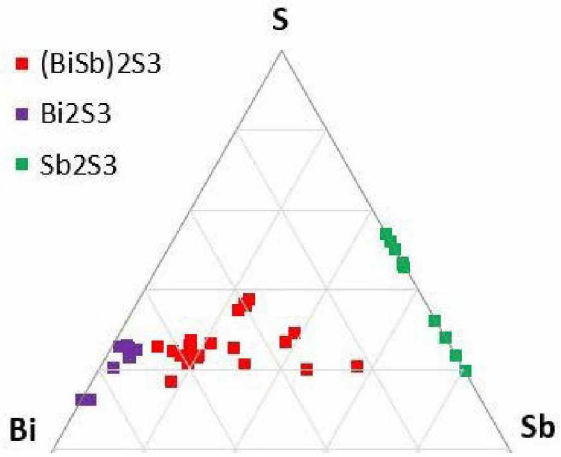

Figure 3-2: Upper half of a ternary diagram showing composition of stibnite-bismuthinite minerals present at Dolphin.

Bi-Te minerals

I identified numerous Bi-Te ± S minerals in thin gold-bearing sulfide veins and as inclusions in pyrite. Plotting these minerals on a ternary diagram (Figure 3-3) shows the sulfides to be primarily bismuthinite, joseite-B, tetradymite and hedleyite (Figure 3-4). The Bi-Te minerals are representative of earlier, higher temperature low fS_2 mineralizing events, with Bi-Te-S minerals forming later under lower, higher fS_2 events.

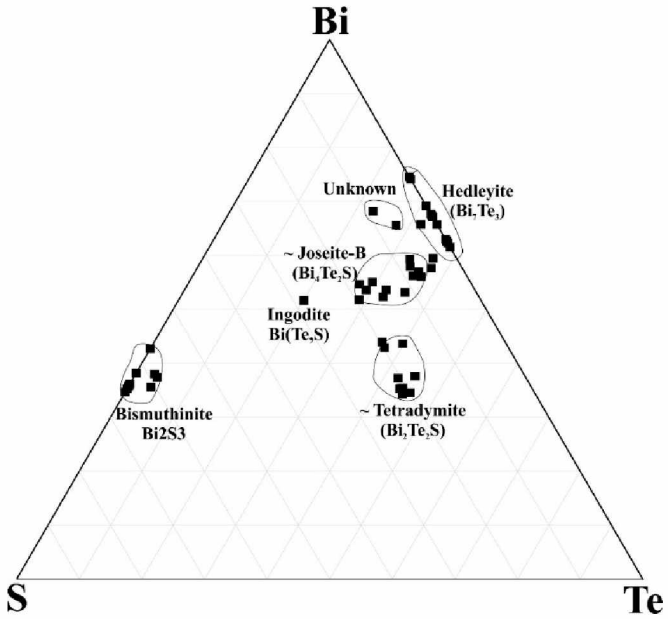

Figure 3-3: Ternary diagram showing composition of Bi-Te-S minerals at Dolphin. Modified from Cook et al., 2007.

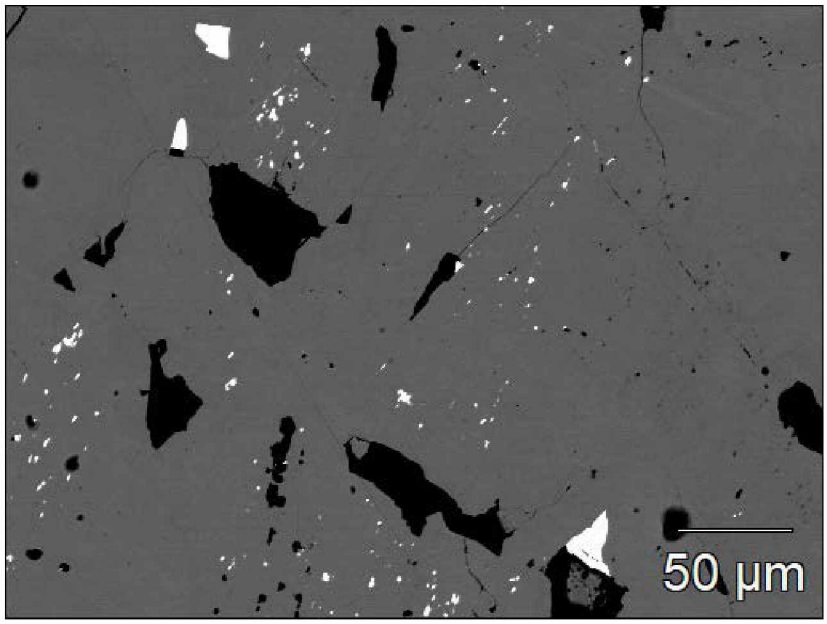

Figure 3-4: Backscatter electron (BSE) image of hedleyite (Bi_7Te_3) inclusions (bright) in pyrite (dark) from sample GSDC1130-222.

Lead and Antimony minerals

The primary lead-bearing minerals at Dolphin are boulangerite ($Pb_5Sb_4S_{11}$) and galena (PbS). Boulagerite is common in Dolphin and occurs as disseminated crystals in intrusive rock, inclusions in pyrite and in semi-massive sulfide zones. It has traditionally been logged at Dolphin as jamesonite ($Pb_4FeSb_6S_{14}$), which is nearly identical in hand specimen and reflected light microscopy. My EDS analyses show that boulangerite is common and jamesonite is rare. Other rare Pb sulfosalts contain Pb ± Bi ± Sb ± Ag + S; these have all been identified from a single sample taken from a thin gold-sulfide veinlet. Gudmundite (FeSbS) was present in a single sample, intergrown with aurostibite and partly enclosed by arsenopyrite.

Copper Minerals

The primary copper minerals at Dolphin are chalcostibite ($CuSbS_2$) and chalcopyrite ($CuFeS_2$) with rare tetrahedrite $Cu_6[Cu_4(Fe,Zn)_2]Sb_4S_{13}$ and freibergite ($Ag_6[Cu_4Fe_2]Sb_4S_{13}$), which is Ag-rich tetrahedrite. High Sb-Cu correlation coefficients (see ahead) in high grade gold intercepts indicate that tetrahedrite and (or) chalcostibite are common in gold-rich materials. I identified chalcostibite inclusions in pyrite which also contains Au° inclusions. Complex copper minerals are primarily seen as inclusions in pyrite; chalcopyrite is common as inclusions in sphalerite.

Table 3-1: Sulfide and associated minerals seen in Dolphin thin sections

x = EDS o = reflected light	Pyrite	Barren ASP	Auriferous ASP	Pyrrhotite	Au°	Aurostibite	Maldonite	Bi°	Bismuthenite	(BiSb)2S3	Stibnite	Boulangerite/Jamesonite	Galena	Chalcopyrite	Cu-Sb-Fe-S(Ag)	Tetradymite	Sphalerite	Bi-Te minerals	Bi-Te-S minerals	Bi-Sb-S(Ag)	FeSbS (Gudmundite)	Freibergite	Pb-Bi-Sb-S(Ag)	Pb-Sb-S(Ag)	PbSbTeS	Silicate
1132-1469	x	?	?	X	x	x					x															b
1132-1480	x	?	?	X		x					x											x				b
1132-49	x	?	?		x																					k
1135-503.8	x	x		x	o							x	x	x			x					x				k
1135-550	x	x		x	x				x				x			x								x		k
1148-257	x	x			x							o		x	x		o									k
1148-527	x	x			x				x	x		x	x	o		x										k
1213-227.5	x	?	?		x																					k
1304-1685.5	x	x	x		o					x	x		x										x			k
1304-742	x	x	x		x							x												x		k
TLD0404-367.5	x		x																							k
TLD0404-368	x		x																							k
TLD0404-372	x		x																							k
1129-273	x	x			x							x	x	x	x	x				x			x	x		
1129-401	x	x	x	x									x											x			
1130-222	x	x			x		x	x	x	x	x	x	x			x		x	x	x			x	x	x	
1130-273																x			x							
1130-314.5	x	x			x					x		x				x			x							
1130-328.5	x	x		o	x	x	x	x						x		x		x	x							
1132-1449.5	x	?	?		x																					
1132-1468.5	x	?	?		x	x																				
1135-411	x	x								x		x								x				x		
1148-1510.5	x		x		x							o	x													
1213-439.9	x	?	?		x								x				x							x		
1218-608.5	x	?	?		x																					
1304-1429	x	x		x	x	x						x	x	x	x									x		
1304-1752-1	x		x	x										o												
1304-1754		x		o	x	x						o	x							o?	x					
TLD0404-358	x		x																							
TLD0404-378	x	x	x																							

Notes: x = mineral identified in EDS. o = mineral only identified in reflected light. b = secondary biotite, k = kaolinite.? = arsenopyrite identified, of unknown type.

3.3 Visible Gold and Gold Minerals

Gold at Dolphin occurs as fine- to coarse-grained inclusions in low-sulfide quartz veins, in sulfide-carbonate ± quartz veinlets, as fine-grained (<1-50 μm) inclusions in disseminated pyrite and arsenopyrite, and as solid-solution in compositionally zoned arsenopyrite (see chapter 4). Visible gold occurs primarily as native gold (Figure 3-5; Figure 3-6) or a mixture of Au^o + Bi^o resulting from maldonite exsolution. Maldonite (Au_2Bi) and aurostibite ($AuSb_2$) are less common.

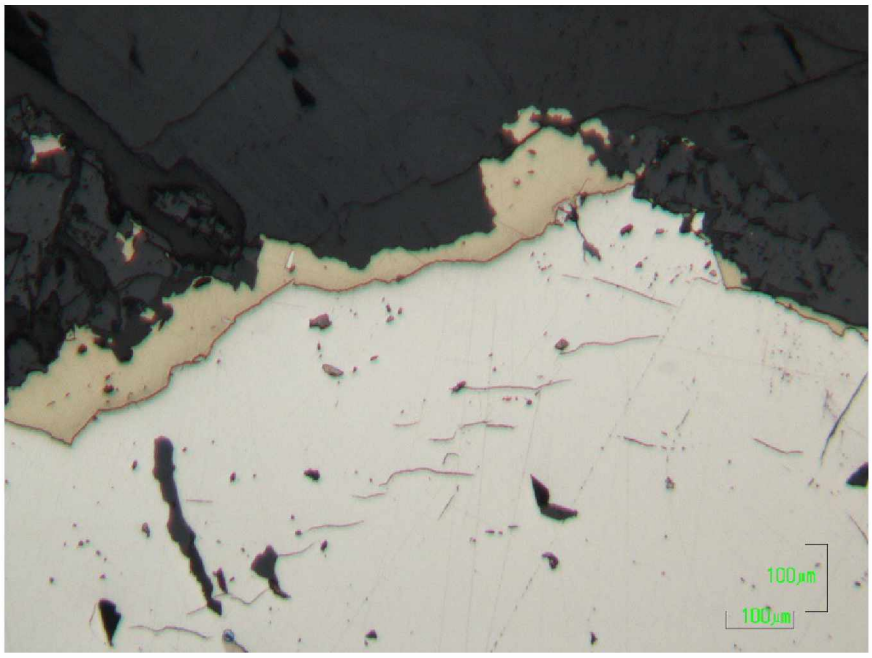

Figure 3-5: Reflected light photomicrograph of gold rimming pyrite grain

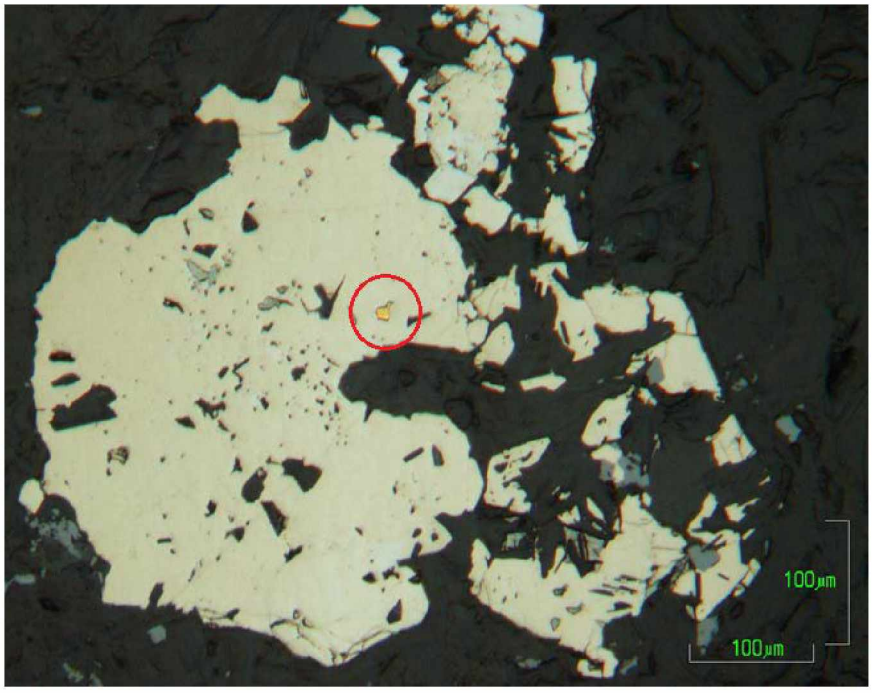

Figure 3-6: Reflected light photomicrograph of "ragged" arsenian pyrite with Au^o inclusion (red circle) in pyrite and sulfosalt (gray) inclusions.

3.4 Discussion

3.4.1 Sulfides

The sulfide assemblages identified in samples displayed in Table 3-1 provide evidence of two mineralizing events. The minerals Au_2Bi, $AuSb_2$, Bi-Te, Bi, FeS, and FeSbS are products of a low fS_2 mineralizing fluid. Gudmundite (FeSbS) in particular has a maximum temperature of 280 °C (Seal et al., 1992) and is only stable at low fS_2 (well below pyrite stability). It decomposes by reactions such as $2FeSbS + 5/2S_2 = 2FeS_2 + Sb_2S_3$. Sulfur fugacity must have increased dramatically to make pyrite stable. Under such conditions maldonite and aurostibite are not stable: maldonite (Au_2Bi) exsolves to Au° + Bi° ➔ Bi_2S_3 and aurostibite to Au° + stibnite (Sb_2S_3). Hydrothermal kaolinite is only stable below 300° C (see section 2.7.8) and is always present with pyrite; the lack of aurostibite and maldonite in samples with kaolinite are consistent with a major change in the fluids that led to both an increase in pH and in fS_2 at a temperature of about 300°C.

The high sulfide content in the pluton differentiates Dolphin from other Alaskan Intrusion-related gold deposits (IRGDs), including the nearby Ft. Knox deposit. Although less than 10 km from Fort Knox and of essentially the same age (McCoy and Olson, 1997), Dolphin contains much higher % sulfides than Fort Knox. Anomalously high Pb, Ag, and Sn compared to other interior Alaskan IRGDs (Table 3-2) is also unique to Dolphin.

Table 3-2: Average metal concentrations (ppm) for some Alaskan IRGDs

Deposit	Reference	Ag	Sn	As	Sb	Pb	%S	Cu	Zn
Shotgun	1	3	3	3200	20	12	0.2	700	70
Donlin	2	1.9	6	4400	140	32	1.2		90
Livengood	3	0.4	5	2200	220	19	1.4	42	190
Dolphin	4	5.4	30	1350	120	420	0.7	24	220

References: 1 = Rombach & Newberry (2001), 2 = Goldfarb et al. (2004), 3 = Cutner et al. (2013), 4 = this study

This high sulfide content combined with the extensive low-temperature (T < 300°C) hydrothermal alteration (section 2.7) suggest that Dolphin is a shallow expression of an IRGD system.

3.4.2 Relations between alteration and gold mineralization

Ideally there would be some straightforward relationship between the type (and intensity) of hydrothermal alteration and the gold concentration. Unfortunately, examination of the data does not reveal any simple pattern. The strongest correlation is between Ag and Pb, consistent with the anomalous

abundance of both elements (Table 3-2) at Dolphin. Correlation coefficients for the highest 156 gold grade intercepts from granite (all intercepts >0.5ppm Au) show strong correlation between Au and Bi, Ag and Pb and Cu and Sb (Table 3-3). Au and Bi correlation is likely the result of maldonite or Au°+Bi° as the result of exsolution of maldonite, both of which have been identified in reflected light and EDS. Tetrahedrite and (or) chalcostibite are common in gold rich intercepts which are both Cu + Sb bearing minerals. Chalcostibite and Au° inclusions are commonly identified together in pyrite through EDS. Ag and Pb commonly occur together in Pb-sulfosalts and argentiferous galena.

Table 3-3: Correlation coefficients among elements for the highest Au grade Dolphin granite intercepts.

	Au	*Ag*	*Be*	*Ca%*	*Cd*	*Cu*	*Fe%*	*Mg%*	*Pb*
Bi	**0.94**								
Cd		**0.69**							
Cu		0.43							
Fe%		0.59			0.59	**0.73**			
Mg%			0.62	0.61					
Mn			0.43	0.59				0.68	
Pb		**0.82**			0.56	0.61	0.67		
Sb		0.45				**0.95**	**0.71**		**0.71**
Zn		0.61			**0.68**				0.42

Figure 3-7 shows gold concentrations vs. wt % Na_2O, with alteration regions as distinguished in the Na_2O vs. K_2O diagram. The reason for lack of correlation between gold and any major element (Table 3-3) is evident: there is no obvious pattern of relationship between a particular alteration type (recognizable by Na_2O contents) and gold concentration. All three of the major types are associated with a wide variety of gold concentrations.

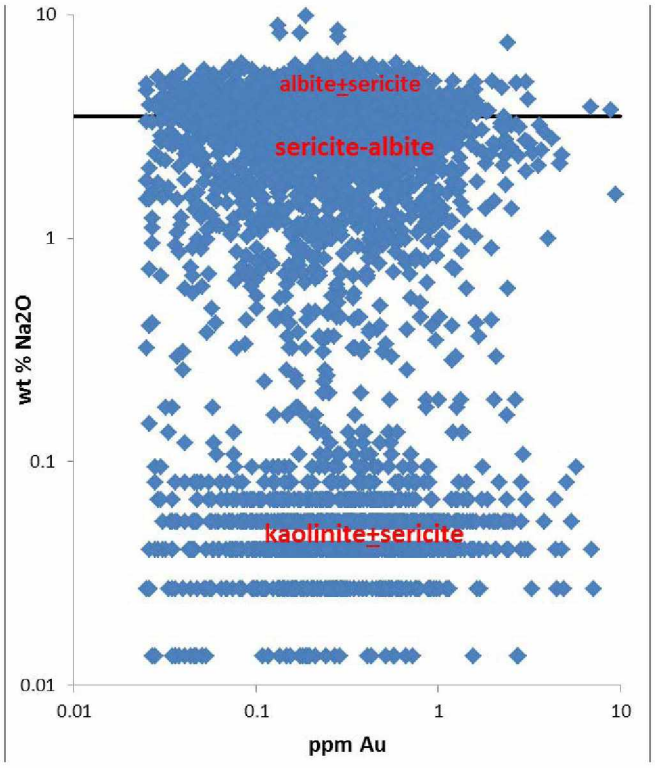

Figure 3-7: Na_2O vs. ppm Au for ~3500 Dolphin altered granitic rock drill core 4-Acid Digest multi-element analyses. No one alteration type is exclusively associated with either high or low Au concentrations

Data from drill hole 1127 (Figure 3-8, left) may show some part of the solution: a thick (150') zone of albitic alteration (zero kaolinite) between 0 and150' depth shows modest gold concentrations, but the higher concentration zones are deeper in the hole, where there are rapid alternations between high and low kaolinite zones. Drill hole 0404 (Figure 3-8, right) appears to show similar patterns of higher gold grades associated with sharp changes in calculated kaolinite abundance.

Another perspective on alteration-mineralization can be seen by the spatial pattern in average gold concentration in drill holes that contain mostly Dolphin pluton (Figure 3-9A). No attempt has been made to determine average gold concentrations above a particular grade cut-off; rather, the average grade has simply been calculated for the granitic rock intervals in each drill hole. Comparing the patterns for average gold concentration to the patterns of tonalite abundance (Figure 2-3) and alteration types (Figure 2-21) indicates that the highest average grades are in the two drill holes with abundant kaolinite-sericite alteration and some tonalite. However, several drill holes with both abundant kaolinite-sericite alteration and abundant tonalite also have low average gold concentrations. Further, many of the drill holes with moderate average gold concentrations, in the middle of the body, contain only granite (no tonalite) and abundant albitic (high Na) alteration with little kaolinite-sericite. One possibility is that much of the gold present was originally deposited with the presumably higher-temperature, lower fS_2, and earlier albite-

sericite alteration, and then variably remobilized during later and lower-temperature kaolinite-sericite alteration.

Figure 3-9B shows that the As distribution largely reflects the gold pattern; presumably because gold commonly occurs as inclusions in arsenopyrite and in gold-enriched arsenopyrite (chapter 4). Higher concentrations are present at the north edge of the pluton. The pattern for Pb (Figure 3-9C) is significantly different; the area of highest Pb partly overlaps that of highest Au & As but is mostly well south of the northern pluton margin. The zone of highest Pb matches best with area of strong kaolinite alteration, between the central and easternmost cross-section lines. This clearly indicates that base metal mineralization (as indicated by Pb) is distinct from gold-rich mineralization at Dolphin. Finally, the W distribution map (Figure 3-9D) is the least similar to the Au-As maps. The zone of highest tungsten has a distinct N-S orientation that closely matches the zone of strong kaolinite alteration. In porphyry Mo deposits, highest tungsten is associated with sericitic alteration; perhaps a similar phenomenon happened at Dolphin.

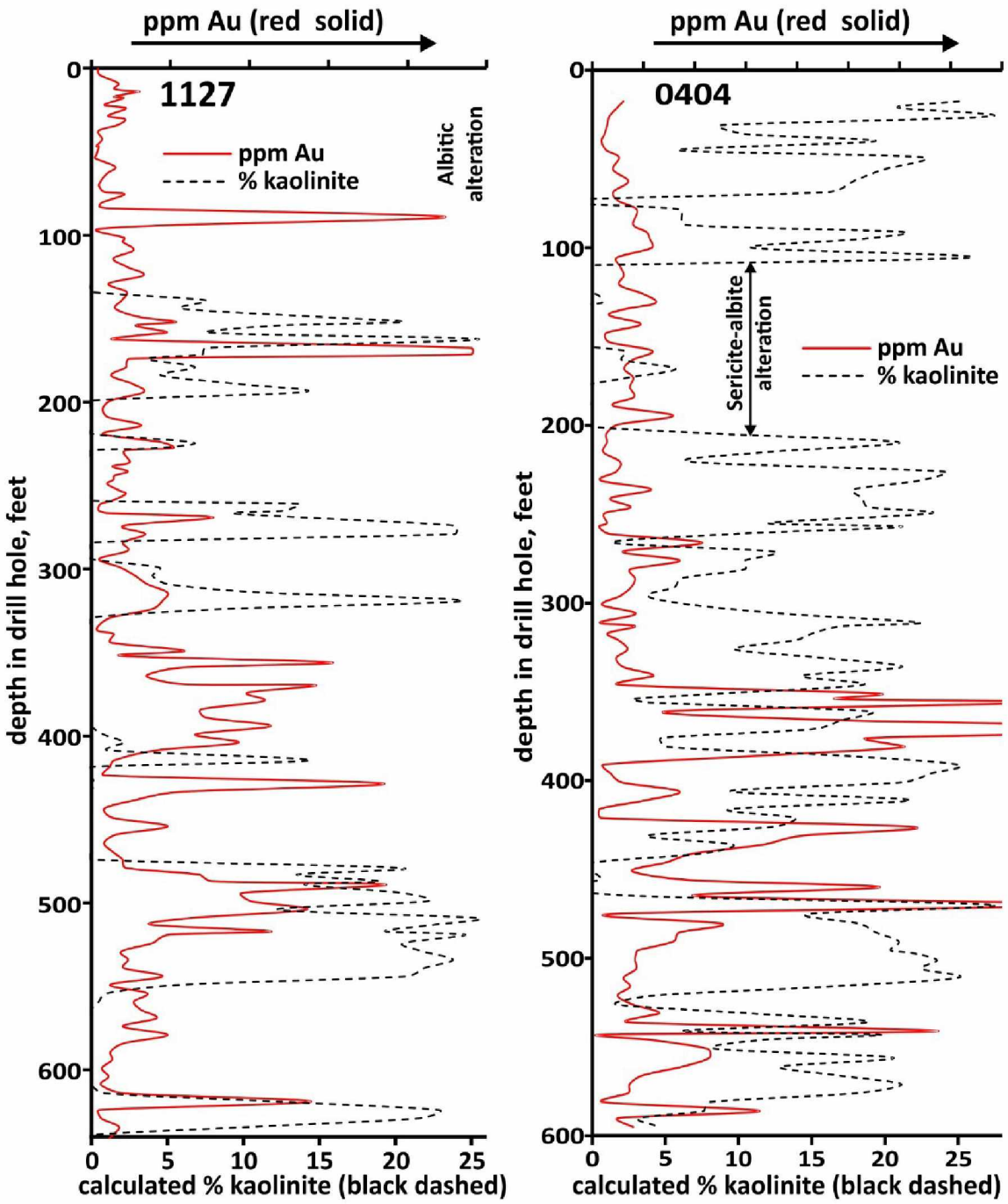

Figure 3-8: Calculated % kaolinite (black dashed) and ppm Au (solid red) vs. depth in drill holes GSDC1127 (left) and TLD0404 (right). 1127 is from the westernmost cross-section, in a region dominated by albitic alteration; 0404 is from the easternmost cross-section, where kaolinite-rich alteration dominates. Both show complex patterns, but higher gold concentrations are commonly at depths where major changes in % kaolinite take place.

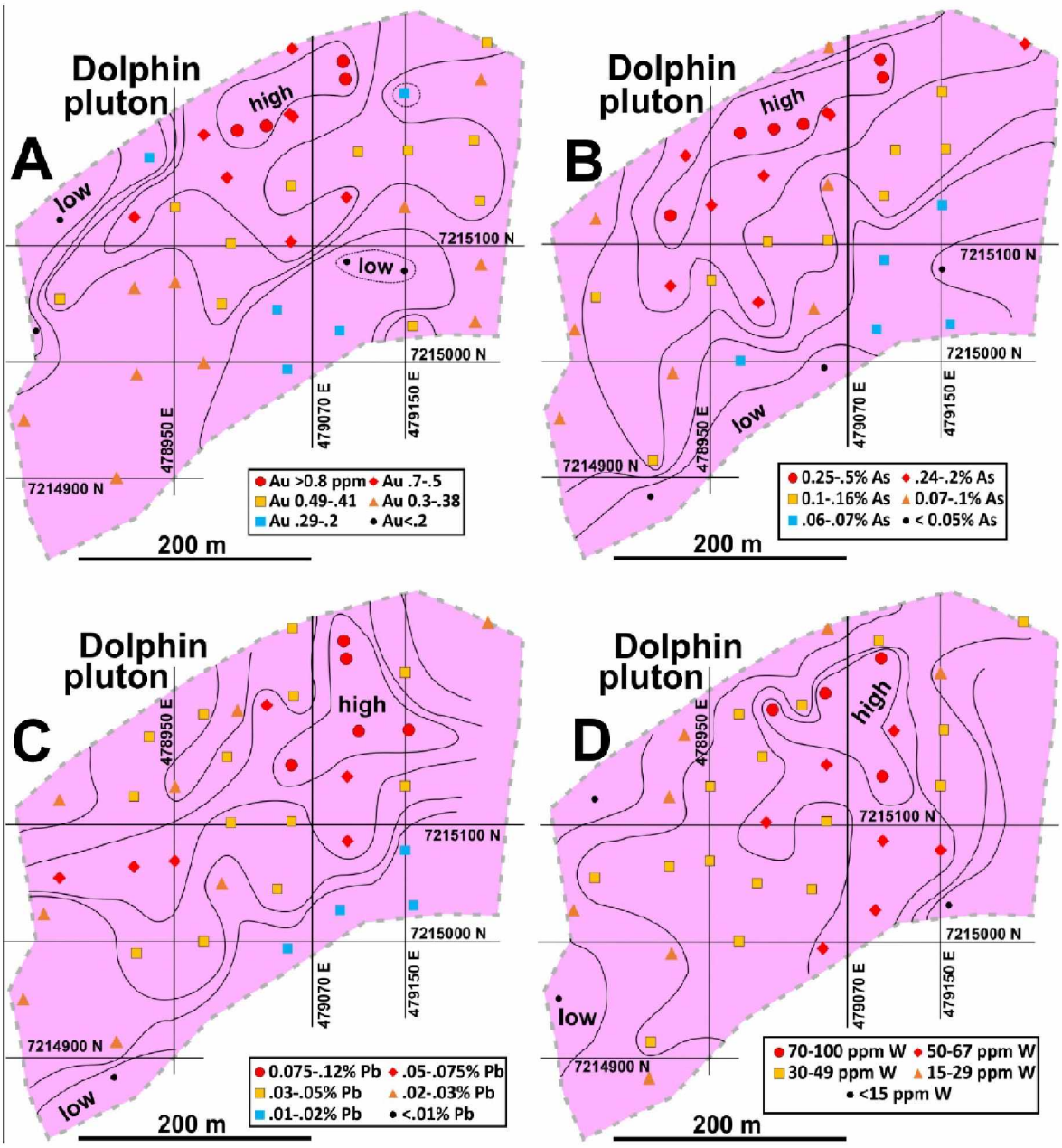

Figure 3-9: Average concentration in granitic parts of drill holes containing mostly Dolphin pluton, as indicated by drill core logs (where available) and (or) 4-acid digest compositions. A larger number of drill holes were used for this compilation, as all holes were analyzed for gold and many of the earlier holes were analyzed with a 2-acid digest multi-element technique. This digest doesn't dissolve silicates but does dissolve all sulfide minerals (and scheelite) and yields accurate results for most common ore elements. A= gold, B= arsenic, C= lead, D= tungsten

Figure 3-10 shows gold grade modified from Abrams et al. (2016) overlaid on a leapfrog model of alteration in granite and the granite-tonalite contact. Higher gold grades are largely restricted to the area immediately around the granite-tonalite contact. This contact could have provided a fluid pathway for fluids to transport and precipitate Au and associated arsenopyrite. This physical relationship suggests that

the volume of fluid flow, along that structural pathway, was more important than alteration per se in determining gold deposition. Unfortunately, there are no drill holes from the immediate vicinity of the northern contact for which I have compositional data so as to gauge alteration. The gap in alteration shown on the cross-section close to the contact is due to lack of information. It might be possible to go back to holes that were drilled close to the contact and extract alteration information.

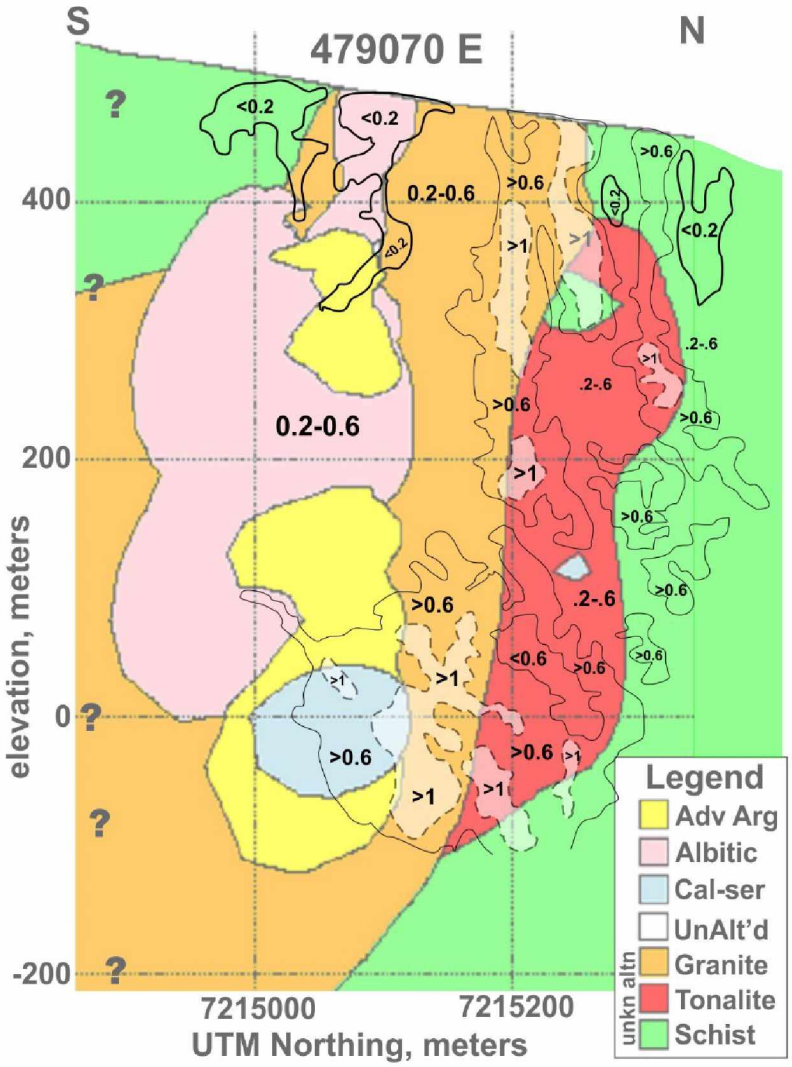

Figure 3-10: Cross section showing gold grades (g/t, modified from Abrams et al., 2016) overlaid on the alteration cross section from section 479070 east. Zones of higher grade gold (outlined in dashed lines and labeled >1) are generally present at or near the granite-tonalite contact and (or) the contact between tonalite and metamorphic rocks.

4 Sub-microscopic Au analysis

4.1 Introduction

I had a dozen polished thin sections made (plus another dozen I inherited) from Au-rich assay intervals, for which I intended to better characterize the occurrence and distribution of gold at Dolphin. Much to my chagrin, however, I was usually unable to find Au° in rocks from high-Au core intervals using both reflected light (all samples) and microprobe EDS (several samples). At the same time, I became aware of another study of Dolphin materials (Di Prisco, 2013) where the same difficulties finding Au° in polished sections from Au-rich core assay intervals were encountered. Finally, studies of gold recovery from Dolphin materials became available (e.g., Abrams et al., 2016) that indicated much of the gold was not readily extractable—indicating that much of it was not simple grains of Au°. All this data pointed to the likelihood of 'invisible' (AKA 'sub-micron' or 'refractory') gold at Dolphin.

Such gold is present as some combination of (a) grains too small to be visible in reflected light, i.e., < 1 micron, and (b) gold present in solid solution in sulfide minerals. Depending on the grain size, one might be able to find gold of the first type with the microprobe as isolated high gold concentrations. Depending on the concentration, one might be able to find the latter type by performing highly sensitive wavelength-dispersive EMPA analyses on appropriate minerals.

Dozens of papers have been written about invisible gold in sulfides (e.g., Cabri et al.,, 1989; Cook & Chryssoulis, 1990; Fleet et al., 1993; Yang et al., 1998; Genkin et al., 1998; Ashley et al., 2000). The consensus is that gold mostly occurs in solid solution in arsenian pyrite and in arsenopyrite, but also as tiny Au° particles. Considerable debate in the literature concerning the manner of that solid solution is built around the problem of the oxidation state of Au, which effects charge balance in the mineral. Based on Mossbauer spectroscopy, however, Yang et al. (1998) showed that gold in sulfide solid solution is neither Au^{+} nor Au^{3+}, but rather is covalently bonded and formal oxidation state is meaningless. They propose substitution of neutral $AuAs_2^0$ clusters for $FeAsS^0$ and FeS_2^0 clusters in arsenopyrite and pyrite, and consequently side-step the question of oxidation states for any of the components.

Arsenopyrite is a complicated mineral. Its formula is usually given as FeAsS, but many compositional studies show that the formula $FeAs_{1-x}S_{1+x}$ better describes the mineral. Based on experimental studies (e.g., Kretschmar & Scott, 1976), arsenopyrite composition varies with $\log f S_2$ and temperature (Figure 4-1). Arsenopyrite that grew in equilibrium with pyrite always contains less than 33 atomic % As and shows a simple relationship between composition and temperature of formation (Figure 4-1). Arsenopyrite is known to be one of the most non-reactive sulfide minerals; it retains its original composition despite conditions changing around it (e.g. Kretchmar & Scott, 1976). Consequently, it is

employed as a geothermometer, but with the proviso that it yields temperatures of original formation, not temperature of last conditions.

My investigations into the problem of sub-microscopic gold at the Dolphin deposit used several analytical tools and strategies. Following visual non-identification of gold in polished materials, I needed to ensure that the thin section actually contained significant gold concentrations. That is, just because a 5-foot core interval yields an average gold concentration of (say) 1 ppm, there's no reason to think that every thin-section sized piece of core from that interval contains that concentration. I assumed that gold accompanies sulfides, but not knowing which sulfides complicates pulling out gold-rich samples for further study. I investigated such by performing high-sensitivity XRF analyses for Au on the 'billets' used to make the sections (where available) and directly on the thin sections where billets were not available. After my initial studies, I used that XRF routine to screen potential additional slabs to ensure that they contained significant gold concentrations before having them made into polished thin sections.

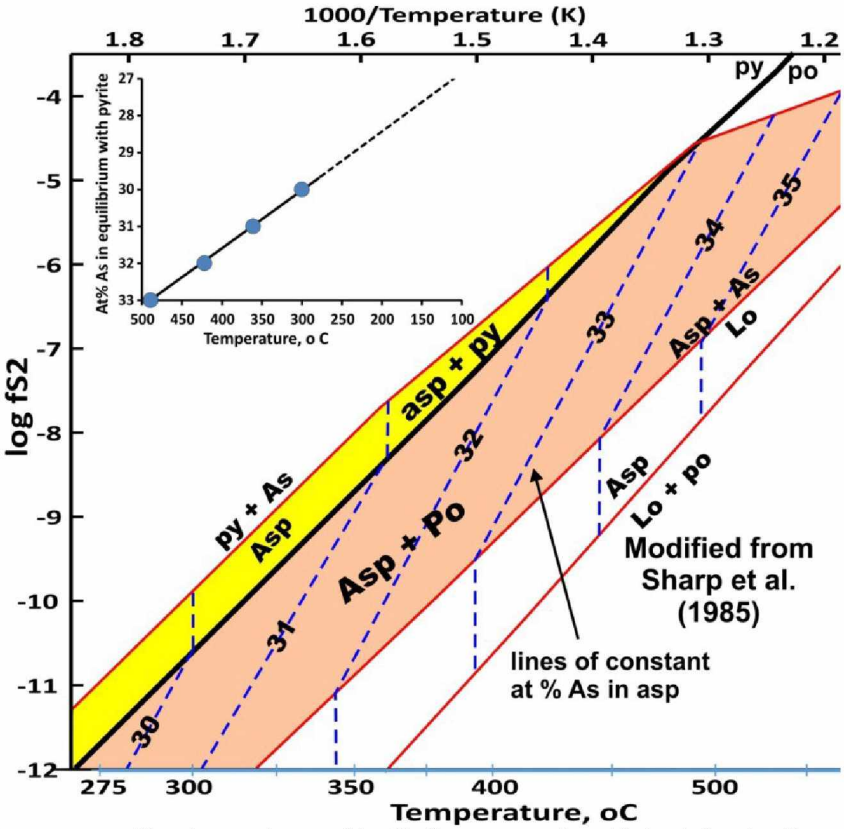

Figure 4-1: Relations between composition, temperature, and logfS_2 for arsenopyrite, with inset showing linear relation between temperature and composition for arsenopyrite formed with pyrite. Modified from Sharp et al. (1985), who used the diagram from Kretschmar & Scott (1976), with isopleths vertical in the pyrite-stable field. Note that arsenopyrite with less than 28 atomic % As yields an impossibly low temperature; such compositions are not typically observed.

Following the identification of likely candidate samples, I used the Laser Ablation ICP-MS at UAF-AIL on one sample to investigate gold concentrations in sulfide minerals. I found evidence for anomalous gold concentrations in arsenopyrite and pyrite in that sample, but also recognized the limitations of that approach. The biggest single problem is that the technique creates 10-micron wide trenches through a sample, and (given the small size of many Dolphin sulfide minerals) basically obliterates the mineral. One cannot 'go back' and re-analyze the same area twice. The other problem is that one can't get accurate major element compositional information with the LA-ICP-MS, that is, one can determine the Au concentrations in arsenopyrite, but not the As-Fe-S concentrations. (Indeed, one has to assume a major element concentration (e.g., Fe) and then use the Au/Fe ratio with the major element to determine the Au concentration.)

Once I determined that sulfide minerals in the Dolphin deposit at least locally contain several hundred ppm gold, I resolved to create a microprobe routine that would allow me to perform repeated analyses and for which I could simultaneously determine major element and gold concentrations in sulfide minerals. Once I created a routine that I felt sufficiently confident in, I analyzed gold and major element concentrations in arsenopyrite (and some pyrite) from 30 samples from the Dolphin intrusion. These samples were taken from nine different drill holes and represent a variety of spatial locations, depths, associated alteration types, and host rocks (although most were taken from Dolphin granite).

4.2 Methods

4.2.1 X-Ray Fluorescence

I began by 'cannibalizing' an existing routine for trace concentrations of gold by XRF but found that it yielded somewhat unreliable results, tested against pressed pellets made from pulverized, certified low-level gold standards. The problem was that the most intense gold peak—the Lα line—is very close to the energy of a large-intensity W line, a smaller intensity Zn line, and a very small intensity Pb line. Assays of Dolphin core indicate W concentrations > 1000 ppm are relatively common and scheelite can be seen in many samples with a UV light. Also, XRF scans of high-purity silica blanks show small tungsten peaks, which means that the Rh filament which generates X-rays contains small amounts of W. Sphalerite is variably common in the ore and both galena and Pb-sulfosalt minerals (Chapter 3) are also variably abundant. I eventually gave up on using the highest intensity Au line and settled for the lower intensity Lb line. This suffers from interferences from As, W, and Pb, but none of the peaks are particularly close to the Au Lb peak. Additional complications include the problem that standard thin section glass contains approximately 0.1% As, but eventually the various interferences were dealt with for the final routine. To get detection limits as low as possible, a count time on the gold peak of 998 seconds (17 minutes) was employed. The theoretical lower limit of detection (LLD) based on counting statistics is

approximately 0.3 ppm but replicates of blanks indicate it's closer to 1 ppm. I prepared polished surfaces on slabs prior to analysis and kept the sample spinning during analysis to even out concentration inhomogeneity in the samples. Each sample was analyzed 3 times and the results averaged.

Analyzing polished thin sections is problematic because the X-ray penetration distance (employing 60 kv conditions) is significantly greater than the thickness of a standard thin section (30 microns). Consequently, the observed concentrations are significantly smaller than they would be for a rock of the same composition, but greater thickness. To adjust for this effect, polished thin sections with available billets (other part of the rock cut off as part of the thin section preparation) were analyzed. The results (Table 4-1, left) show a relatively consistent proportionality between billet and thin sections. They also show that both billet and thin sections which lack visible gold contain appreciable gold concentrations. Using the proportionality factor from thin sections to billets, the 'effective' gold concentrations for those polished thin sections (for which I lacked billets (Table 4-1, right)) were calculated. Numerous thin sections yielded significant gold concentrations despite lack of visible gold.

Table 4-1: XRF compositional data for billets and polished thin sections from the Dolphin deposit

sample #	**Au conc. (ppm)**		**observed**		**sample #**	**Au conc. (ppm)**	**observed**
	billet	**thin section***				**thin section****	
1138-4	1	1	no Au°		**1132-1469**	**7**	**many Au°**
1138-8	2	**1**	no Au°		**1132-1480**	**4**	**some Au°**
1138-8	4.1	2.2	no Au°		**1132-49.5**	**2**	**1 big Au°**
1138-9	3	1.9	no Au°		1132-316	2	no Au°
1138-10	**11**	4.3	no Au°		9801-41	**5**	**several Au°**
1138-11	**5**	**3.5**	**several Au°**		9801-111	7	no Au°
1138-13	4	3.2	no Au°		9801-280	2	no Au°
1138-15	1	1	no Au°		9801-282	2	no Au°
1313-580	**102**		**many Au°**		9801-302	3	no Au°
9801-865.5	4		no Au°		9801-388'	4	no Au°
					9801-805	7	no Au°

*value is the measured concentration; lower than the billet because the thin section is thinner than the X-ray penetration distance;
**value is the calculated concentration for the rock from which the thin section was made.

4.2.2 LA-ICP-MS

Two arsenian pyrite and two arsenopyrite grains from sample 1138-10 were analyzed utilizing laser ablation inductively coupled plasma mass spectrometry (ICP-MS) to test for the presence of submicroscopic gold in the sulfides. The sample analyzed contained 11 ppm Au (as determined by XRF analysis, Table 4-1) but no obvious gold grains of any size as observed by reflected light microscopy and backscatter

electron spectroscopy (BSE). Several 100μm lines were ablated across the grains at 1μm/second. Gold concentrations were calculated based on average Au/Fe ratios measured on the artificial sulfide standard (MASS-1) combined with the Au/Fe ratios measured on the samples. Due to the destructive nature of the analysis and the unreliability of the equipment (various parts and pieces kept breaking), I did not pursue this technique past my initial analyses.

4.2.3 Wavelength Dispersive Spectrometry (WDS) Gold Routine

I created a wavelength dispersive spectrometry (WDS) routine for electron probe microanalysis (EPMA) using Probe for EPMA software. The routine was used to investigate and quantify elemental composition of gold bearing pyrite and arsenopyrite. The routine was performed on a JEOL JXA-8530F electron microprobe located in the Advanced Instrument Laboratory at the University of Alaska Fairbanks.

Probe conditions were set at 5-micron beam size at 15 KeV. A "combined conditions" routine was used where current was set at 500nA for Au analysis and then reduced to 100nA for Fe, As, and S analysis. Three spectrometers were set to detect the Au-Mα line simultaneously using TAP crystals. Analysis lasted for 300 seconds on peak and 75 seconds on each of 4 multipoint background off-peaks (two high and two low) for a total of 600 second analysis for Au. The Fe-Lα line was analyzed using a TAP crystal for 60.0 seconds on peak and 5.81 seconds for background off-peak high and low. The As-Lα line was analyzed using a TAP crystal for 60.0 seconds on peak and 4.74 seconds background off-peak high and low. The S-Kα line was analyzed using a PET crystal for 60.0 seconds on peak and 3.51 seconds background off-peak high and low. (Table 4-2). (Screenshots of routine setup windows can be found in Appendix 1).

Table 4-2: General Conditions employed for high-sensitivity Au EMPA Analysis

Channel	Element	Spectro	Crystal	On-Peak	Hi-Peak	Lo-Peak
1	au ma	1	PETL	300.00	75.00	75.00
2	au ma	2	PETL	300.00	75.00	75.00
3	au ma	3	PETL	300.00	75.00	75.00
4	s ka	4	PETL	60.00	3.51	3.51
5	fe la	5	TAPL	60.00	5.81	5.81
6	as la	5	TAPL	60.00	4.74	4.74

Standards used were: *C.M. Taylor Pyrite* for Fe and S, *C.M. Taylor Gallium Arsenide* for As, and *C.M. Taylor Gold* for Au. *ASP 200* (a natural arsenopyrite standard provided by S.D. Scott) was used as a blank correction sample assignment for Au in arsenopyrite and as a secondary monitoring standard. *C.M. Taylor Pyrite* was similarly used for the blank correction for Au in pyrite. Based on repeated analyses of

these two minerals, the lower limit of detection for gold is approximately 50 ppm in arsenopyrite and 60 ppm in pyrite. A total of 881 analyses were conducted on 36 pyrite and 121 arsenopyrite grains from 30 polished thin sections made from 9 different drill holes.

4.2.4 Laser Ablation ICP-MS

Representative examples of data for arsenopyrite (Figure 4-2A) and pyrite (Figure 4-2B) show that both yield gold concentrations above the detection limit of approximately 10 ppm which indicates submicroscopic Au is present. Arsenopyrite yielded much higher (up to 430 ppm) gold concentration than pyrite and—based on comparison with the BSE image for the grains--showed an apparent correlation with increased S (lower As). Pyrite yielded lower concentrations (maximum of 20 ppm) but also seemed to show higher Au concentrations with lower As (Figure 4-2B). Gold most likely occurs as solid solution in the sulfide, as the gold values occur in bands that correlate with major element composition (seen as darker shades in the BSE images). If the gold occurred as nanoparticles instead, one would expect abrupt narrow spikes in gold concentration that do not correlate with major element composition. Based on the results of this preliminary investigation, I proceeded to create the EPMA gold routine (section 4.2.2) to further investigate sub-microscopic gold in pyrite and arsenopyrite.

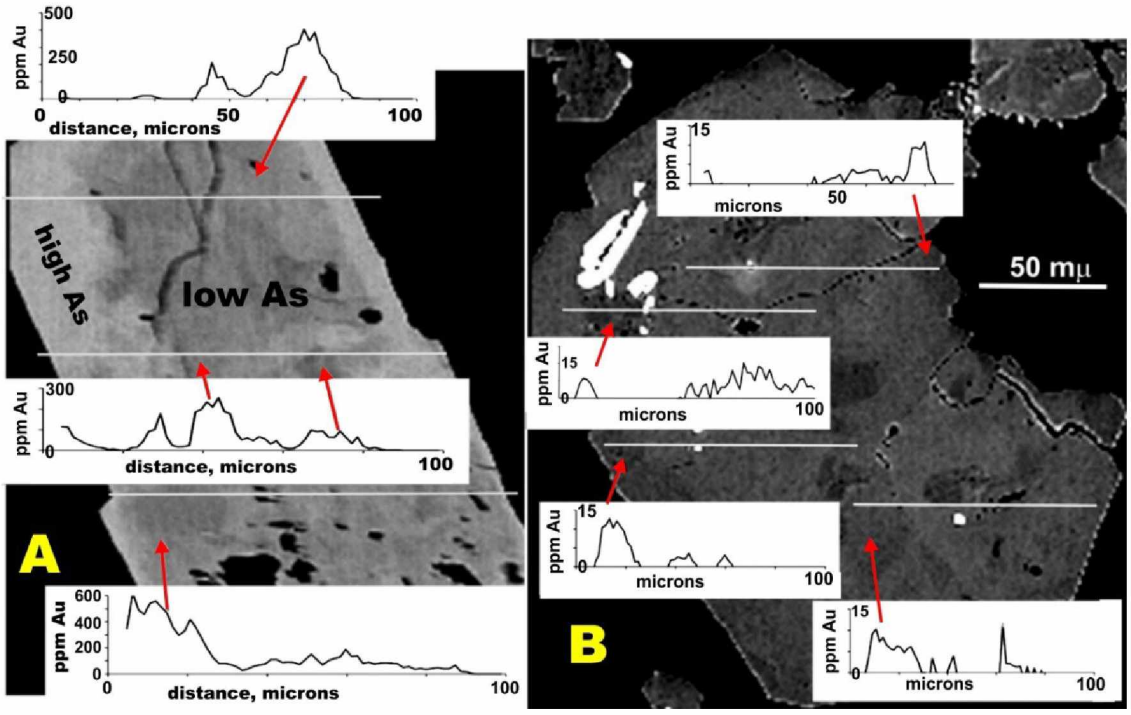

Figure 4-2:Gold values (ppm) across zoned arsenopyrite (A, right) and arsenian pyrite (B, left) from laser ablation ICP-MS superimposed on electron microprobe BSE images of the grains (pre-analysis). Brighter areas for both indicate higher As (lower S) concentrations. Black spots in the arsenopyrite are quartz inclusions. Bright spots in the pyrite are arsenopyrite inclusions. Darker areas (higher S) in both images appear to correlate with higher Au concentrations

4.2.5 Wavelength Dispersive Spectrometry (WDS)

Of the 121 arsenopyrite grains analyzed, sub-microscopic Au was detected (detection limit of 50 ppm) in 90. Table 4-3 gives summary characteristics for the arsenopyrite analyses. My EMPA data (Table 4-3) show there are two major compositional types of arsenopyrite in the Dolphin pluton: (1) an essentially unzoned, compositionally uniform, gold-absent, type, and (2) a strongly zoned, compositionally variable, Au-bearing type.

As illustrated by numerous grains in sample 1138-398, auriferous arsenopyrites commonly have a distinct pattern with a low As core, moderate As middle, and higher As rim. This zoning pattern is seen in backscatter electron (BSE) images with the brighter zones containing higher As (Figure 4-3). The cores of these arsenopyrites are barren and contain ~25-27.5 atomic % As. Au is restricted to the zone of moderate As, which surrounds the As poor core. This zone contains 28-31.6 atomic % As and up to 0.24% Au. Finally, an Au barren, As rich (~31.1-37 at %) zone commonly rims the arsenopyrite (Figure 4-3). Zoned arsenopyrite from other well-characterized samples yields similar compositions (Figure 4-4); that is, Au-bearing arsenopyrite displays a wide range of atomic % As, but is gold-bearing over a relatively restricted range in atomic % As.

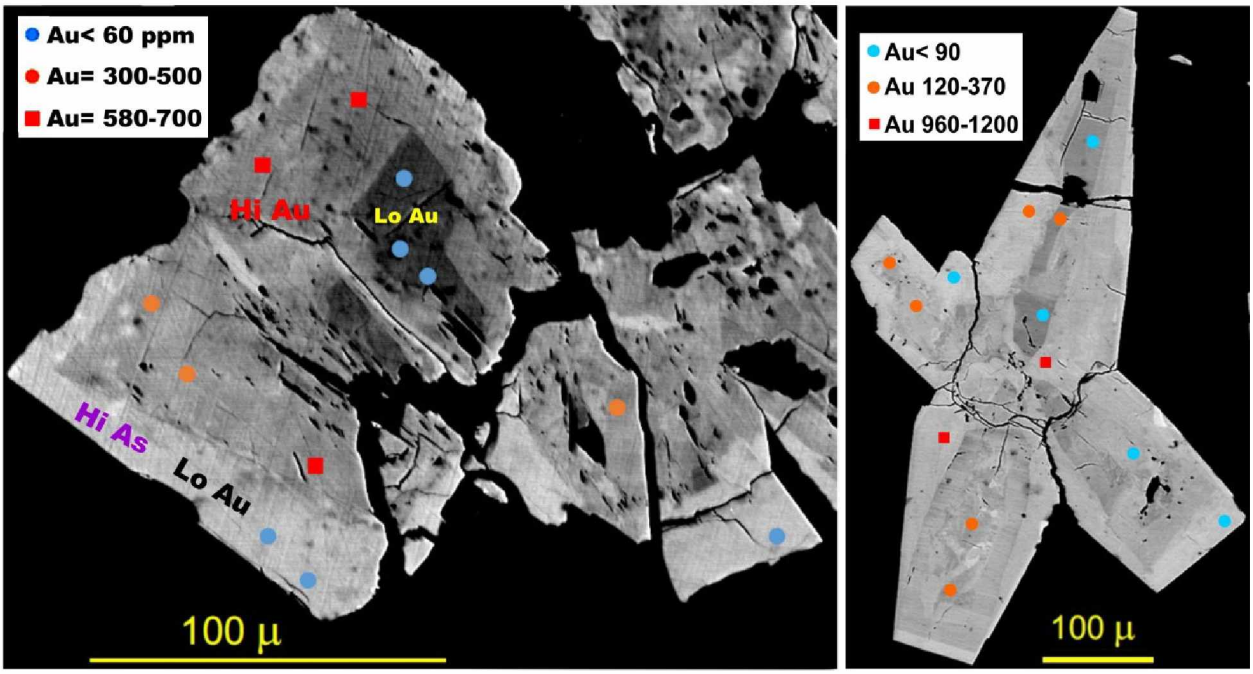

Figure 4-3: Backscatter electron (BSE) images of zoned arsenopyrite grains from GSDC1138-10, showing dark, As depleted cores (26.7-27 atomic %), middle zones of moderate As concentrations (29.7-32.2 atomic %), and bright, As rich rims (As >32.5 atomic %). Significant Au concentrations are restricted to zones of moderate As.

Table 4-3: Data for arsenopyrite examined by EPMA for this study

DDH	feet	ppm Au in Asp		At% As in	Avg[2]at%	stdev	"T"	+/-	altn[4]	vg?
		range[1]	Avg[2]	asp (range)	As in asp		°C[3]			
1138	**398**	0-1350	280	24-33			--		kaol	**N**
9801	41	0-29	8		32.8	0.3	**473**	17	kaol-mu	Y
9801	111		low?		33.2	0.2	**>400**	10	kaol-mu	**N**
9801	280	0-38	5		30.4	0.3	**326**	22	alb-mu	**N**
9801	282	0-69	9		30.6	0.6	**335**	38	alb-mu	**N**
9801	302		low?		29.9	0.1	**291**	6	kaol-mu	**N**
9801	388	8-1480	550	27-32					alb-mu	**N**
9801	805	0-76	27		31.8	0.5	**412**	34	mu-kaol	**N**
9801	873		low?		29.7	0.2	**282**	11	kaol-mu	**N**
1132	316	0-140	33	25-33					kaol-mu	**N**
404	358	47-2470	535	25.8-32.4					MUSC	**N**
404	368	29-1067	250	29.1-36.3					**kaol**	**N**
404	367.5	51-1483	460	26.2-37.3					**kaol**	**N**
404	372	57-2054	425	27.4-32.4					**kaol**	**N**
404	378	40-1231	285	27-32.3					alb-mu	**N**
1129	273		10		32.6	**0.4**	**459**	25	alb-mu	Y
1129	401	41-2135		30.9-33.9	32.0	0.5	**424**	31	alb-mu	**N**
1130	222		35		32.9	0.7	**484**	46	alb-mu	Y
1130	328.5	37-102		33-37	33.8	0.4	**>420**		alb-mu	Y
1130	314.5	32-87		33-37	34.1	**0.5**	**>450**		alb-mu	Y
1135	550	14-196	38	23.7-31.7					alb-mu	Y
1135	503.8		12		34.4	**0.3**	**>460**	18	kaol-mu	Y
1148	257	0- 18	**8**	**only 1 grain**	32.6	0.2	**464**	12	kaol-mu	Y
1148	527	81-92	**87**	28.5-30.6	**only 3 analyses**				kaol-mu	Y
1148	1510.5	3-279	83	28.1-32.3					musc-alb	Y
1304	742	34-195	96	28.7-34.6					kaol-mu	Y
1304	1429	15-287	64	29.5-33.5					alb-mu	Y
1304	1685.5	25-2238		26-33	32.0	0.5	**424**	31	kaol-mu	Y
1304	1752	55-600	225	**29.3-32.1**					alb-mu	**N**
1304	1754	31-110	63	28-32.2					alb-mu	Y

Notes: [1]Range in gold composition (ppm) observed in arsenopyrite; detection limit is approximately 50 ppm. [2]Avg = average, given if a single population is in the sample; [3]Temperature based on composition of homogeneous arsenopyrite with fS_2 buffered by surrounding minerals (usually pyrite or pyrrhotite); [4]Altn = alteration: alb = albite, mu= muscovite, kaol = kaolinite. Other abbreviation: vg = 'visible gold' observed in the polished section.

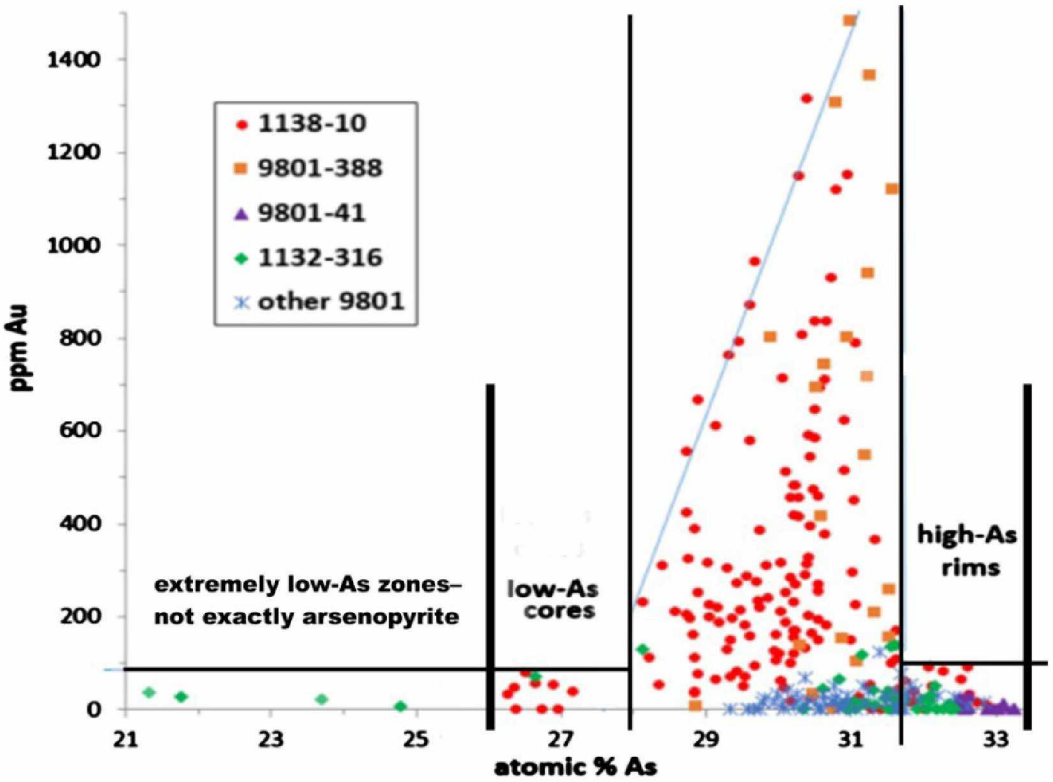

Figure 4-4: Summary of compositional patterns seen in several well-studied Dolphin samples. Highly zoned arsenopyrite grains possess a wide range of compositions, but the Au-bearing portions typically contain 28-32 atomic % As. However, unzoned, compositionally homogeneous arsenopyrite can have compositions in that same range

Not all grains in a sample exhibit the complete zoning pattern. For example, I performed numerous analyses on the arsenopyrite that was subjected to Laser ablation (Figure 4-2) while testing out various permutations of my microprobe routine (Figure 4-5). Given the small size of the grain, the large Laser ablation trenches, and the 5-micron beam size, finding places to analyze was frequently tricky. However, repeated analyses clearly show an As-enriched, Au-depleted rim (Figure 4-5). In contrast, the interior appears compositionally complex and my attempted contouring shows several zones with > 250 ppm Au. A distinct, low-Au, low-As core that is seen in many arsenopyrite grains (Figure 4-3) in the sample (1138-398) does not appear to be present. I suspect that this pattern of complex internal zoning is relatively common.

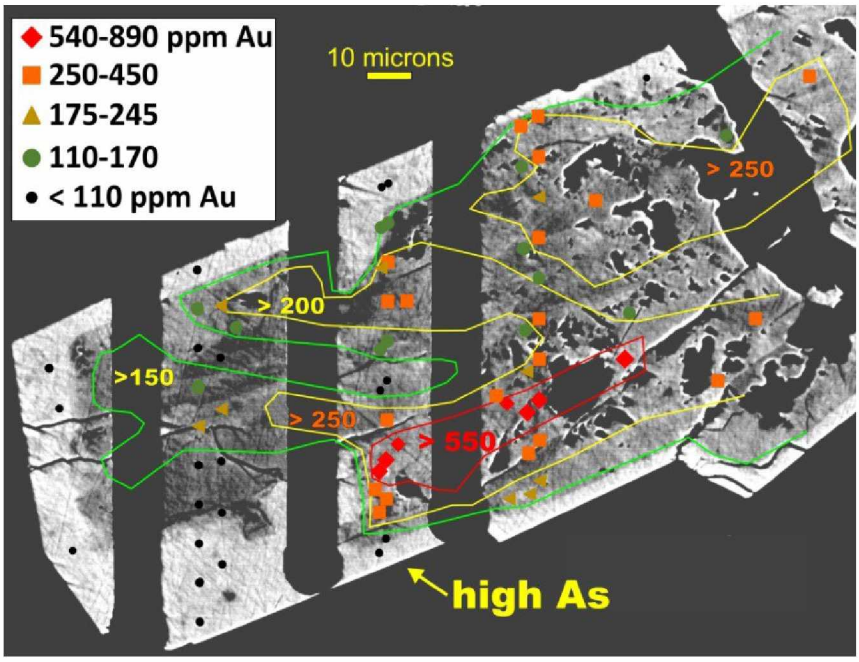

Figure 4-5: Compositional zoning in arsenopyrite that was first analyzed by LA-ICP-MS. The Au-poor, As-rich (bright) rim is obvious (black points) but the internal zoning is complex. Several low-Au points in the interior might indicate an Au-poor core, but due to the damage caused by the laser made it difficult to perform follow-up analyses.

Au-poor arsenopyrite does not display strong zoning and yields relatively homogenous compositions, with a standard deviation in at % As of 0.1-0.7% (Table 4-3). All arsenopyrite grains showed some degree of compositional zoning in BSE imaging, but only grains with the strongest zoning yielded significant Au concentrations. Unzoned grains yielded average compositions of 29.7 $\pm$ 0.2 to 34.4 $\pm$ 0.3 at % As; assuming that they grew in equilibrium with pyrite, many yield temperatures of approximately 300°C. Many yield significantly higher temperatures, and grains from drill holes 1130 and 1135 have As contents greater than possible for equilibrium with pyrite (Table 4-3, Figure 4-1). Such is consistent with the presence of pyrrhotite (especially as inclusions in arsenopyrite) in those samples.

In a few samples (Table 4-3), compositionally unzoned and compositionally zoned arsenopyrite occur in the same thin section (e.g., Figure 4-6). In this case, five of the seven arsenopyrite grains analyzed possess large compositional variability (26-33 atomic %As); two are essentially homogeneous (32.2 $\pm$ 0.3 at % As). Most of the zoned ones are in a cluster about 30 microns away from the unzoned ones (Figure 4-6). One zoned grain (#5) is closest to the unzoned ones, but still too distant (about 4 mm) to see any textural relationship.

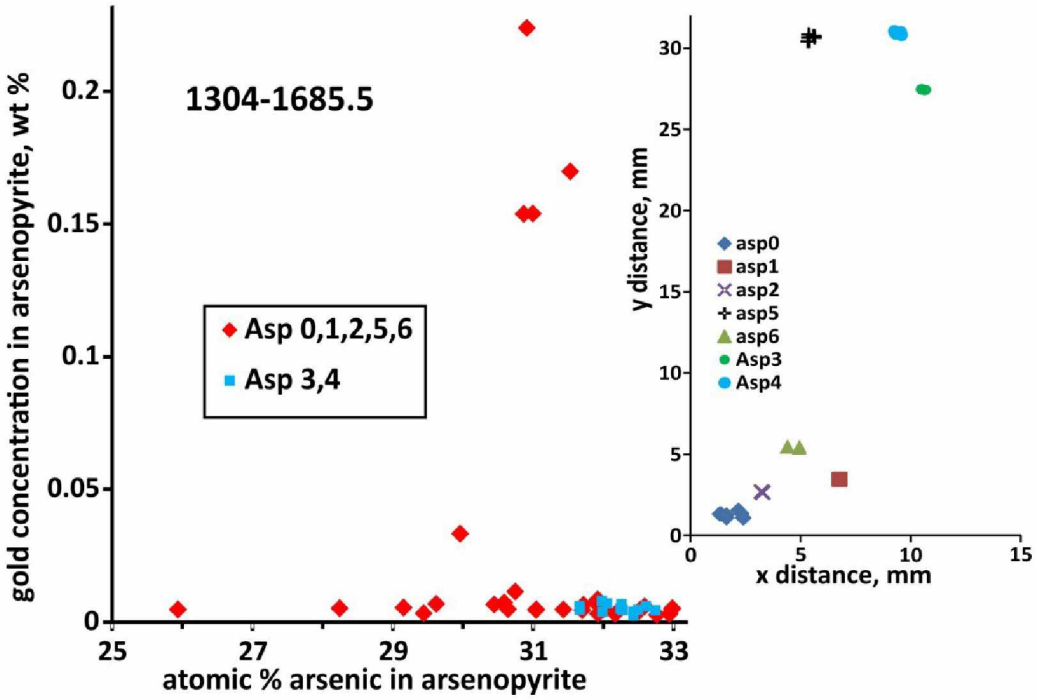

Figure 4-6: Compositions (left) and spatial locations (right) of zoned and unzoned arsenopyrite grains in sample 1304-1685.5.

Out of the 191 analyses of 36 pyrite grains, only 6 analyses yielded Au concentrations above detection level, both in arsenian pyrite. Five of these analyses are from a single gold-bearing pyrite grain which contains up to 320 ppm Au and nearly 3 wt% As (Figure 4-7, left) and shows a highly irregular zoning pattern in BSE (Figure 4-7, right). Oddly, the one arsenopyrite grain analyzed in that sample (1148-257) showed no compositional zoning and gold concentrations below detection (Table 4-3). Unfortunately, additional analyses are needed to determine if that is just an unrelated coincidence.

The other gold-bearing analysis yielded 0.39% Au and 0.4 weight percent As. Eight other analyses in this same grain all failed to detect gold above level of detection but contained up to 3.3 weight percent As. This number (0.39 wt%) is the highest gold concentration I detected in any sulfide analysis using my EMPA-WDS routine. This fact coupled with the low As concentration suggests that the analysis detected a Au° nanoparticle rather than solid-solution gold. The other 185 analyses on pyrite grains (e.g., Figure 4-7) show that pyrite at Dolphin is commonly, although not always, arsenian.

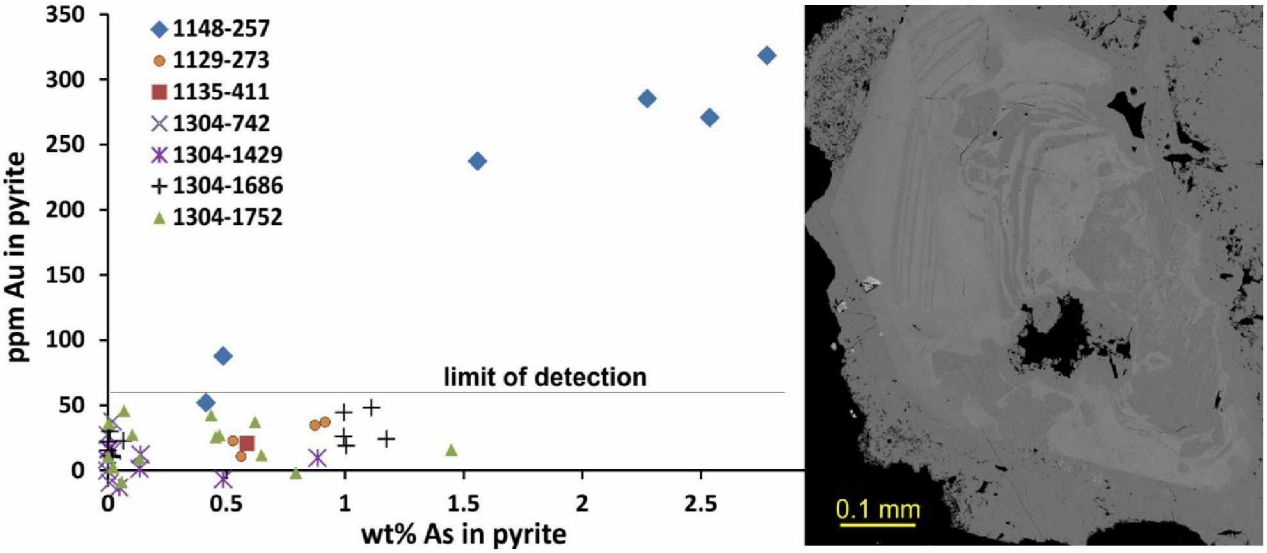

Figure 4-7: Weight% As vs ppm gold for many analyzed Dolphin pyrites (left). Pyrite showing strong and irregular compositional zoning (brighter = higher As) (right) for pyrite 6 from 1148-257.

A rough calculation of the size of the particle needed to generate 0.4% Au is based on the assumption that the particle is essentially pure gold. For a 20 kV beam in pyrite, the X-ray generating electron penetration depth is about 0.5 microns and the BSE-penetration depth is about half of that distance. Thus, the volume affected by the 5-micron beam is approximately 2.5^2 x 0.5 x 3.14 micron^3 = 9.8 cubic microns. The density of gold is nearly 20, that of pyrite is close to 5, so for a gold grain in pyrite, volume % = .25 x wt %.The volume of the gold grain is thus 9.8 cubic microns x 0.4% x .25 = 1x 10^{-2} cubic microns. If the grain is approximated as a cube, it has sides that are $(10^{-2})^{.333}$ microns long = 0.2 microns. If this hypothetical grain was buried .25 microns below the surface, then it could not be detected by BSE but would still show up in the analysis. Such a grain, approximately 0.2 microns in diameter, would be too small to be visible in reflected light and frankly would take very diligent searching to find even with the microprobe. That I only encountered such a grain for 1 analysis suggests that such sub-micron inclusions are relatively rare at Dolphin.

4.3 Discussion

Results of the WDS routine show that there are two distinct arsenopyrite populations in the Dolphin pluton: barren homogenous arsenopyrite with compositions of 27.7 $\pm$ 0.2 to 34.4 $\pm$ 0.3 atomic % As; and auriferous, compositionally zoned arsenopyrite with compositions that typically span at least 3 atomic % As (Table 4-3, Figure 4-8). These arsenopyrite grains are generally (but not always) arsenic poor compared to stoichiometric arsenopyrite (FeAsS) in that even the As "enriched" rims commonly contain <33 atomic % As (Figure 4-8). Compositional zoning (as measured by variation in the atomic % As) appears to be crucial to the presence of solid-solution Au at Dolphin. In Au-bearing arsenopyrite,

atomic percent As varies tremendously; by at least 2.3% and up to 11 atomic %. By contrast, Au-barren arsenopyrite is relatively homogeneous, with variation as little as 0.5 atomic % and at most 1.8 atomic % (Figure 4-8). In several cases, I only managed to generate a small number of analyses for a single thin section, e.g., only three for the zoned arsenopyrites in sample 1148-527. Thus, the likely compositional range for the zoned types is larger than the amount shown.

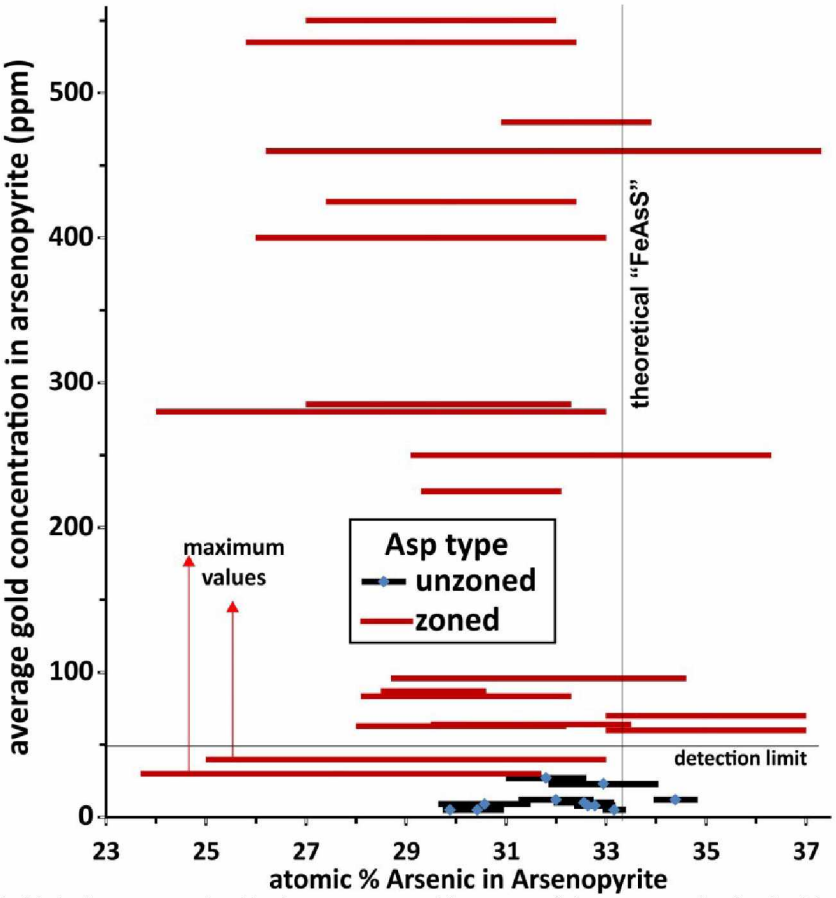

Figure 4-8: Range in atomic % As in arsenopyrite (Asp) vs. average gold content of the arsenopyrite for the 30 samples studied. A single sample can possess both types. For the zoned arsenopyrites, the maximum gold concentration (not shown) is typically 3-5 times that of the average. The detection limit of 50 ppm Au is based on repeated analyses of standard ASP 200.

Based on experimental data, Kretschmar and Scott (1976) demonstrated that atomic % As in arsenopyrite ($FeAs_{1-x}S_{1+x}$) that formed in the presence of pyrite and pyrrhotite decreases with decreasing temperature of formation. S and As are inversely proportional, as they substitute for each other. If arsenopyrite formed at high temperature and continued to grow as temperature dropped, the As content of the arsenopyrite should progressively decrease away from the core. This is the opposite of the pattern seen in the Dolphin zoned arsenopyrite, so unless the temperature was somehow increasing as the arsenopyrite crystals formed, another explanation is needed. Kretschmar and Scott (1976) studied both

natural and synthetic arsenopyrite and noted a similar problem (high –As rim) for a few natural samples. They concluded that such zoning is caused by growth under non-equilibrium conditions.

Figure 4-9 shows compositions for 247 high-quality analyses taken from samples of coexisting arsenopyrite and pyrite. The bulk of the analyses span the range of 29-33 at % As, although the full range is from 28 to 34 at % As. Based on the experimental relations between arsenopyrite composition and temperature arsenopyrite with 28 and 29 atomic % As yield highly unrealistic temperatures of 235 and 175°C, respectively. That is, such compositions cannot reflect equilibrium growth conditions. In addition, arsenopyrite that grows in equilibrium with pyrite cannot contain more than 33 atomic % As (Figure 4-1). Most of the zoned, Au-bearing arsenopyrite at least locally yields < 29 atomic % As or > 33atomic % As (Figure 4-8) which also indicates growth under non-equilibrium conditions.

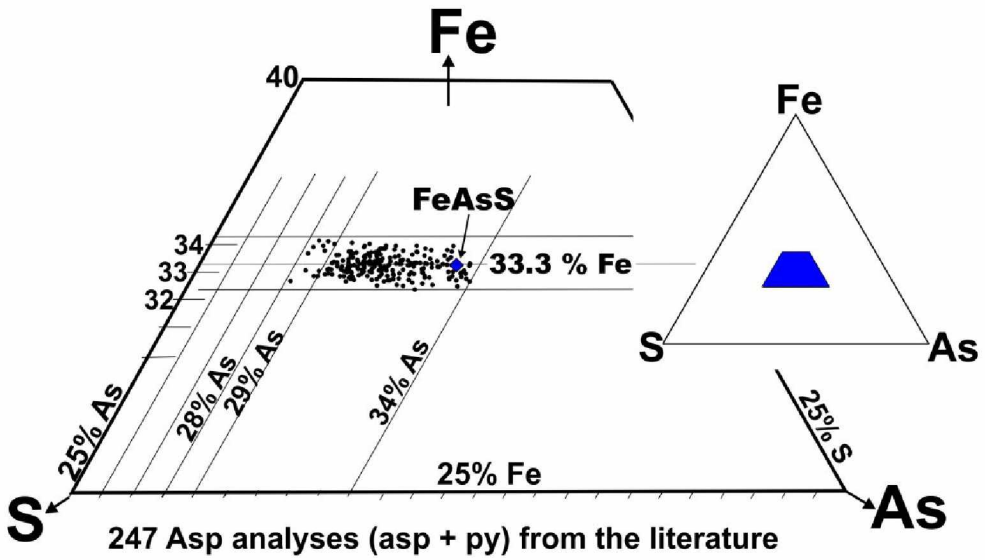

Figure 4-9: Compositions of arsenopyrite for grains present with pyrite, taken from the literature. Atomic % Fe shows little variation and the bulk of analyses are in the range of 29-33 atomic % As. Compilation by R.J. Newberry, writ. comm., 2018.

In contrast, I assume that arsenopyrite which does not display significant compositional zoning grew under equilibrium conditions, but not necessarily with pyrite. Given the known refractory character of arsenopyrite (retention of original composition), I infer that homogeneous arsenopyrite that contains > 33 atomic % As grew with pyrrhotite and not pyrite. This is consistent with the presence of pyrrhotite inclusions in arsenopyrite in those samples. The temperatures given in Table 4-3 reflect such assumptions about the associated sulfide at the time of formation. Two groups are apparent: (a) calculated

temperatures of approximately 300°C (282 ± 11 to 335 ± 38 °C) and (b) calculated temperatures > 400 °C (412 ± 34 to 484 ± 46 °C for those assumed in equilibrium with pyrite).

In several cases the apparently higher-temperature arsenopyrite is present with a silicate assemblage that includes kaolinite. This requires that the sample experienced temperatures < 300 °C for a long enough time to grow kaolinite in the rock. If the temperature given by the arsenopyrite composition is approximately correct, then the arsenopyrite grew during a pre-kaolinite hydrothermal event and did not subsequently re-equilibrate. Apparently higher-temperature arsenopyrite is also present with albite-muscovite alteration (Table 4-3), which is compatible with either that alteration taking place at temperatures > 300 °C or else that the arsenopyrite grew earlier and did not re-equilibrate.

The homogeneous arsenopyrite grains with compositions that yield temperatures of approximately 300°C occur with both kaolinite-muscovite and albite-muscovite alteration (Table 3-4). If these also represent equilibrium growth (as suggested by the uniform compositions within individual grains and between different grains in the sample) then these arsenopyrites grew at temperatures of about 300° C. If true, this requires that both alteration types occurred at a relatively low temperature, although those with kaolinite yield 282 ± 11 to 291 ± 6 °C and those with albite-muscovite yield 326 ± 22 to 335 ± 38 °C. These differences might not be significant.

My results show that sub-microscopic or "invisible" gold is present in both arsenian pyrite and arsenopyrite at Dolphin, although the latter greatly predominates. The fact that I detected Au in only two out of 36 pyrite grains I analyzed (one apparently solid solution, one a nanoparticle) suggests that pyrite is the less-favored host for invisible gold at Dolphin. Further, I suspect that solid solution Au is restricted to pyrite that exhibits strange and complex BSE patterns (e.g., Figure 4-7, right), which I only encountered in that one sample. If the single Au nanoparticle I encountered is typical, then they are restricted to higher-As pyrite which I have seen commonly at Dolphin. Unfortunately, as they are not visible by BSE, I don't know how to quantify their abundance at Dolphin. Because they are so small they don't likely add to the gold budget; unless they are more common than they seem to be.

There is a close association between Au and As in arsenian pyrite with Au occurring as nanoparticles (Au°) of native metal and as cations in solid-solutions (Reich et al., 2005; Deditius et al., 2011). Arsenian pyrite containing dissolved gold is especially present in Carlin-type Au deposits. Reich et al. (2005) demonstrate that the amount of Au that can be dissolved in arsenian pyrite is directly related to the pyrite As content.

In contrast, the dissolved gold contents I found inDolphin arsenopyrite commonly accounts for the gold concentration in the rock. To make such a calculation, I employed samples that (a) lacked (or had

tiny amounts of) visible gold, (2) had sufficient microprobe analyses to generate a viable 'average' Au grade, and (3) were derived from billets for which I had reliable XRF gold and As concentrations (from which I could estimate arsenopyrite abundance). Samples that satisfy those requirements are listed in Table 4-4. For all but one of the samples that met the criteria, there is reasonably good agreement between the calculated Au concentration and that measured by XRF in the associated billet.

Table 4-4: Gold accounting in some samples with Au-bearing arsenopyrite

drill hole	footage	XRF Au (ppm)	~% Asp	avg Au in Asp (ppm)	calc'd Au in rock (ppm)
1138	**398**	**11**	5	280	**14**
404	358	**2.9**	0.5	535	**2.7**
404	368	1.6	0.3	250	0.8
404	367.5	**2.7**	0.8	460	**3.7**
404	372	**19**	4	425	**17**
404	378	**3.7**	1	285	**3.4**
1129	401	**1.9**	0.4	346	**1.5**

Notes: ~% Asp = approximate wt% arsenopyrite, calculated from XRF As concentration; calc'd Au in rock = ppm Au in arsenopyrite x wt% arsenopyrite/100. Bold numbers show good agreement between XRF and calculated values, underlined one is significantly low.

The problem samples are those for which no visible gold was noted and Au-bearing arsenopyrite or pyrite was not found, namely most of the samples from drill hole 9801 (Table 4-3). The two possibilities are that (a) my estimated gold concentrations from thin section XRF are too high, and the samples really don't contain much gold; or (b) gold is present as not-yet detected nanoparticles in those samples. I know of no easy way to address either possibility.

From a theoretical perspective, one would expect that rapidly precipitated arsenopyrite would do so under dis-equilibrium conditions, which could result in both unusual (i.e., not thermodynamically stable) As contents and also in solid solution Au. Similarly, arsenian pyrite is not a stable mineral (it ought to decompose to pyrite + arsenopyrite) and its presence indicates that disequilibrium sulfide formation took place. But when and how did such dis-equilibrium growth take place?

To begin with (Figure 4-10), I found highly zoned, Au-bearing, arsenopyrite at locations throughout the Dolphin pluton and in samples from all the different alteration zones. However, seven of the eight samples with high (>200 ppm) average Au in arsenopyrite came from the zone of strong kaolinite

alteration. However, samples with zoned, Au-bearing, arsenopyrite came from all but the shallowest depths, with a range of nearly 500 vertical meters (Figure 4-10). In contrast, samples with homogeneous arsenopyrite are all from elevations 200 m ASL or higher. Oddly, samples yielding higher temperatures (> 400°C) are present in the shallowest and deeper exposures. Arsenopyrite yielding low (~300°C) temperature is exclusively from drill hole 9801, at elevations between 370 and 190 m ASL.

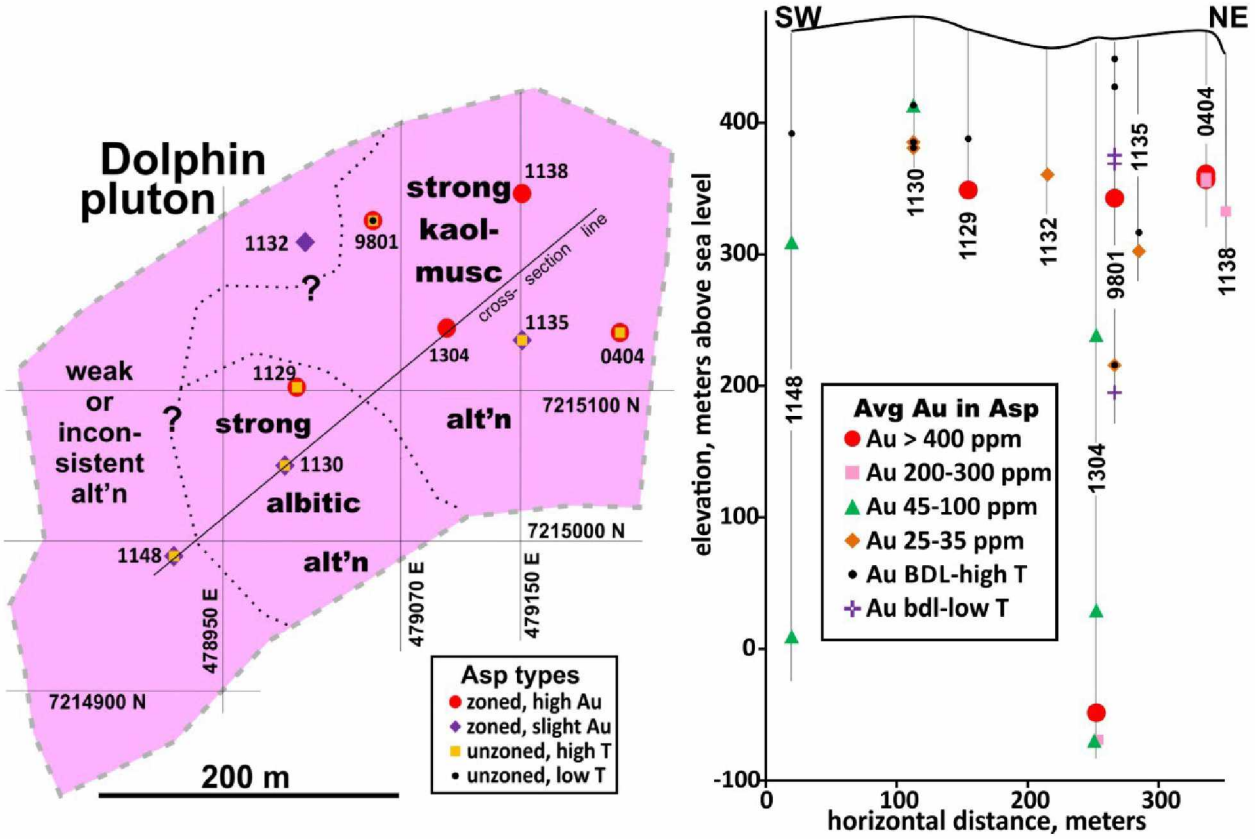

Figure 4-10: Plan map (left) and projected cross-section (right) showing types of arsenopyrite (Asp) found at Dolphin and their locations. Numbers next to drill holes are the hole number. BDL = below detection limit, i.e. average Au concentration in arsenopyrite < 50 ppm. High and low temperature refers to calculated value (Table 4-3) based on average at % As in compositionally homogeneous grains. High T = calculated T > 400C, low T = calculated T ~ 300 C. Many samples are projected a long distance from the cross-section line (above, left); their spacing is unimportant but drill holes NE of 1132 are all from the area of extensive kaolinite-bearing alteration. Abbreviations: kaol = kaolinite, musc = muscovite, alt'n = alteration.

Because Au-enriched arsenopyrite occurs with a variety of alteration types, it does not necessarily represent a lower-temperature phenomenon. Indeed, if the arsenopyrite that yields lower temperatures does represent equilibrium (as suggested by the homogeneous compositions) then there is no clear tie between declining temperature and formation of the highly zoned, Au-enriched arsenopyrite at Dolphin. (This, of course, does not rule it out, either.) An alternative to growth at exceptionally low temperature is the possibility of rapid growth, due to abrupt changes in the fluid during arsenopyrite growth. An example of which is the exsolution of CO_2 ('boiling') from a mixed CO_2-H_2O fluid. Investigation of this

phenomenon at Dolphin is well beyond the scope of this thesis, but the abundance of carbonate minerals in the deposit does require that the associated fluids contained significant CO_2.

5 Discussion and Conclusion

5.1 Comparison with Ft. Knox

The age and metallogeny of intrusive rocks indicate Dolphin and Fort Knox are part of the mid-Cretaceous (89-93 Ma) magmatic event referred to as the "Tombstone" suite by Mortenson et al. (2000). McCoy and Olson (1997) reported $^{40}Ar/^{39}Ar$ plateau ages of 90±1.5 and 88±1.5 Ma from Dolphin sericite. Sericite and biotite from the Ft Knox deposit have yielded nearly identical (within uncertainties) ages of 86-88 (±1.5) Ma (McCoy et al., 1997).

Besides the obvious age similarities and spatial proximity (Figure 1-2) of Dolphin and Ft. Knox, there are startling differences in hydrothermal alteration and sulfide content. Ft. Knox has significantly lower sulfide content (<1% vs > 10% at Dolphin) and Au° is hosted in sericitic shear zones. It is thought that due to the close proximity of the deposits and similar radiometric ages, the deposits are related and share the same batholith at depth. If this is true the question of why the deposits are so different must be addressed. These similarities and differences have been noted in the past (e.g., Adams and Giroux, 2011, and Abrams and Giroux, 2013). The prevailing explanation is that Dolphin is a shallower deposit in the Intrusion-related gold deposit (IRGD) model than Ft. Knox (Figure 5-1). This is supported by the extensive lower-temperature hydrothermal alteration at Dolphin which is a symptom of shallow emplacement, especially compared to Ft. Knox. The offset in depositional depth over such a short distance is likely the result of vertical displacement over the series of northeast trending high angle faults mapped by Newberry et al. (1996). However, either the 'break' between largely non-refractory gold (deeper) and gold present in solid solution (shallower) is much deeper than shown on Figure 5-1 or else the Dolphin deposit was formed at much shallower depth than shown on Figure 5-1.

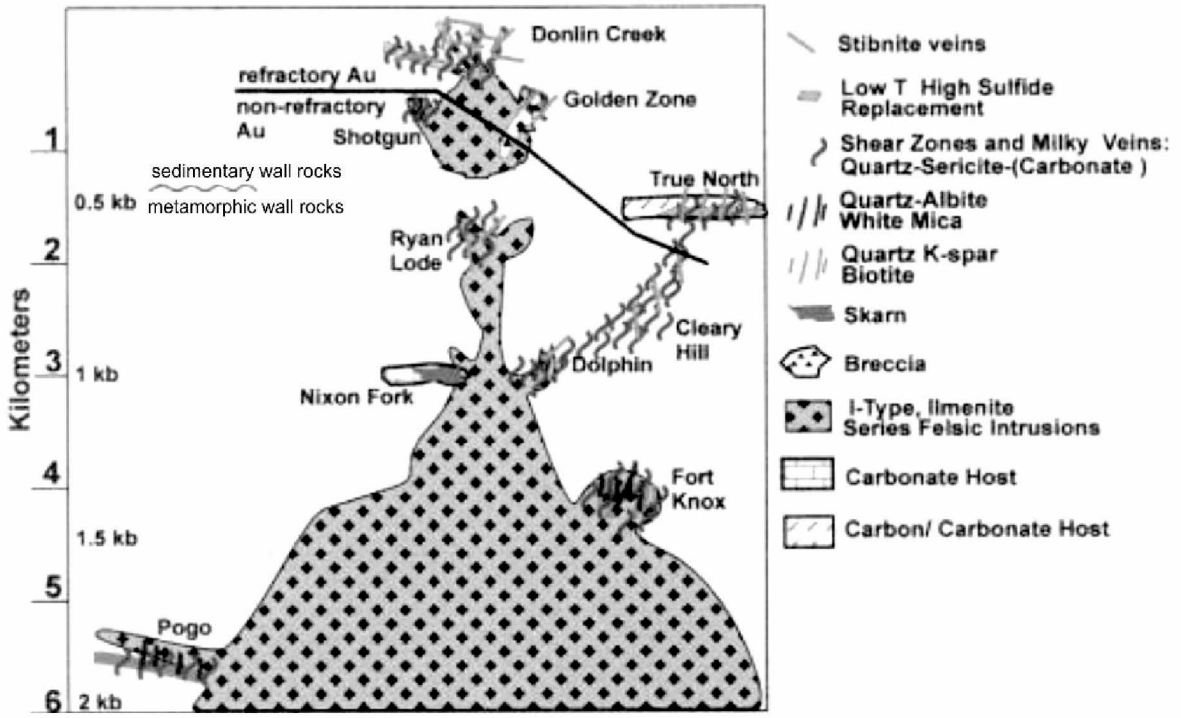

Figure 5-1: Cartoon showing Alaskan Intrusion-related gold (IRG) deposits and relative depths. Note that Dolphin is located approximately 1km shallower than Ft. Knox. Modified from McCoy et al. (1997).

5.2 Arsenopyrite

Based on data from my WDS routine (Table 4-3), I identified two types of arsenopyrite: smaller compositionally zoned arsenopyrite with highly variable As contents, and larger homogenous arsenopyrites. Arsenopyrite is a refractory mineral that does not readily change composition once it has formed, which can be useful for determining conditions under which it formed (Kretschmar and Scott, 1976). By plotting the As concentrations of the homogenous arsenopyrite, the temperature at the time of formation can be determined. These homogenous arsenopyrites contain two ranges of As: higher temperature (~33-34.5 atomic % As) and lower temperature (~30 atomic % As). Compositions of seven homogenous arsenopyrites are plotted on Figure 5-2 and labeled with relevant minerals identified in the thin section. Homogenous arsenopyrite is found in all styles of mineralization as is zoned, gold-bearing arsenopyrite. In the few samples where I identified homogenous and gold bearing arsenopyrite in the same thin section (Table 3-1), the homogenous arsenopyrite has always been the higher temperature type.

Plotting homogenous arsenopyrite compositions and associated minerals on Figure 5-2 shows fluid evolution from higher to lower temperature and fS_2. The identification of gudmundite (FeSbS) (a low temperature and low fS_2 mineral) with low As homogenous pyrite in one sample and low As arsenopyrite with pyrite in others shows that the fS_2 must have increased without a corresponding increase in temperature. The nature of this event is unknown, but apparently is related to the occurrence of

hydrothermal kaolinite at Dolphin. Something happened to the hydrothermal system that caused (a) a radical increase in sulfur fugacity, (b) a significant decrease in fluid pH, and (c) the formation of irregularly zoned and Au-bearing arsenopyrite. I hypothesize that this was a sudden and drastic event, one reflecting non-equilibrium (rapid?) arsenopyrite growth.

A strong correlation between Au and As concentrations at Dolphin does not occur due to the fact that solid solution gold exists within zoned arsenopyrite but not homogenous arsenopyrite, and because Au^{o} inclusions are seen in both types of arsenopyrite. In other words, there isn't a consistent relation between gold and arsenopyrite. Additionally, the upper limit for As in four-acid digest assays is 10,000 ppm (1%). This concentration is commonly present in mineralized Dolphin rocks, further confounding an Au-As correlation.

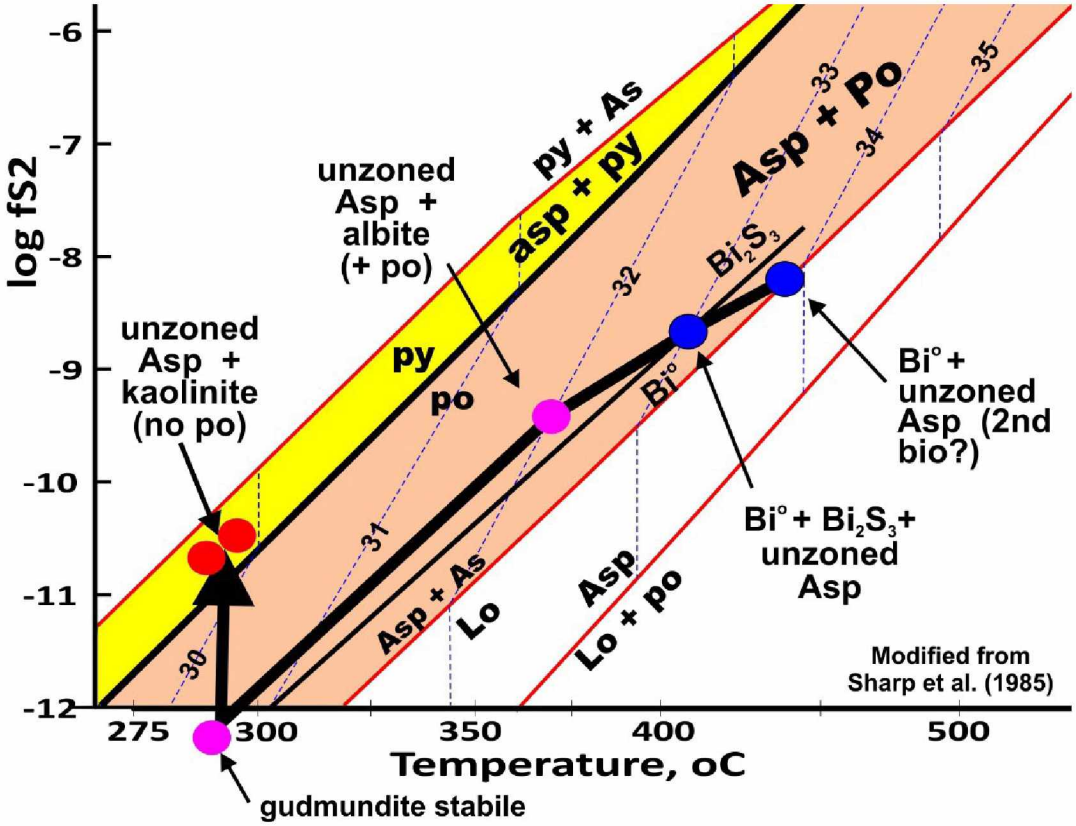

Figure 5-2: Phase diagram showing mineral stabilities with relation to arsenopyrite (Asp) compositions, modified from Sharp et al. (1985). Additional abbreviations: po = pyrrhotite, py = pyrite, Lo = lollingite. Pink field = arsenopyrite with pyrrhotite, yellow = arsenopyrite with pyrite.

5.3 Recommendations for future work

Based on the results of my findings, the following recommendations should be considered for work which could prove useful to further understand the nature of the Dolphin pluton:

- Diamond core drilling has not defined the extent of the pluton to the east or south. Further drilling in these areas could expand the resource.
- Gold grade has been seen to increase with depth in some drill holes (e.g., GSDC1132). Drilling to further depth could also expand the resource.
- A structural analysis of the deposit could be undertaken. This thesis did not dive into the complicated structural nature of this area. Elevated gold grades are seen in some shear zones in the deposit and coarse-grained gold is found in sheeted, and stockwork quartz veins.
- Investigate the relationship between vein density and Au grade through electronic core logs and assay data.

5.4 Conclusions

The Dolphin deposit is a mid-Cretaceous gold deposit largely hosted by a composite, highly altered, granite and tonalite composition pluton. The tonalite is older and is primarily located along the northern margin of the pluton. Gold mineralization was associated with the granite, as gold is found in both intrusive units. Investigations of hydrothermal alteration (based on chemical analyses, X-ray diffraction, and thin section examination) show albitic and advanced argillic (kaolinite-quartz) alteration are the dominant styles with sericite common throughout. Advanced argillic is a low temperature (<300°C) low pH alteration style that has only rarely been identified in mid-Cretaceous intrusion-related gold deposits in interior Alaska. Albitic alteration probably resulted from higher temperature, more neutral pH fluids.

Gold occurs as fine- to coarse-grained Au°, aurostibite, and maldonite in quartz + sulfide veins; fine-grained Au° in the oxide zone; and in many forms in disseminated sulfide. These include as Au° inclusions in pyrite and arsenopyrite, solid-solution Au with compositionally zoned arsenopyrite, and as Au° nanoparticles in pyrite and arsenopyrite. Solid-solution gold occurs only in arsenopyrite with strong compositional zoning. These commonly have low As cores; gold-bearing mantles with moderate % As; and high As rims. In contrast, compositionally homogenous arsenopyrite does not contain solid-solution gold and contains ~30% to 34.5 atomic % As. Pyrite is commonly arsenian and carries dissolved gold (if any) near detection limits. Gold mineralization has not been tied to any lithology or alteration style; however, gold does seem to correlate with abrupt changes in alteration, especially between sericite + albite and kaolinite + sericite alteration, and gold-bearing, zoned arsenopyrite is associated with advanced argillic alteration. That is, the nature of the gold occurrence appears to change with alteration type, but not the overall abundance of gold.

6 References

Abrams, M., Blumberg, J., Giroux, G., Johns, C., Michael, N., Richers, D., Scharnhorst, V., Spiller, D.E., Thompson, K., 2016, NI 43-101 Technical Report Golden Summit Project Preliminary Economic Assessment Fairbanks, Alaska USA, Document 910054-REP-R0001-01, 232 p.

Abrams and Giroux, 2013, Technical Report for the Golden Summit Project, Fairbanks Mining District, Alaska: Prepared for Freegold Ventures Ltd., 118 p.

Adams and Giroux, 2011, Geology and Mineralization and Mineral Resource Estimate for the Golden Summit Project, Fairbanks Mining District, Alaska: Prepared for Freegold Ventures Ltd., 193 p.

Ashley, P., Creagh, C. & Ryan, C., 2000, Invisible gold in ore and mineral concentrates from the Hillgrove gold-antimony deposits, NSW, Australia: Mineralium Deposita, Vol. 35, p. 285-301.

Bakke AA, 1995, The Fort Knox 'Porphyry' Gold Deposit – Structurally controlled stockwork and shear quartz vein, sulfide-poor mineralization hosted by a Late Cretaceous pluton, east central Alaska. In: Schroeter TG, ed, Porphyry Deposits of the Northwestern Cordillera of North America. Canadian Institute of Mining, Metallurgy and Petroleum Special Volume 46, p. 795-802.

Brathwaite, R.L., Simpson, M.P., Faure, K., and Skinner, 2001, D.N.B., Telescoped porphyry Cu-Mo-Au mineralization, advanced argillic alteration, and quartz sulfide-gold-anhydrite veins in the Thames District, New Zealand: Mineralium Deposita, Vol. 36, p. 623-640.

Burns, L.E., Newberry, R.J., and Solie, D.N., 1991, Quartz normative plutonic rocks of interior Alaska and their favorability for association with gold: Alaska Division of Geological & Geophysical Surveys Report of Investigation 91-3, 71 p.

Cabri, L.J., Chryssoulis, S.L., De Villiers, J.P.R., Laflamme, H.H.G., and Buseck, P.R., 1989, The nature of "invisible" gold in arsenopyrite, Canadian Mineralogist, Vol. 27, p. 353-362.

Cook, N.J., Ciobanu, C.L., Wagner, T., Stanley, C.J., 2007, Minerals of the system Bi-Te-Se-S related to the tetradymite archetype: review of classification and compositional variation, Canadian Mineralogist, Vol. 45, p. 665-708.

Cook, N.J., and Chryssoulis, S.L., 1990, Concentrations of "invisible gold" in the common sulfides, Canadian Mineralogist, Vol. 28, p. 1-16.

Deal, M.L., 2012, Origins and zoning of the Buckhorn gold skarn, NE Washington: unpublished MS thesis, University of Alaska Fairbanks, 235 p.

Deditius, A.P., Utsunomiya, S., Reich, M., Kesler, S.E., Ewing, R.C., Hough, R., and Walshe, J., 2011, Trace metal nanoparticles in pyrite, Ore Geology Reviews, Vol. 42, p. 32-46.

DGGS, 1995, Airborne magnetic survey of the Fairbanks Mining District, Alaska: Alaska Division of Geological & Geophysical Surveys, PDF 95-6, 2 maps.

Di Prisco, G., 2013, Mineralogy Examination of the Golden Mineralization from the Golden Summit Project, Alaska, USA: unpublished report for Freegold Ventures LTD. TerraMS-13SEP-002 – Golden Summit – Gold Mineralization, 30 p.

Dusel-Bacon, C., Lanphere, M.A., Sharp, W.D., Layer, P.W., and Hanson, V.L., 2002, Mesozoic thermal history and timing of structural events for the Yukon-Tanana Upland, east-central Alaska—$^{40}Ar/^{39}Ar$ data from metamorphic and plutonic rocks: Canadian Journal of Earth Sciences, Vol. 39, p. 1013–1051.

Fleet, M.E., Chryssoulis, S.L., MacLean, P.J., Davidson, R., and Weisener, C.G., 1993, Arsenian pyrite from gold deposits: Au and As distribution investigated by SIMS and EMP, and color staining and surface oxidation by XPS and LIMS, Canadian Mineralogist, Vol. 31, p. 1-17.

Francis, K., 2008, Donlin Creek Project NI 43-101 Technical Report Southwest Alaska, U.S.: Prepared for Nova Gold Resources Inc., 397 p.

Freeman, C.J., 1991, Golden Summit Project Final Report - Volume 2: Historical summary of lode mines and prospects in the Golden Summit project area, Alaska: Geol. Rept. GS91-1, Avalon Development Corp., internal report to International Freegold Mineral Development, 159 p.

Gagnon, J.E., Samson, I.M., Fryer, B.J., and Williams-Jones, A.E., 2004, The composition and origin of hydrothermal fluids in a NYF-type granitic pegmatite, S. Platte District, Colorado: Canadian Mineralogist, Vol. 42, p. 1331-1355.

Genkin, A.D., Bortnikov, N.S., Cabri, L.J., Wagner, F.E., Stanley, C.J., Safonov, Y.,G., McMahon, G., Friedl, J., Kersin, A.L., and Gamyanin, G.N., 1998, A multidisciplinary study of invisible gold in arsenopyrite from four mesothermal gold deposits in Siberia, Russian Federation, Economic Geology, Vol. 93, p. 463-487.

Goldfarb, R.J., 1997, Metallogenic evolution of Alaska, in Mineral Deposits of Alaska, Goldfarb, R.J., and Miller, L.D. ed. Economic Geology Monograph 9, p. 4-34.

Goldfarb, R., Ayuso, R., Miller, M., Ebert, S., Marsh, E., Petsel, S., Miller, L., Bradley, D., Johnson, C., and McClelland, W., 2004, The Late Cretaceous Donlin Creek Gold Deposit, Southwestern Alaska: Controls on Epizonal Ore Formation. Economic Geology, Vol. 99, p. 643–671.

Hill, J.M., 1933, Lode deposits of the Fairbanks district, Alaska: U.S. Geological Survey Bulletin 849-B 163 p.

Kretschmar, U. and Scott, S.D., 1976, Phase Relations Involving Arsenopyrite in the system Fe-As-S and their application: Canadian Mineralogist, Vol. 14, p. 364-386.

Kunter, R., Rehn, C., Prenn, N., Carew, T., and Levy,. M.; 2013, Canadian National Instrument 43-101Technical Report on the Livengod Gold Project Feasibility Study, Livengood, Alaska – Prepared for: International Tower Hill Mines Ltd., September 4, 2013, 347 p.

Lang, J., and Baker, T., 2001, Intrusion-Related Gold Systems: The Present Level of Understanding. Mineralium Deposita, Vol. 36, p. 477-489.

McCoy, D., and Olson, I., 1997, Thermochronology and mineralogy of the Dolphin Deposit and other selected Golden Summit Deposits, February 1997: Prepared for Freegold Ventures Ltd., 19 p.

McCoy, D. T, Newberry, R.J., Layer, P.W., DiMarchi, J.J., Bakke, A., Masterman, J.S. and Minehane, D.L. 1997, Plutonic Related Gold Deposits of Interior Alaska in Goldfarb, R.J., ed. Ore Deposits of Alaska, Economic Geology Monograph, No. 9, p. 191-241.

Mortenson, J.K., Hart, C.J.R., Murphy, D.C., and Heffernan, S., 2000, Temporal evolution of early and mid- Cretaceous magmatism in the Tintina Gold Belt: The Tintina Gold Belt: concepts, exploration and discoveries, BCYCM Spec. Vol. 2 (Cordilleran Roundup Jan. 2000), p. 49-57.

Newberry, R.J.; Clautice, K., Bundtzen, T.K.; Combellick, R.A.; Douglas, T., Laird, G.M.; Liss, S.A.; Pinney, D.S., Reifenstuhl, R.R. and Solie, D.S., 1996, Preliminary geologic map of the Fairbanks Mining District, Alaska: Alaska Division of Geological & Geophysical Surveys, PDF 96-16, 35 p., 2 maps.

Newberry, R.J., 1996, Major & trace element analyses of Cretaceous plutonic rocks in the Fairbanks mining district, AK: Alaska Division of Geological & Geophysical Surveys, PDF 96-18, 19 p.

Raymond, L., 2017, The Dolphin deposit, Fairbanks: yet another variation on the 'Fort Knox-type' theme: 2017 Alaska Miners Association Convention Abstracts, p. 5.

Reich, M., Kesler, S.E., Utsunomiya, S., Palenik, C.S., Chryssoulis, S.L., and Ewing, R.C., 2005, Solubility of gold in arsenian pyrite, Geochimica et Cosmochimica Acta, Vol. 69, p. 2781-2796.

Robinson, M.S., Smith, T.E., and Metz, P.A., 1990, Bedrock geology of the Fairbanks Mining District: Alaska Division of Geological & Geophysical Surveys, Professional Report 106, 2 sheets, scale 1:63,360.

Seal, R.R., Robie, R.A., Barton, P.B.,Jr., and Hemingway, B.S., 1992, Superambient heat capacities of synthetic stibnite, bertheirite, and chalcostibite: reviwed thermodynamic properties and implications for phase equilibria, Economic Geology, Vol. 87, p. 1911-1918.

Sharp, Z., Essene, E., and Kelly, W., 1985, A re-examination of the arsenopyrite geothermometer; pressure considerations and applications to natural assemblages: Canadian Mineralogist, Vol. 23, p. 517-534.

Rombach, C.M., and Newberry, R.J., 2001, Shotgun deposit: granite porphyry-hosted gold-arsenic mineralization in southwestern Alaska, USA: Mineralium Deposita, Vol. 36, p. 607–620.

Van Wyck, N. and Armitage, A., 2013, Technical Report on the Shotgun Gold Project, Southwest Alaska, Prepared for TNR Gold Corp, 185 p.

Yang, S., Blum, N., Rahders, E., and Zhang, Zh, 1998, The nature of invisible gold in sulfides from Xiangxi Au-Sb-W ore deposit in northwestern Hunan, People's Republic China, Canadian. Mineralogist, Vol. 36, p. 1361-1372.

APPENDIX A: Microprobe Routine Setup Screenshots

The following screenshots are included in order to display the analytical conditions utilized for the wavelength-dispersive spectroscopy (WDS) routine developed for this study. The software used for this routine and captured in these screenshots is Probe for EPMA v 11.8.8 by John J. Donovan, Probe Software Inc.

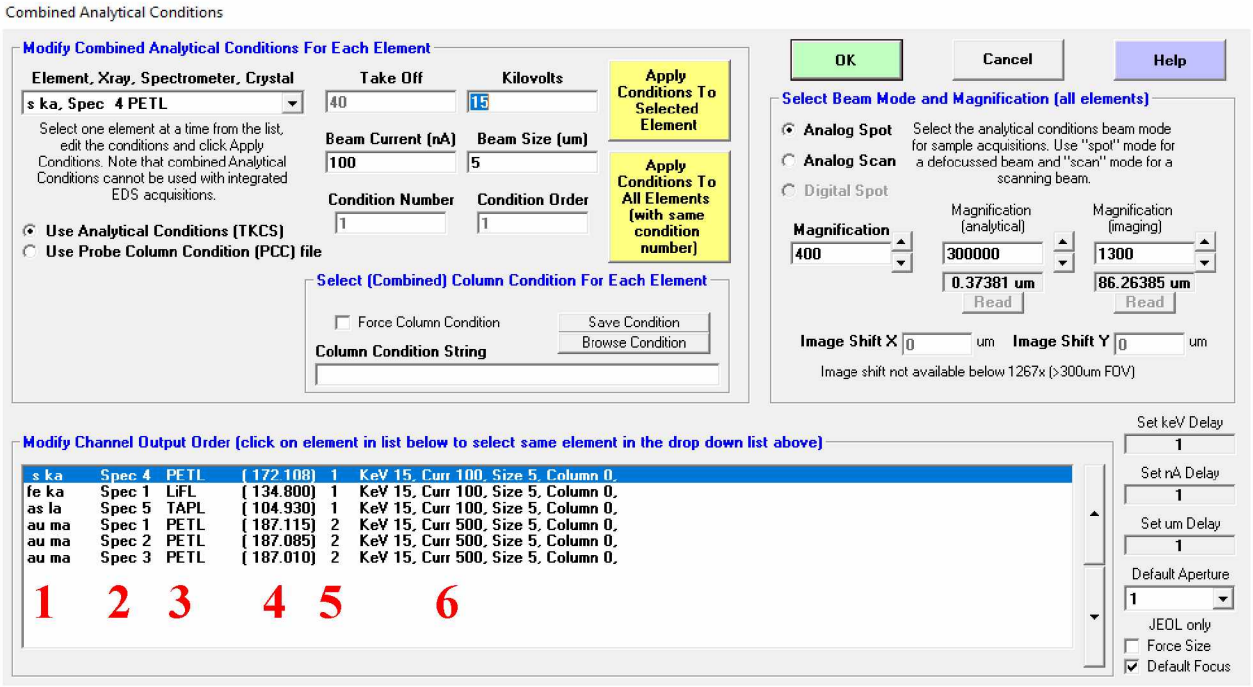

Figure A-1: Screen grab of combined analytical conditions setup in Probe for Windows software used for this study. 1) Element x-ray line analyzed 2) Spectrometer number 3) Crystal type 4) Peak position 5) Analysis order 6) Voltage, Current and beam size

Channel	Element	Spectro	Crystal	On-Peak	Hi-Peak	Lo-Peak
1	au ma	1	PETL	300.00	75.00	75.00
2	au ma	2	PETL	300.00	75.00	75.00
3	au ma	3	PETL	300.00	75.00	75.00
4	s ka	4	PETL	60.00	3.51	3.51
5	fe la	5	TAPL	60.00	5.81	5.81
6	as la	5	TAPL	60.00	4.74	4.74

Figure A-2: Screen grab showing on-peak and off-peak counting times (in seconds) for each element. Note that the Hi-Peak and Lo-Peak count times are for individual off-peak locations. Au analyses uses a multi-point background for a total of two Hi-Peak and two Lo-Peak sites (Figure 6-3). This means during Au analyses, Hi-Peak and L-Peak runs for 150 seconds each (75 seconds x2) for a total of 300 seconds off-peak and 300 seconds On-Peak. S, Fe, and As analyses use only one Hi-Peak and Lo-Peak site.

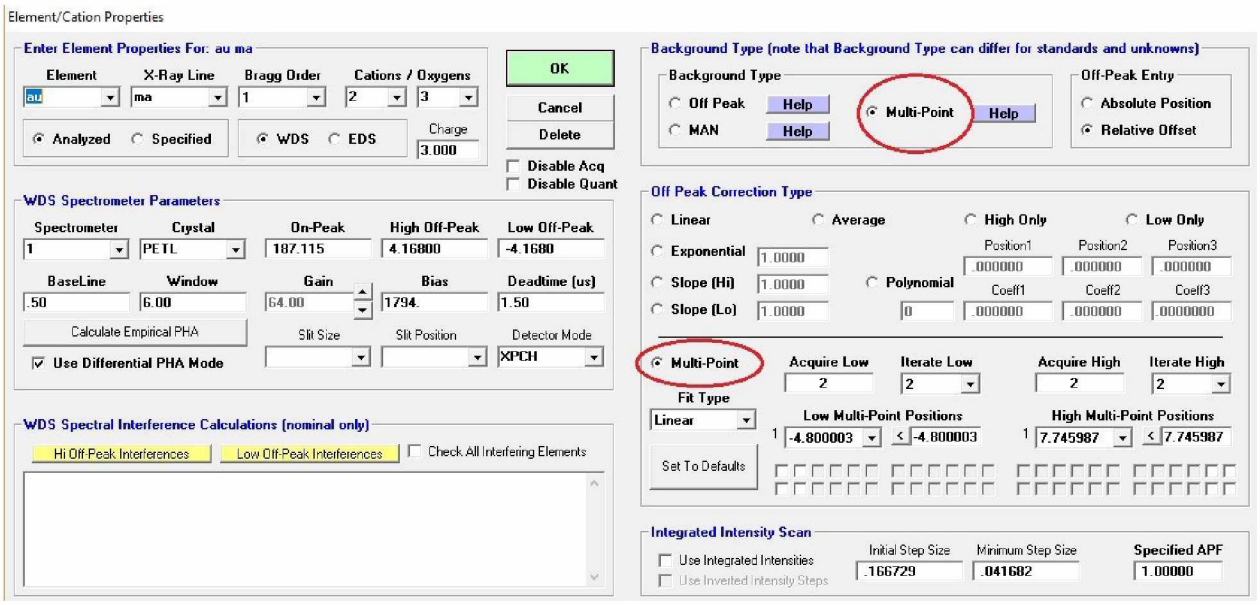

Figure A-3: Screenshot showing the Element/Cation Property window setup for multi-point background points utilized for Au analysis

Appendix B: Supplemental Electronic Files

The supplementals electronic files provide data tables that were created during this course of this study or historic data that was modified to match conclusions drawn from this thesis.

File Name:	Description
DolphinLithology.xlsx	Lithology of all drill hole intercepts.
DolphinAlteration.xlsx	Alteration of all drill hole intercepts.
DolphinSulfideEDS.xlsx	Quantified data from EDS analyses of sulfides hosted in plutonic rock.
DolphinWDSdata.xlsx	WDS data from pyrite and arsenopyrite analyzed in this study.